COMPUTER SIMULATION OF NANOPARTICLES TRANSLOCATION THROUGH PHOSPHOLIPID MEMBRANES WITHIN SINGLE CHAIN MEAN FIELD APPROACH

Sergey Pogodin

Dipòsit Legal: T. 290-2012

UNIVERSITAT ROVIRA I VIRGILI
COMPUTER SIMULATION OF NANOPARTICLES TRANSLOCATION THROUGH PHOSPHOLIPID MEMBRANES WITHIN SINGLE CHAIN MEAN FIELD APPROACH
Sergey Pogodin
DL: T. 290-2012

Universitat Rovira i Virgili
Departament d'Enginyeria Química

Doctoral Thesis

Computer Simulation of Nanoparticles Translocation through Phospholipid Membranes within Single Chain Mean Field Approach

by Sergey Pogodin

Tarragona, Spain, 2012

UNIVERSITAT ROVIRA I VIRGILI
COMPUTER SIMULATION OF NANOPARTICLES TRANSLOCATION THROUGH PHOSPHOLIPID MEMBRANES WITHIN SINGLE CHAIN MEAN FIELD APPROACH
Sergey Pogodin
DL: T. 290-2012

UNIVERSITAT ROVIRA I VIRGILI
COMPUTER SIMULATION OF NANOPARTICLES TRANSLOCATION THROUGH PHOSPHOLIPID MEMBRANES WITHIN SINGLE CHAIN MEAN FIELD APPROACH
Sergey Pogodin
DL: T. 290-2012

UNIVERSITAT ROVIRA I VIRGILI
COMPUTER SIMULATION OF NANOPARTICLES TRANSLOCATION THROUGH PHOSPHOLIPID MEMBRANES WITHIN SINGLE CHAIN MEAN FIELD APPROACH
Sergey Pogodin
DL: T. 290-2012

Sergey Pogodin

Computer Simulation of Nanoparticles Translocation through Phospholipid Membranes within Single Chain Mean Field Approach

---

Doctoral Thesis
Supervised by Dr. Vladimir A. Baulin

Departament d'Enginyeria Química
Molecular Simulation Group

UNIVERSITAT ROVIRA I VIRGILI

Tarragona, 2012

UNIVERSITAT ROVIRA I VIRGILI
COMPUTER SIMULATION OF NANOPARTICLES TRANSLOCATION THROUGH PHOSPHOLIPID MEMBRANES WITHIN SINGLE CHAIN MEAN FIELD APPROACH
Sergey Pogodin
DL: T. 290-2012

UNIVERSITAT ROVIRA I VIRGILI

Departament d'Enginyeria Química

Av. Països Catalans, 26
43007 Tarragona
Tel.: +34 977 55 8675
Fax.: +34 977 55 9621

I STATE that the present study, entitled "Computer Simulation of Nanoparticles Translocation through Phospholipid Membranes within Single Chain Mean Field Approach", presented by Sergey Pogodin for the award of the degree of Doctor, has been carried out under my supervision at the Departament d'Enginyeria Química of this university, and that it fulfils all the requirements to be eligible for the European Doctorate Award.

Doctoral Thesis Supervisor

Dr. Vladimir A. Baulin
Tarragona, January 10, 2012

UNIVERSITAT ROVIRA I VIRGILI
COMPUTER SIMULATION OF NANOPARTICLES TRANSLOCATION THROUGH PHOSPHOLIPID MEMBRANES WITHIN SINGLE CHAIN MEAN FIELD APPROACH
Sergey Pogodin
DL: T. 290-2012

UNIVERSITAT ROVIRA I VIRGILI
COMPUTER SIMULATION OF NANOPARTICLES TRANSLOCATION THROUGH PHOSPHOLIPID MEMBRANES WITHIN SINGLE CHAIN MEAN FIELD APPROACH
Sergey Pogodin
DL: T. 290-2012

Acknowledgements

It is a great pleasure to acknowledge here all the people and organizations who were supporting me all the way through my PhD study, and made this thesis completion possible. First of all it is my supervisor, Dr. Vladimir A. Baulin, who made essential contribution to the project and provided me an attentive guidance in the course of the work, and the rest of the members of the Molecular Simulation Group of the Chemical Engineering Department of the Rovira i Virgili University, especially Prof. Josep Bonet Ávalos, and Prof. Allan Mackie. Special thank goes to the group secretary, Teresa Mármol, whose help with a lot of paperwork was priceless.

For financial support, I would like to thank Agència de Gestió d'Ajuts Universitaris i de Recerca of the Generalitat de Catalunya, which provided me with the scholarship to perform this study, and supported our research group with number of others grant. I also acknowledge Spanish Ministry of Education and Science, which also funded part of the work.

Important scientific contribution to this work, in form of inspiring and fruitful discussions, was done by many colleagues from different institutes. I'd like especially mention here Professor Nigel Slater from University of Cambridge, UK, who brought a lot of ideas concerning our studies and became coauthor of few papers, forming this thesis report, and Professor Jens-Uwe Sommer from Institute of Polymer Research in Dresden, Germany, who was very kind to invite me for three-months stage in his research group at the final part of work at my PhD-project.

Finally, I'd like to thank all my friends and relatives for the nice atmosphere in my life and support in hard moments. And the last, but not the least, thanks go to my parents, Marina Pogodina and Alexei Fedorov, without them I'd have no chance to write down these words ever.

Sergey Pogodin
Tarragona, January 10, 2012

UNIVERSITAT ROVIRA I VIRGILI
COMPUTER SIMULATION OF NANOPARTICLES TRANSLOCATION THROUGH PHOSPHOLIPID MEMBRANES WITHIN SINGLE CHAIN MEAN FIELD APPROACH
Sergey Pogodin
DL: T. 290-2012

UNIVERSITAT ROVIRA I VIRGILI
COMPUTER SIMULATION OF NANOPARTICLES TRANSLOCATION THROUGH PHOSPHOLIPID MEMBRANES WITHIN SINGLE CHAIN MEAN FIELD APPROACH
Sergey Pogodin
DL: T. 290-2012

Abstract

Present work is devoted to development and usage in practical applications of the Single Chain Mean Field (SCMF) method of computer simulation of molecular systems. It covers the theoretical bases of the approach in general and special cases, as well as peculiarities of efficient numerical implementation of the method. Few coarse-grained models of DMPC lipid membrane, reproducing within the SCMF method essential characteristics of the lipid bilayer, such as its thickness, density and elasticity, are proposed. One of these models is used to study features of interaction between the membrane and different homogeneous and patterned nano-objects, such as carbon nanotubes with different coverings and LEA-protein-like objects.

UNIVERSITAT ROVIRA I VIRGILI
COMPUTER SIMULATION OF NANOPARTICLES TRANSLOCATION THROUGH PHOSPHOLIPID MEMBRANES WITHIN SINGLE CHAIN MEAN FIELD APPROACH
Sergey Pogodin
DL: T. 290-2012

UNIVERSITAT ROVIRA I VIRGILI
COMPUTER SIMULATION OF NANOPARTICLES TRANSLOCATION THROUGH PHOSPHOLIPID MEMBRANES WITHIN SINGLE CHAIN MEAN FIELD APPROACH
Sergey Pogodin
DL: T. 290-2012

Contents

1 Motivation and goals of the study **3**
1.1 Foreword . . . 3
1.2 Role of phospholipid membranes in nature . . . 4
1.3 Experimental methods to study phospholipid membranes . . . 7
1.4 Theoretical approaches to study phospholipid membranes . . . 8
1.5 Implementation of the Single Chain Mean Field method . . . 10
1.6 Goals of the project and research overview . . . 11
1.7 My contribution to the project . . . 12
1.8 References . . . 13

2 Phospholipid membranes within SCMF approach **17**
2.1 Introduction . . . 17
2.2 Theory . . . 18
2.3 Application to phospholipid membranes . . . 20
2.4 Results and discussion . . . 21
2.5 Conclusions . . . 25
2.6 Appendix A. Computational details . . . 25
A.1. Conformational sampling generation . . . 25
A.2. Discretization of space . . . 25
A.3. Numerical implementation . . . 26
2.7 Acknowledgements . . . 27
2.8 References . . . 27

3 Insertion of nanoscale objects into phospholipid bilayer **29**
3.1 Introduction . . . 29
3.2 Theory . . . 29
3.3 Results and discussion . . . 32
3.4 Conclusions . . . 33

3.5 Acknowledgements 33
3.6 References 33

4 Carbon nanotube vs. phospholipid bilayer 35
4.1 Introduction 35
4.2 Free energy of the nanotube insertion 36
4.3 Results and discussion 37
4.4 Conclusions 40
4.5 Methods 40
4.6 Acknowledgements 41
4.7 References and notes 41

5 Translocation of patterned carbon nanotube 43
5.1 Introduction, results and discussion 43
5.2 Acknowledgements 47
5.3 References and notes 47

6 Adsorption of patterned biomolecule 49
6.1 Abstract 49
6.2 Introduction 49
6.3 Results and discussion 50
6.4 Conclusion 53
6.5 Materials and methods 53
6.6 Acknowledgement 53
6.7 References and Notes 53

7 Conclusions 55

8 Publications, conferences and summer schools 57
8.1 Publications in refereed journals with ISI citation index 57
8.2 Participation in conferences and summer schools 59

UNIVERSITAT ROVIRA I VIRGILI
COMPUTER SIMULATION OF NANOPARTICLES TRANSLOCATION THROUGH PHOSPHOLIPID MEMBRANES WITHIN SINGLE CHAIN MEAN FIELD APPROACH
Sergey Pogodin
DL: T. 290-2012

Chapter 1

Motivation and goals of the study

1.1 Foreword

The regulations [1] of the Chemical Engineering Department of the Universitat Rovira i Virgili permit to a student to compile his doctorate thesis out of his publications in peer-reviewed journals with high impact factors, if at least two appropriate articles were published in the course of his doctorate study. The use of this option explains the format of the present thesis book. First chapter presents the introduction, motivation and goals of the study. Next five chapters contain reprints of the following articles written during the study:

- "Coarse-grained models of biological membranes within the Single Chain Mean Field theory" by Sergey Pogodin and Vladimir A. Baulin, published in *Soft Matter*, 2010, **6**, 2216-2226 (ISI impact factor is 4.457, AIF[1] 2.458, the article is cited 7 times)

- "Can a carbon nanotube pierce through a phospholipid bilayer?" by Sergey Pogodin and Vladimir A. Baulin, published in *ACS Nano*, 2010, **4**, 5293-5300 (ISI impact factor is 9.865, AIF 4.154, the articles is cited 7 times)

- "Surface patterning of carbon nanotubes can enhance their penetration through a phospholipid bilayer" by Sergey Pogodin, Nigel K. H. Slater and Vladimir A. Baulin, published in *ACS Nano*, 2011, **5**, 1141-1146 (ISI impact factor is 9.865, AIF 4.154, the articles is cited 4 times)

- "Equilibrium insertion of nanoscale objects into phospholipid bilayers" by Sergey Pogodin and Vladimir A. Baulin, published in *Current Nanoscience*, 2011, **7**, 721-726 (ISI impact factor is 1.879, AIF 4.154)

[1] ISI aggregated impact factor of the most relevant journal category

- "Biomolecule surface patterning may enhance membrane association" by Sergey Pogodin, Nigel K. H. Slater and Vladimir A. Baulin, published online in *ACS Nano*, 2012 (ISI impact factor is 9.865, AIF 4.154)

The last chapter summarizes the results of the articles and provides general conclusions of the study.

1.2 Role of phospholipid membranes in nature

Biological cells, elementary building blocks of the live matter, are presented in large amounts on our planet, and they are extremely important for us, because all we are made of them. An essential component of every cell is the cell membrane, protecting the cell from the environment and also controlling the transport of chemicals between the interior and exterior of the cell [2–4]. When an extraneous nanoobject approaches the cell membrane, important questions about their destiny arise naturally. Will be the nanoobject able to pass through the membrane, or will the membrane stop it? Will the nanoobject severely damage the membrane machinery, causing the cell death, or not? One can image numerous practical applications of specific interactions possible between a nanoobject and the membrane. They may be used, for example, to deliver a necessary medicine inside a deceased cell [5–9], or to kill some specific harmful cells by destruction of their membranes or by suppression of their proper functioning [10–13].

The questions outlined above are hard to answer at the present day, both using experimental or theoretical methods. The major difficulty is the complex structure of the cell membrane (Fig. 1.1), consisting of lipid bilayer with numerous proteins embed into it and anchored to it. The lipid basement of the membrane is formed by mixture of phospholipids, glycolipids, and cholesterol, and the phospholipids are the major compound of the bilayer. Thus a pure phospholipid bilayer can be considered as a model of a real cell membrane both in experimental and theoretical studies. It can be used to estimate mechanical properties of the biological membrane, its permability for different chemicals and nanoobjects, to study its interaction with single proteins.

Chemical structures of some typical phospholipids being widely used in experiments are shown in Figure 1.2. Each of them consists of two carbon hydrophobic tails and one polar hydrophilic headgroup. Such amphiphilic nature explains spontaneous self-assembly of phospholipid molecules in solutions into stable spacial structures, with tails gathered together in regions pure of solvent and heads formed

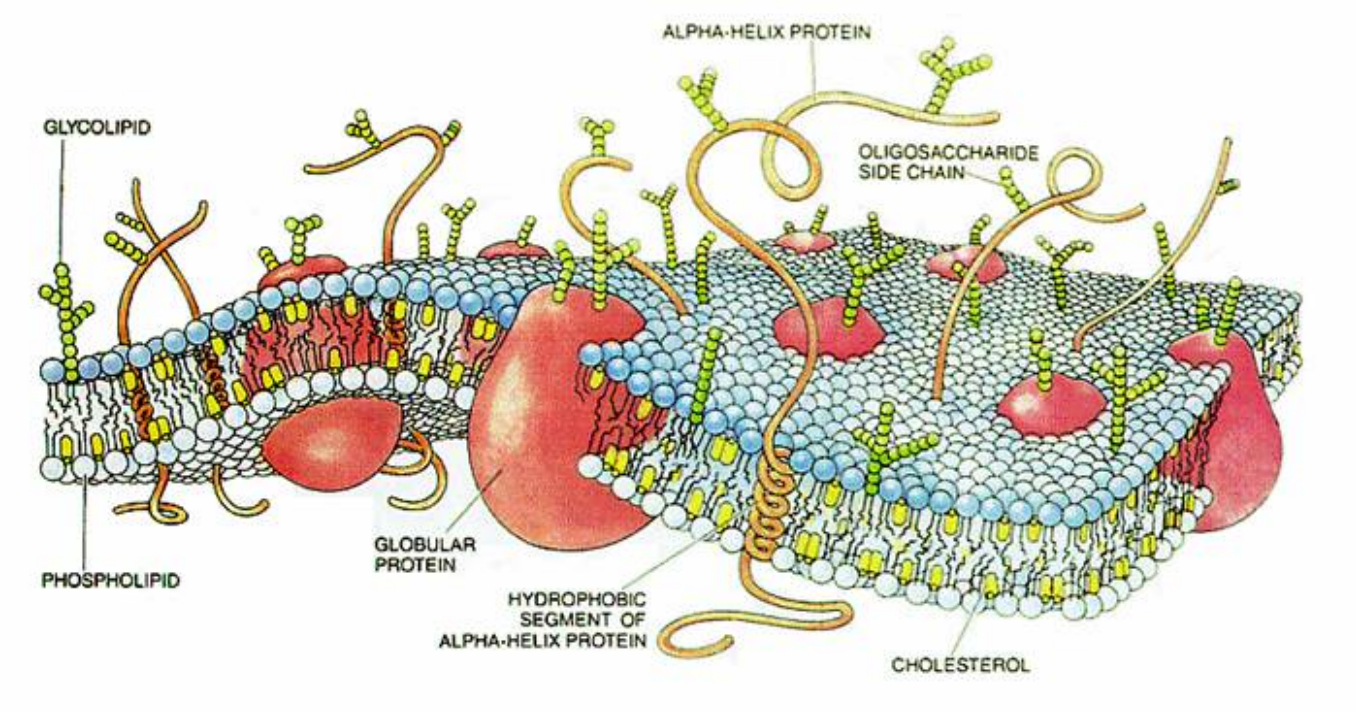

Figure 1.1: Schematic image [14] of the cell membrane, composed of mixture of phospholipids with cholesterol and embed proteins.

Table 1.1: Experimental data [15, 16] on DMPC, DPPC, DOPC, EPC and DLPE membranes.

Lipid	DMPC	DPPC		DOPC	EPC	DLPE	
Temperature, $^\circ C$	30	20	50	30	30	20	35
Thickness of the bilayer, $\AA$	44.2	52.4	46.5	45.1	45.1	47.0	42.8
Thickness of the hydrophobic core, $\AA$	26.2	34.4	28.5	27.1	27.1	30.0	25.8
Interfacial area per lipid, $\AA^2$	59.6	47.9	64.0	72.5	69.4	41.0	51.2
Lipid molecular volume, $\AA^3$	1101	1144	1232	1303	1261	863	907
Stretching modulus, dyn/cm	257	—	—	251	—	—	—

surfaces dividing those regions, poor and rich in solvent. Depending on concentration of lipids in the solution and conditions of the process, number of biologically relevant structures, such as micelles, vesicles, and membranes, can be formed. Table 1.1 shows some experimentally measured mechanical properties of the membranes assembled from the lipids shown in Figure 1.2.

An important feature of lipid membranes is the presence of phase transition between so called gel and fluid phases. While in the fluid phase the lipids can freely diffuse in the membrane plane, in the gel phase they are much more ordered, and are not able to move around the bilayer. The critical temperature, at which this transition occurs, vary significantly for different lipids [17], depending on the length of their tails and the presence of double bonds inside them. This transition is also

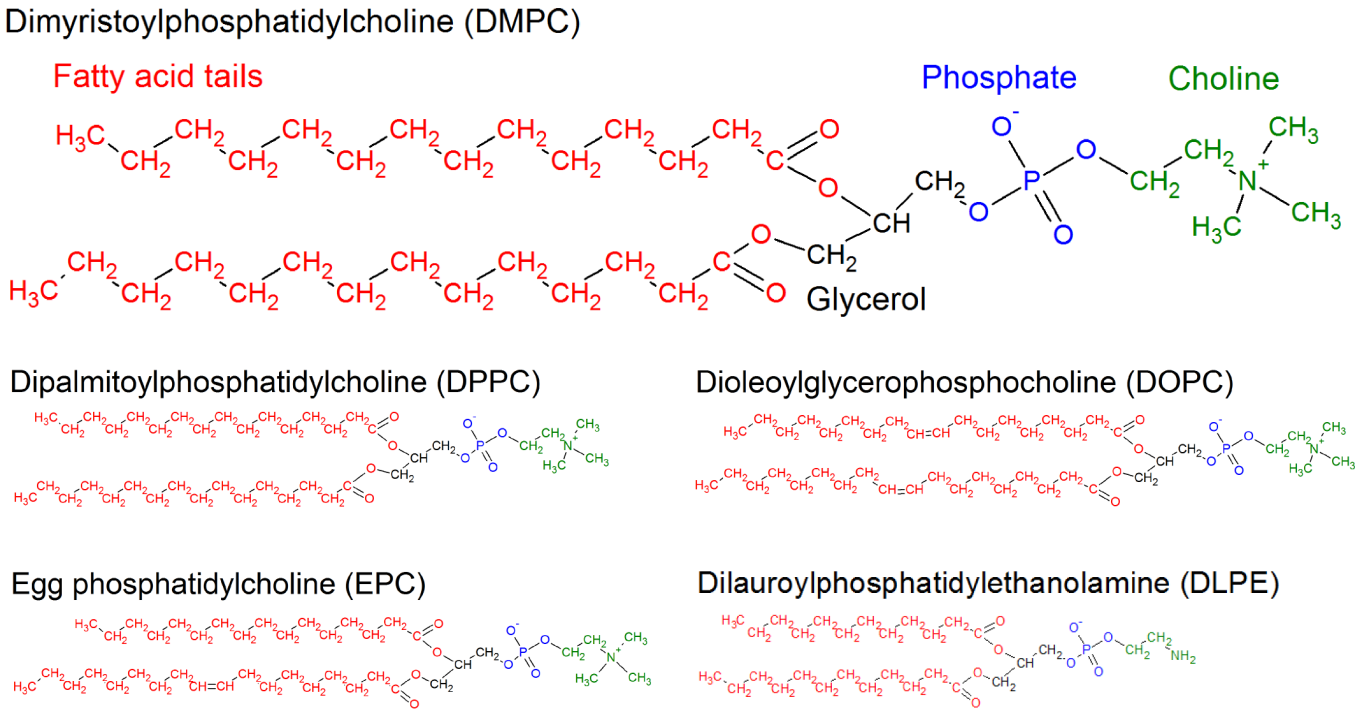

Figure 1.2: Chemical structures of some of the most popular phospholipids.

referred as the main transition due to possibility of other transitions. The biological membranes at relevant conditions stay in fluid phase, but not far from the gel-liquid transition [18], and this may play important role in transport of chemicals through them [19], taking into account that all the proteins inserted into the membrane have influence at the critical temperature of the phase transition in their vicinity, and on the other hand phase behavior of the membrane around a protein may have influence on it function.

As for the model phospholipid membranes composed of one type of lipids there are few possible mechanisms of transport of molecules through them. One is by thermal diffusion through the lipid bilayer, when the transported object has to cross the membrane, physically overcoming potential barriers of size depending on the object size, structure, and surface properties. The alternative possibility is the transport by endocytosis, when a part of the membrane wrap around the transported object into a vesicle, and that vesicle, containing the object, eventually separates from the membrane and float into opposite side of the membrane. Then the vesicle with its content may diffuse to a region of space, where it is being destructed, releasing the load. Another way of transmembrane transport is a collective interaction of transported objects with the membrane, when the group of the objects internalize into the membrane, creating a pore inside it, and other objects then cross the membrane

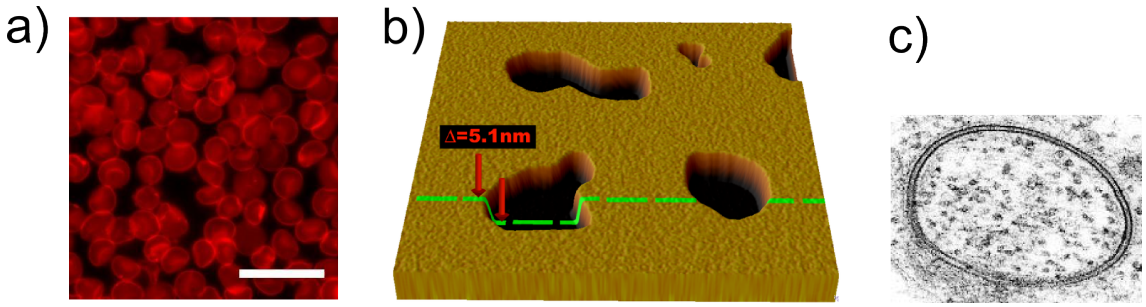

Figure 1.3: Examples of microscopy images of lipid bilayers, obtained by different methods: a) Fluorescence microscopy image [20] of human red blood cells supported on a glass slide. Scale bar is 20 microns. b) AFM scan [21] of a supported lipid bilayer. c) Transmission electron microscopy image [22] of lipid vesicle.

via that pore.

1.3 Experimental methods to study phospholipid membranes

Number of experimental methods are successfully applied to characterize lipid membranes, but at present they are not able to answer all questions about behavior of the membranes and their interaction with other objects. This is because the thickness of the membrane and the size of nano-objects are close to the maximum resolution of existing methods. Another problem is that the preparation of the samples for those methods usually assume some modifications of the membrane, and it can be hard to find out, how much the pretreatment of the membrane during the sample preparation alters the membrane properties.

To visualize a phospholipid membrane different microscopy methods may be used. Fluorescent microscopy [23] (Fig. 1.3a) is performed by coloring with a fluorescent dye the membrane, or the objects which translocation through the membrane is studied. Resolution of the method is limited by wavelength of light and is typically of order 100 nm. Although some special techniques of the fluorescent microscopy can improve the resolution further, usually the thickness of the membrane is smaller than the resulting resolution. Severe disadvantage of the method is that the introduction of dye molecules into the membrane affects the system properties, and the influence of this effect is hard to estimate. In addition, the fluorescent microscopy can only indicate the fact of translocation or accumulation of nanoobjects in the membranes, but cannot suggest on the molecular mechanism of translocation.

Atomic Force Microscopy (AFM) [24] method (Fig. 1.3b) can be used for imaging of phospholipid membranes with high resolution of order of nanometer. However, this method is limited to supported bilayers, where the membrane is adsorbed at

the surface and thus, the properties of the membrane can be changed. Although its is easy to damage the bilayer with the AFM probe.

Electron microscopy [25, 26] (Fig. 1.3c) is able to visualize a lipid membrane with resolution of nanometer or higher, but also is very demanding for the sample preparation. Usually the samples for electron microscopy have to be under vacuum, which is not compatible with normal conditions for a phospholipid membrane. To overcome this difficulty samples can be studied under cryogenic conditions (so-called cryo-TEM), when the solvent is frozen inside the bilayer, instead of being removed from it under vacuum. Another problem is the low contrast between the lipids and water, which usually requires introduction of heavy metal compounds inside the bilayer to improve the contrast, thus affecting the normal structure of the membrane.

Neutron [27] and X-ray [28] scattering techniques are suitable for exploration of lipid membranes structure and distribution of embedded objects inside the bilayers. While the neurons scatter at nuclei of atoms, the X-rays scatter at the electron shells of the atoms. As a result these methods have different contrasts for different components of the system. The neutron scattering may distinguish between different isotopes, and detect light-weighted elements like hydrogen. The X-rays on contrary almost don't interact with light atoms, and water is almost transparent for them. Both methods gives spatially averaged structure of the bilayer.

To study transport of chemicals through a phospholipid membrane electrical measurements can be used [18]. In this approach electrodes are placed at different sides of the membrane and conductivity of the circuit is measured. Penetration of objects through the membrane has strong influence at the conductivity, even appearance of tiny nanometer-size pores can be easily detected with this approach.

Number of other approaches are used to measure some properties of phospholipid membranes. Thus optical measurements [29] are useful to study reorganization of the membranes, because the lipids are highly polar molecules. To measure elasticity of the membranes micropipette aspiration technique [30] can be applied.

1.4 Theoretical approaches to study phospholipid membranes

Depending on the task, a phospholipid membrane can be modeled with different levels of approximation. The most detailed description is used in atomistic computer simulations [31], which individually take into account all the atoms of the phospholipid and solvent molecules presented in the system. Unfortunately, such methods are extremely computationally expensive, and their application to simula-

tion of long-term behavior of a large part of a membrane is problematic, because it takes too much time. When this problem emerge, coarse-grained approaches [32–34] are coming into play. The idea is that groups of neighbor atoms can be represented in the model as spherical "coarse-grained" beads, interacting with each other via some effective potentials. This reduces amount of degrees of freedom in the system, and larger sizes and times become accessible in the simulation. Obviously, the accuracy of such methods depends on the strategy used for coarse-graining. On one hand every coarse-grained bead can represent just few atoms, on the other hand the whole lipid molecule can be represented with the use of only few beads. Accurate usage of this technique allows one to study interaction of large parts of the membrane with molecules and particles. Finally, when the system size is even larger, one can think to treat the membrane as an infinitely thin surface without any internal structure, but with a given elasticity and bending resistance.

There is a number of different techniques, how the simulation of the membrane with a chosen approximation can be performed. While some properties of the membrane can be estimated purely analytically, better approach is to run a computer simulation with the use of Molecular Dynamics (MD) or Monte-Carlo (MC) methods. The Molecular Dynamics is the most "brute-force" approach, dealing with numerical solving of Newton's equations of motion for the molecules presented in the system. It gives the most detailed information about the evolution of the system in time, and represents its true dynamics behavior. On the other hand this method is the most computationally expensive, and if the equilibrium properties of the system should be studied, it can take a lot of time to reach the equilibrium with MD method. Unquestionable advantage of the method, emerging from its popularity, is availability of free and commercial program packages for performing the simulations, and existing of good models already fitted for description of phospholipid membranes.

Monte Carlo approach is a stochastic method, base on random exploration of a system's conformational space. At every step it randomly update the current state of the system, and this update is accepted or rejected with a certain probability, depending on the energy change. Dynamical properties of the system, also can be studied with MC method, if the trial updates of the system's state are done in an appropriate way.

Although MD and MC methods are powerful and well-developed at the present day, they cannot be called a "must to use" tools for simulation of lipid membranes, and development of alternative approaches, more suitable for investigation of some

specific properties of the membranes, still looks perspective and promising. The method used in this work, called Single Chain Mean Field (SCMF) approach, was originally developed by Ben-Shaul, Szleifer et al. [35, 36] for simulation of polymer systems. The idea behind it is to approximate the intermolecular interactions in the system with the use of mean-field method, i.e. to replace them by effective interactions of every single molecule with average mean-field distribution of all other molecules. Then the free-energy of the equilibrium state of the system can be written down as a function of the single molecule distributions in the simulation box, and numerical minimization of that function gives the equilibrium values of those distributions, and all the equilibrium properties of the system then can be calculated via direct averaging over the distributions. Thus the SCMF approach looks ideal for the study of equilibrium properties of the phospholipid membranes, and for calculation of the free-energy barriers for translocation of nanoparticles through them.

1.5 Implementation of the Single Chain Mean Field method

In the previous works [35–39] the authors studied different systems using simplest implementations of the SCMF method. It seemed for us too restrictive for the purposes of the present work, so the decision was made to create a new implementation of the method, making its revision, and writing a flexible computer simulation code from scratch.

Our version of the SCMF method consider a system containing molecules constructed of spherical beads interacting with each other via specified potentials. Number of types of the potentials, beads and molecules can be arbitrary. The simulation box may have periodical or "hard-wall" boundary conditions, and contain some additional objects, imitating nano-particles fixed inside the box. In general it allows to represent a model phospholipid bilayer with different level of coarse-graining and study its interaction with different nano-objects.

The computer code was written in C++ language with extensive use of object-oriented programming features. It has flexible modular structure, allowing its easy modification and improvement by adding new modules rather than by rewriting and correcting the existing ones. Parallel execution at shared memory machines is supported via OpenMP protocol. The code is cross-platform and can be compiled and used both under Linux and Windows operative systems.

Detailed description of our general implementation of the method is given in the

Chapter 2, and the Chapter 3 describes its particular view in the case of phospholipid membrane simulation within "three-bead" coarse-grained model.

1.6 Goals of the project and research overview

Apart from implementation and test of working SCMF computer code, the following scientific goals were set in the beginning of the work:

- To fit a coarse-grained model of the DMPC phospholipid membrane, accounting for the peculiarities of the SCMF method, and reproducing experimental properties of the membrane, reported in literature.
- Investigate the possibility of spontaneous translocations of carbon nanotubes through the DMPC bilayer.
- Investigate the influence of a carbon nanotube patterning on its ability to penetrate through the membranes.

To complete the first task few models of the DMPC molecule, 44-, 10-, and 3-beads ones, were approbated and fitted to reproduce the unperturbed membrane with thickness, density and elasticity coinciding with experimental data. Details of this part of the work can be found in the Chapter 2. The 3-beads model, the fastest and simplest model, which is still able to reproduce most essential features of the system of interest, was then chosen for primary use in the future research. Simplified description of the method for the particular case of 3-bead model application for study of nano-objects insertion into the membrane is given in the Chapter 3.

Simulations of the phospholipid bilayer alone were continued with simulations of its interaction with carbon nanotubes, with original hydrophobic, or modified hydrophilic homogeneous surface. Free energy barriers for translocation of such objects through the membrane were calculated, and conclusions about the ability of such objects spontaneously penetrate through the bilayer via thermal diffusion were made. Such study is useful in view of ongoing discussions of the carbon nanotubes cytotoxicity and their impact on biological systems. Chapter 4 describes the results of this part of the work.

Further the influence of the nanotube patterning on the translocation through the membrane was explored. It was shown that some periodical patterns at the nanotube surface, composed of regions with higher and lower hydrophobicity, can significantly enhance the abilities of the nanotube to diffuse through the phospholipid bilayer. These results are reported in the Chapter 5.

In the last part of the work, a new object interacting with the membrane was studied. Cells of some plants and animals contain so-called Late Embryogenesis Abundant (LEA) proteins, playing important role in their protection against desiccation, freezing and osmotic shocks. In case of such dangers the LEA proteins may fold into helical structure with hydrophobic and hydrophilic stripes going along the helix main axis. In this conformation they are able to adsorb onto the membrane and modify its mechanical properties to resist the dangerous conditions. Our investigation of the LEA-protein-like objects adsorption onto the phospholipid bilayer is described in the Chapter 6.

1.7 My contribution to the project

During my PhD study I have done myself most of the work which results forming this thesis:

- Derivation of the general Single Chain Mean Field theory in our interpretation (with help and advise by Dr. Vladimir Baulin).
- All the programming from scratch of the computer simulation code used in this project.
- Active participation in choice of the scientific goals together with Dr. Vladimir Baulin and Prof. Nigel Slater.
- All the computer simulations runs and output data processing.
- Preparation of all artworks for the articles forming this thesis.
- Active participation in the working out articles texts together with Dr. Vladimir Baulin (Articles [41–45]) and Prof. Nigel Slater (Articles [44, 45]).

In addition, I have presented our research at number of scientific conferences, both as poster presentation and as oral talks (the list of attended conferences can be found in the end of this book, in the section 8.2).

Apart of the work on this thesis, I have participated in two side projects with Dr. Vladimir Baulin and others, doing some part of theoretical analysis and numerical calculations. Two articles [46, 47] based on the results of those projects were prepared, but their subject falls out of the scope of this thesis.

1.8 References

[1] See "Normativa per a la Presentació d'una tesi doctoral per compendi de publicacions", Departament d'Enginyeria Química of the Universitat Rovira i Virgili, Tarragona, October 2009.

[2] Alberts, B. *Molecular Biology of the Cell*, 5th ed.; Garland Science: New York, 2008.

[3] Yeagle, P. L. *The Structure of Biological Membranes*, 2nd ed.; CRC Press: Boca Raton, FL, 2005.

[4] Cooper, G. M.; Hausman, R. E.; *The Cell: a Molecular Approach*, 5th ed.; Sinauer Associates Inc.: Sunderland, MA, 2009.

[5] Stewart, K. M.; Horton, K. L.; Kelley, S. O. Cell-Penetrating Peptides as Delivery Vehicles for Biology and Medicine. *Org. Biomol. Chem.* **2008**, *6*, 2242-2255.

[6] Moghimi, S. M.; Hunter, A. C.; Murray, J. C. Nanomedicine: Current Status and Future Prospects. *FASEB J.* **2005**, *19*, 311-330.

[7] Kamada, H.; Okamoto, T.; Kawamura, M.; Shibata, H.; Abe, Y.; Ohkawa, A.; Nomura, T.; Sato, M.; Mukal, Y.; Sugita, T.; et al. Creation of Novel Cell-Penetrating Peptides for Intracellular Drug Delivery Using Systematic Phage Display Technology Originated from Tat Transduction Domain. *Biol. Pharm. Bull.* **2007**, *30*, 218-223.

[8] Pack, D. W.; Hoffman, A. S.; Pun, S.; Stayton, P. S. Design and Development of Polymers for Gene Delivery. *Nature* **2005**, *4*, 581-593.

[9] Plank, C.; Zauner, W.; Wagner, E. Application of Membrane-Active Peptides for Drug and Gene Delivery across Cellular Membranes. *Adv. Drug Delivery Rev.* **1998**, *34*, 21-35.

[10] Tew, G. N.; Liu, D.; Chen, B.; Doerksen, R. J.; Kaplan, J.; Carroll, P. J.; Klein, M. L.; DeGrado, W. F. De Novo Design of Biomimetic Antimicrobial Polymers. *Proc. Natl. Acad. Sci. U.S.A* **2002**, *99*, 5510-5114.

[11] Jenssen, H.; Hamill, P.; Hancock, R. E. W. Peptide Antimicrobial Agents. *Clin. Microbiol. Rev.* **2006**, *19*, 491-511.

[12] Brogden, K. A. Antimicrobial Peptides: Pore Formers or Metabolic Inhibitors in Bacteria. *Nature* **2005**, *3*, 238-250.

[13] Hancock, R. E. W.; Sahl, H.-G. Antimicrobial and Host-Defense Peptides as New Anti-Infective Therapeutic Strategies. *Nat. Biotechnol.* **206**, *24*, 1551-1557.

[14] The image is taken from the NIST website:
http://www.ncnr.nist.gov/programs/reflect/rp/biology/cell_membranes.html
The drawing was made by Dana Burns, and can also be found in Scientific American, 1985, 253(4), pages 86-90, in the article "The molecules of the cell membrane" by M.S. Bretscher.

[15] Nagle, J. F.; Tristam-Nagle, S. Structure of Lipid Bilayers. *Biochem. et Biophys. Acta* **2000**, *1469*, 159-195.

[16] Mathai, J. C.; Tristam-Nagle, S.; Nagle, J. F.; Zeidel, M. L. *J. Gen. Physiol.* **2008**, *131*, 77-85.

[17] Critical temperatures of different phase transitions in phospholipid membranes, can be consulted for large amount of phospholipids in the free Internet database Lipidat: www.lipidat.tcd.ie

[18] Heimburg, T. *Thermal Biophysics of Membranes*; Wiley-VCH Verlag: Weinheim, Germany, 2007.

[19] Gallaher, J.; Wodzińska, K.; Heimburg, T.; Bier, M. Ion-Channel-Like Behaviour in Lipid Bilayer Membranes at the Melting Transition. *Phys. Rev. E* **2010**, *81*, 061925.

[20] Image is taken from Wikipedia Commons
en.wikipedia.org/wiki/File:Sedimented_red_blood_cells.jpg and is allowed by author for use for any purposes without restrictions.

[21] Image is taken from Wikipedia Commons
en.wikipedia.org/wiki/File:Bilayer_AFM_schematic.png and is allowed by athour for use for any purposes without restrictions.

[22] Image is taken from Wikimedia Commons http://en.wikipedia.org/wiki/File:Annular_Gap_Junction_Vesicle.jpg and is allowed by author for use for any purposes without restrictions.

[23] http://www.microscopyu.com/articles/fluorescence/fluorescenceintro.html

[24] Giessibl, F. J. Advances in Atomic Force Microscopy. *Rev. Mod. Phys.* **2003**, *75*, 949-983.

[25] Bozzola, J. J.; Russell, L. D. *Electron Microscopy*, 2nd ed.; Jones and Bartlett Publishers, Inc.: 1999.

[26] Williams, D. B.; Carter, C. B. *Transmission Electron Microscopy. A Textbook for Materials Science*, 2nd ed.; Springer: New York, 2009.

[27] Pynn, R. *Neutron Scattering - A primer* http://knocknick.files.wordpress.com/2008/04/neutrons-a-primer-by-rogen-pynn.pdf

[28] http://www.mrl.ucsb.edu/mrl/centralfacilities/xray/xray-basics/index.html

[29] Mashaghi, A.; Swann, M.; Popplewell, J.; Textor, M.; Reimhult, E. Optical Anisotropy of Supported Lipid Structures Probed by Waveguide Spectroscopy and Its Application to Study of Supported Lipid Bilayer Formation Kinetics. *Anal. Chem.* **2008**, *80*, 36663676.

[30] Hochmuth, R. M. Micropipette aspiration of living cells. *J. Biomech.* **2000**, *33*, 15-22.

[31] Tieleman, D. P.; Marrink, S. J; Berendsen, H. J. C. A Computer Perspective of Membranes: Molecular Dynamics Studies of Lipid Bilayer Systems. *Biochem. Biophys. Acta* **1997**, *1331*, 235-270.

[32] Venturoli, M.; Sperotto, M. M.; Kranenburg, M.; Smit, B. Mesoscopic Models of Biological Membranes. *Phys. Rep.* **2006**, *437*, 1-54.

[33] Saiz, L.; Klein, M. L. Computer Simulation Studies of Model Biological Membranes. *Acc. Chem. Res.* **2002**, *35*, 482-489.

[34] Scott, H. L. Modeling the Lipid Component of Membranes. *Curr. Opin. Struct. Biol.* **2002**, *12*, 495-502.

[35] Ben-Shaul, A.; Szleifer, I.; Gelbart, W. M. *J. Chem. Phys.* **1985**, *83*, 3597.

[36] Ben-Shaul, A.; Szleifer, I.; Gelbart, W. M. *J. Chem. Phys.* **1986**, *85*, 5345.

[37] Mackie, A. D.; Panagiotopoulos, A. Z.; Szleifer, I. *Langmuir* **1997**, *13*, 5022.

[38] Al-Anber, Z. A.; Bonet-Avalos, J.; Mackie, A. D. *J. Chem Phys.* **2005**, *122*, 104910.

[39] Al-Anber, Z. A.; Bonet-Avalos, J.; Floriano, M. A.; Mackie, A. D. *J. Chem. Phys.* **2003**, *118*, 3816-3826.

[40] Shvartzman-Cohen, R.; Ren, C.; Szleifer, I.; Yerushalmi-Rozen, R. *Soft Matter* **2009**, *5*, 5003-5011.

[41] Pogodin, S.; Baulin, V. A. Coarse-Grained Models of Phospholipid Membranes within the Single Chain Mean Field Theory. *Soft Matter* **2010**, *6*, 2216-2226.

[42] Pogodin, S.; Baulin, V. A. Can a Carbon Nanotube Pierce through a Phospholipid Bilayer? *ACS Nano* **2010**, *4*, 5293-5300.

[43] Pogodin, S.; Baulin, V. A. Equilibrium Insertion of Nanoscale Objects into Phospholipid Bilayers. *Current Nanoscience* **2011**, *7*, 721-726.

[44] Pogodin, S.; Slater, N. K. H.; Baulin, V. A. Surface Patterning of Carbon Nanotubes Can Enhance Their Penetration through a Phospholipid Bilayer. *ACS Nano* **2011**, *5*, 1141-1146.

[45] Pogodin, S.; Slater, N. K. H.; Baulin, V. A. Biomolecule Surface Patterning May Enhance Membrane Association. *ACS Nano* **2012**, published online.

[46] Yaroshchuk, A.; Zholkovskiy, E.; Pogodin, S.; Baulin, V. Coupled Concentration Polarization and Electroosmotic Circulation near Micro/Nanointerfaces: Taylor-Aris Model of Hydrodynamic Dispersion and Limits of Its Applicability. *Langmuir* **2011**, *27*, 11710-11721.

[47] Ivanova, E. P.; Hasan, J.; Webb, H. K.; Truong, V. K.; Watson, G. S.; Watson, J. A.; Baulin, V. A.; Pogodin, S.; Wang, J. Y.; Tobin, M. J.; L'obbe, C.; Crawdord, R. J. Natural Antibacterial Surfaces: Cicada (Psaltoda Claripennis) Wings Kill Pseudomonas Aeruginosa Cells. *Just submitted.*

PAPER www.rsc.org/softmatter | Soft Matter

Coarse-grained models of phospholipid membranes within the single chain mean field theory

Sergey Pogodin[a] and Vladimir A. Baulin*[ab]

Received 5th January 2010, Accepted 25th February 2010
First published as an Advance Article on the web 1st April 2010
DOI: 10.1039/b927437e

The single chain mean field theory is used to simulate the equilibrium structure of phospholipid membranes at the molecular level. Three levels of coarse-graining of DMPC phospholipid surfactants are present: the detailed 44-beads double tails model, the 10-beads double tails model and the minimal 3-beads model. We show that all three models are able to reproduce the essential equilibrium properties of the phospholipid bilayer, while the simplest 3-beads model is the fastest model which can describe adequately the thickness of the layer, the area per lipid and the rigidity of the membrane. The accuracy of the method in description of equilibrium structures of membranes compete with Monte Carlo simulations while the speed of computation and the mean field nature of the approach allows for straightforward applications to systems with great complexity.

1 Introduction

Phospholipid membranes and self-assembled bilayers of block copolymers have many common features originating from the amphiphilic nature of the molecules. Phospholipids comprise of hydrophilic head group and two hydrophobic acyl chains and the driving force of self-assembly in membranes, as in case of block copolymers, is the hydrophobic effect.[1] Thus, theoretical methods developed for the self-assembly of block copolymers can be applied for the description of phospholipid membranes.[2]

Theoretical description and computer simulation of phospholipid bilayers and biological membranes has been a challenging task for many decades.[2,3] Although phospholipids are relatively short chains in comparison to polymers and block copolymers, the configurational space of conformations and the number of interactions are extremely large. In addition, the simulation of phospholipid bilayers and membranes is a problem involving many interacting molecules, thus full description of collective behavior would require simultaneous simulation of a large number of molecules. That is why, full atomistic molecular dynamics models,[4–12] describing membranes with chemical accuracy, are limited to short times and short lengths. Usually, atomistic models on times exceeding microseconds and lengths larger than nanometres are not practical,[2] especially when the equilibrium structures of large systems are considered.

One of the strategies to overcome this problem is to group atoms into effective particles that interact *via* effective potentials within so-called coarse-grained models.[13] Coarse-graining can reduce considerably the degrees of freedom and the configurational space such that larger systems and longer times can be reached. Monte-Carlo (MC) simulations of phospholipid membranes with coarse-grained models of phospholipids[14–19] are proved to capture the essential properties of self-assembly of phospholipids into membranes, their molecular structure and collective phenomena.

However, if the objective of the research is the equilibrium properties and the molecular details of the self-assembled structures, the equilibration time may largely exceed microseconds and thus, may not be reached with MD simulations in a reasonable time. An alternative strategy is to reach directly the minimum of the free energy using methods based on mean field theories, thus, avoiding computationally expensive equilibration process used in MC and MD simulations.

The method of the single chain mean field (SCMF) theory[20–25] is particularly suitable for such purposes: it combines analytical theory of the mean field type with the conformational variability accessible in MC simulations. Thus, the accuracy of the method in describing the molecular details of equilibrium structures can compete with MC simulations while the speed of obtaining the results depends only on the speed of the numerical solution of equations, thus it can be much faster than MC simulations.

The advantage of this method is the speed in localization of the free energy minimum and the equilibrium properties as well as the precision in the measurement of the equilibrium free energy which is not straightforwardly accessible with MD and MC simulations. The disadvantage is the mean-field nature of the solution that does not include fluctuations and inter-particle correlations. Nevertheless, the shortcomings of the approach can be compensated by the combination of the SCMF theory with MD simulations which can complement the method. Fast mean field method provides for equilibrium structure with molecular details which, in turn, can be used as input initial configuration for MD simulations and provide the lacking dynamic information and fluctuations.

The SCMF theory, originally developed for the micellization problem of low-molecular surfactants,[20,21] describes a single molecule in the molecular fields. The multichain problem is reduced to a single chain in the external self-consistent field problem. The position, orientation and configuration of the molecule depend on the surrounding fields while the fields

[a]*Universitat Rovira i Virgili 26 Av. dels Paisos Catalans, 43007 Tarragona, Spain. E-mail: vladimir.baulin@urv.cat*
[b]*ICREA, 23 Passeig Lluis Companys, 08010 Barcelona, Spain*

depend on the configurations of the molecules, and finally the equilibrium fields are found self-consistently by numerical solution of a system of nonlinear equations. This method gives a detailed microscopic information on the configurations and averaged positions of the molecules, the optimal shape and structure of self-assembled structures, the distribution of molecules in the aggregates, the critical micellar concentrations as well as the optimal aggregation number and the size distributions of the micelles and the aggregates.[23,24] This method is quite universal: it can be applied to solutions of linear or branched polymers, solutions of low-molecular weight surfactants and various additives, mixtures of various components and structural and shape transitions. However, the limiting factor restraining the use of the SCMF theory is the computational realization of a stable code that can efficiently solve self-consistent equations. There are no standard packages with universal implementation of the SCMF theory, which could make the use of the method accessible for a large number of people like Mesodyn package[26,27] for mesoscopic modeling of phase separation dynamics or an integrated simulation system for soft materials (OCTA) for multiscale modeling.[28–30] Most of the previous works on SCMF theory[20–24] use iterative methods or external mathematical libraries, which are not optimized for a given problem and thus, computationally unstable and highly demanding in computer resources, especially in RAM memory. Thus, problems involving long molecules, large systems and geometries more than 1D confront with the limit of available computer resources and thus, making the solution of the problem without special technical skills to be a quite difficult task. A modification of the method, single chain *in* mean field calculations,[31–33] avoids the necessity to solve self-consistent equations. The direct solution of the self-consistent equations is replaced by MC equilibration of the chains in the *quasi-instantaneous* fields maintained at the most recent values and updated after a predetermined number of MC moves. In practice, the MC equilibration would slow down the calculation with respect to direct solution of the equations, but it is still much faster than the direct MC method.

It is noteworthy that the SCMF method is similar in spirit to one of the first mean field model of the phospholipid membranes by Marcelja[34,35] constructed for modeling of the fluid–gel phase transition and based on phenomenological potential of the Maier–Saupe type between the segments of the tails. The boundary between the solvent and the membrane is modeled as a planar surface with the phospholipid tails attached with a fixed grafting density. Each tail interacts with the neighbors *via* mean field which is found self-consistently.

In this work we report a computational tool providing relatively fast and stable solution of the equations of the SCMF theory in different geometries and different molecule structures. The SCMF theory is applied to model phospholipid membranes. We show that three different coarse-grained models of phospholipids can adequately describe the equilibrium properties and the molecular structure of phospholipid membranes.

The paper is organized as follows. Theoretical principles of the SCMF theory and main equations of the method are introduced in the section 2 in the most general way. This theory is then applied to the simulation of phospholipid bilayers and three coarse-grained models of phospholipid molecule are introduced in section 3. These models and the resulting equilibrium phospholipid bilayers are compared with experimental data and between each other in section 4. Last, section 5 summarizes the obtained results while the computational details which are necessary for the implementation of the method are described in the Appendix A.

2 Theory

The SCMF theory is an example of the self-consistent field (SCF) method where a single chain is described at the molecular level while the interactions between different chains are described through a mean molecular field which is found self-consistently.

The conformations of a single chain are generated with the Rosenbluth algorithm[36] or MC simulations[13,37] and the intramolecular interactions are calculated exactly using the model potential for interactions between the segments of the chain (see Appendix A.1 for details). The probabilities of individual chain conformations depend on the mean molecular fields, while the values of the fields are calculated as the average properties of individual conformations. The resulting equations for the mean fields and the probabilities of the conformations are solved self-consistently with the original method described in the Appendix A.3. The solution of these equations gives the equilibrium structures and the concentrations profiles of all components in the system as well as the most probable conformations of individual molecules. The power of this method is the speed in obtaining solutions (faster than MC and much faster than MD simulations) and the precise calculation of the energies.

This method is quite universal and can be applied for the mixture of an arbitrary number of molecules of different types interacting with each other through the mean fields. The free energy of a system containing N_1, N_2,..., N_M molecules of types 1, 2,..., M can be written as a sum of three terms, the entropy, intra- and inter-molecular terms, all written in terms of kT,

$$F = -\langle S\rangle + \langle H^{intra}\rangle + \langle H^{inter}\rangle \tag{1}$$

where the angular brackets denote the average over the probability distribution function (pdf) ρ of the system, $\langle\ldots\rangle = \int\ldots\rho\mathrm{d}\rho$. This function contains all information about the equilibrium state of the whole system. If there are no strong correlations between interacting particles, such as ion pair formation or bonds formation, we can neglect the correlations between the molecules and use the mean field approximation: the pdf ρ of many component system factorizes into the product of single molecules pdfs $\rho_\alpha(\Gamma_{\alpha i})$,

$$\rho \approx \prod_{\alpha=1}^{M}\prod_{i=1}^{N_\alpha}\rho_\alpha(\Gamma_{\alpha i}) \tag{2}$$

where $\Gamma_{\alpha i}$ is the conformation of i-th molecule of type α. Such factorization into contributions of individual molecules allows us to derive a close set of equations for $\rho_\alpha(\Gamma_{\alpha i})$.

The entropy term in the expression (1) is written as

$$\langle S\rangle = -\langle \ln \rho\Lambda\rangle \tag{3}$$

where the volume Λ has a quantum mechanics origin,

$$\Lambda = \prod_{\alpha=1}^{M} \Lambda_\alpha^{N_\alpha} N_\alpha! \approx \prod_{\alpha=1}^{M} \left(\frac{N_\alpha \Lambda_\alpha}{e} \right)^{N_\alpha} \tag{4}$$

Since the constants Λ_α do not appear in the final expressions, they can be treated as unknown normalization constants. Thus, after factorizing the pdf ρ (2), the entropy term (3) reads

$$\langle S \rangle \approx - \sum_{\alpha=1}^{M} N_\alpha \left\langle \ln \frac{\rho_\alpha N_\alpha}{e} \Lambda_\alpha \right\rangle \tag{5}$$

where the brackets on the right hand side denote the average over the single molecule pdf ρ_α. Similar arguments allow us to write the intra-molecular energy of the system as a sum of contributions of the single molecules of different types

$$\langle H^{intra} \rangle \approx \sum_{\alpha=1}^{M} N_\alpha \langle H_\alpha^{intra} \rangle \tag{6}$$

Before writing a similar expression for the inter-molecular part, we assume that molecules of each type α comprise of subunits with different chemical structure, and thus different energy parameters. Subunits can represent Kuhn segments in the chain or, in case of coarse-graining description, the groups of atoms or beads in a coarse-grained model. Thus, the interaction energy between a molecule of type α in the conformation state Γ_α and a molecule of type β in the conformation state Γ_β, can be written as a sum over the types of beads a as

$$H_{\alpha\beta}^{inter}(\Gamma_\alpha, \Gamma_\beta) = \sum_a \int u_\alpha^a(\Gamma_\alpha, \boldsymbol{r}) c_\beta^a(\Gamma_\beta, \boldsymbol{r}) d\boldsymbol{r} \tag{7}$$

In this expression $c_\beta^a(\Gamma_\beta,\boldsymbol{r})$ is the concentration of units of type a at the point $\boldsymbol{r}$ of a molecule of type β in the conformation state Γ_β. These units interact with the field $u_\alpha^a(\Gamma_\alpha,\boldsymbol{r})$ created by the molecules of type α. Thus, factorizing the pdf ρ (2) one can write the inter-molecular interaction free energy in the form

$$\langle H^{inter} \rangle \approx \frac{1}{2} \sum_{\alpha,\beta=1}^{M} N_\alpha (N_\beta - \delta_{\alpha\beta}) \sum_a \int \langle u_\alpha^a(\boldsymbol{r}) \rangle \langle c_\beta^a(\boldsymbol{r}) \rangle d\boldsymbol{r} \tag{8}$$

where $\delta_{\alpha\beta}$ is the delta symbol. Thus, the interaction free energy is represented by the interaction of the average concentration of beads with the average fields at each point.

The free energy is usually coupled with the incompressibility condition implying that the sum of the concentrations of all components in a solution is fixed. However, this condition implies the hard core repulsion between all beads in the system, and thus creates computational problems in converging the SCMF equations. To overcome this problem, we introduce the explicit incompressibility condition in every point $\boldsymbol{r}$ in the system,

$$\sum_{\alpha=1}^{M} N_\alpha \langle \phi_\alpha(\boldsymbol{r}) \rangle = \phi_0 \tag{9}$$

where $\langle \phi_\alpha(\boldsymbol{r}) \rangle$ is the average volume fraction occupied by a molecule of type α in the point $\boldsymbol{r}$, while ϕ_0 is the total volume fraction occupied by the molecules of all types.

Combining all terms (5), (6), (8) together with the incompressibility condition (9), the free energy of the system can be written as

$$\begin{aligned} F[\rho_1, \rho_2, ..., \rho_M] \approx & \sum_{\alpha=1}^{M} N_\alpha \left\langle \ln \frac{\rho_\alpha N_\alpha}{e} \Lambda_\alpha \right\rangle + \sum_{\alpha=1}^{M} N_\alpha \langle H_\alpha^{intra} \rangle + \\ & + \frac{1}{2} \sum_{\alpha,\beta=1}^{M} N_\alpha (N_\beta - \delta_{\alpha\beta}) \sum_a \int \langle u_\alpha^a(\boldsymbol{r}) \rangle \langle c_\beta^a(\boldsymbol{r}) \rangle d\boldsymbol{r} + \\ & + \int \lambda(\boldsymbol{r}) \left(\phi_0 - \sum_{\alpha=1}^{M} N_\alpha \langle \phi_\alpha(\boldsymbol{r}) \rangle \right) d\boldsymbol{r} \end{aligned} \tag{10}$$

where $\lambda(\boldsymbol{r})$ is a Lagrange multiplier and all the averages are taken over the single-molecule pdfs ρ_α. Minimization of this functional with respect to ρ_α gives the pdf of a single molecule of type α

$$\rho_\alpha(\Gamma_\alpha) = \frac{1}{Z_\alpha} \exp \left(- H_\alpha^{intra}(\Gamma_\alpha) - \sum_{\beta=1}^{M} (N_\beta - \delta_{\alpha\beta}) \times \right.$$

$$\left. \sum_a \int u_\alpha^a(\Gamma_\alpha, \boldsymbol{r}) \langle c_\beta^a(\boldsymbol{r}) \rangle d\boldsymbol{r} + \int \lambda(\boldsymbol{r}) \phi_\alpha(\Gamma_\alpha, \boldsymbol{r}) d\boldsymbol{r} \right) \tag{11}$$

where Z_α is a normalization constant which is found from the normalization condition $\int \rho_\alpha(\Gamma_\alpha) d\Gamma_\alpha = 1$. This constant has a meaning of a partition function of the system at equilibrium and $-\ln Z_a$ is the total free energy of the system at equilibrium.

Once the average concentrations $\langle c_\beta^a(\boldsymbol{r}) \rangle$ and the volume fractions $\langle \phi_\alpha(\boldsymbol{r}) \rangle$ are known, this expression allows to calculate the probabilities of each conformation $\rho_\alpha(\Gamma_\alpha)$ for all molecules in the system. In turn, if the probabilities $\rho_\alpha(\Gamma_\alpha)$ are known, the average concentrations and volume fractions, being the molecular fields in this problem are found from the self-consistency conditions,

$$\begin{aligned} \langle c_\alpha^a(\boldsymbol{r}) \rangle &= \int c_\alpha^a(\Gamma_\alpha, \boldsymbol{r}) \rho_\alpha(\Gamma_\alpha) d\Gamma_\alpha \\ \langle \phi_\alpha(\boldsymbol{r}) \rangle &= \int \phi_\alpha(\Gamma_\alpha, \boldsymbol{r}) \rho_\alpha(\Gamma_\alpha) d\Gamma_\alpha, \end{aligned} \tag{12}$$

representing the averages over the probabilities of conformations.

The probability of each conformation can be written as $\rho_\alpha(\Gamma_\alpha) = \frac{1}{Z_\alpha} \exp[-H_{eff}(\Gamma_\alpha)]$, where $H_{eff}(\Gamma_\alpha)$ is the effective Hamiltonian given by (11), which describes the system at equilibrium. The last term in the effective Hamiltonian corresponds to the steric repulsion of beads of all types. If one of the components is a one bead solvent, the only degree of freedom of the solvent molecules is the position in space, $\boldsymbol{r}$. Hence, the volume fraction of the solvent, can be found from the incompressibility condition (9)

$$\phi_s(\boldsymbol{r}) = \phi_0 - \sum_{\alpha=1, \alpha \neq s}^{M} N_\alpha \langle \phi_\alpha(\boldsymbol{r}) \rangle \tag{13}$$

In addition, the Lagrange multiplier $\lambda(\boldsymbol{r})$ can be expressed through the concentration of the solvent. The pdf of the solvent $\rho_s(\boldsymbol{r})$, the concentration $c_s(\boldsymbol{r})$ and the volume fraction occupied by the solvent $\phi_s(\boldsymbol{r})$ are related *via* the following expressions

$$\rho_s(\boldsymbol{r}) = \frac{c_s(\boldsymbol{r})}{N_s} = \frac{\phi_s(\boldsymbol{r})}{v_s N_s} \tag{14}$$

where N_s is the number and v_s is the volume of the solvent molecule, while the molecular field

$$\phi_s(\mathbf{r},\mathbf{r}') \approx v_s\delta(\mathbf{r}-\mathbf{r}') \quad (15)$$

where $\delta(\mathbf{r}-\mathbf{r}')$ is the Dirac delta-function. Substitution of (14) and (15) into (11) gives the approximate expression for the Lagrange multiplier $\lambda(\mathbf{r})$

$$v_s\lambda(\mathbf{r}) \approx \ln\phi_s(\mathbf{r}) + \sum_{\beta=1}^{M}(N_\beta - \delta_{s\beta})\sum_a \int u_s^a(\mathbf{r},\mathbf{r}')\langle c_\beta^a(\mathbf{r}')\rangle d\mathbf{r}' \quad (16)$$

where we have assumed that $H_s^{intra}(\mathbf{r}) = 0$ and omitted few constants, which will cancel out by the normalization of ρ_α.

It is noteworthy, that in our equations the fields $\langle\phi_\alpha(\mathbf{r})\rangle$ and $\langle c_\alpha^a(\mathbf{r})\rangle$ formally are not related although they both correspond to the concentration of monomers. They are indeed related through the volume of the monomers only if the molecules are composed of *non-overlapping* beads, when the distance between the centers is larger than the the diameter. However, if we want to conserve the possibility of describing the overlapping beads, the coefficient of proportionality between $\langle\phi_\alpha(\mathbf{r})\rangle$ and $\langle c_\alpha{}^a(\mathbf{r})\rangle$ is not known *a priori* and we keep them as independent variables.

The eqn (11),(12),(13) and (16) form a closed set of non-linear equations of the SCMF theory. The solution of these equations gives the equilibrium structures, the self-consistent molecular fields such as the concentration profiles of the beads of each type and the distribution of the solvent, and the probabilities of each conformation of the molecules in the fields and the accurate measure of equilibrium free energies. The implementation of the computational method as well as the technical details related to the solution of the equations are present in Appendix A.

3 Application to phospholipid membranes

The method of the SCMF theory described so far is applied to model the equilibrium structures and properties of phospholipid membranes. The SCMF theory can provide the detailed information on the microscopic structure of the phospholipid layer such as concentration profiles of all groups of atoms of the phospholipid molecule, the thickness of the membrane, the average area per phospholipid head group and the mechanical properties such as compressibility of the membrane and the surface tension. All these parameters can be measured in the experiment[38–40] and thus, allowing the direct comparison with experimental data.

We have developed the C++ code which runs in parallel using OpenMP shared memory platform on the 32-core AMD machines (see Appendix A.3). To simulate a flat phospholipid layer we use one dimensional geometry and discretize the space into parallel cells with the same value of the average fields. The periodic boundary condition is applied together with the assumption of the symmetry of the layer with respect to the central plane.

Despite the complexity of the structure of the phospholipid membranes, the driving force for the self-assembly of phospholipids into bilayers is the amphiphile nature of phospholipids. That is why, we only consider the units of two types, hydrophilic, H, and hydrophobic, T. The units of both types interacts with each other through the square well potentials. We assume that all units, T and H, and the solvent molecules S, have the same size and the same interaction range, while the interaction energies are different. We consider three types of interactions, interactions between hydrophobic units, T-T, interactions between hydrophobic units and solvent, T-S and hydrophilic units with solvent, H–S. In the following we will show that such assumptions are justified for quantitative study of phospholipid layers and, in principle, cohere with approximations used in successful models of phospholipid membranes (see *e.g.* ref. 19). However, if necessary, more types of beads and more complicated potentials can be implemented.

The chemical structure of the DMPC molecule is depicted in Fig. 1a. We present three models of DMPC phospholipid molecule at a different level of coarse-graining.The first, most detailed model, represents the DMPC phospholipid as a two tails molecule of 44 beads (Fig. 1b). A carbon group CH_2 of the molecule is assigned to one T bead. A phosphate group, PO_4, is represented by 5 H overlapping beads, placed at the vertexes and center of a tetrahedron. The choline group NC_4H_{11} is represented in a similar way: one H bead in the center of a tetrahedron is surrounded by 4 T beads placed in the corners. The COO groups are represented by 2 H beads. The angles between most of the bonds are fixed at value 120°. The torsion angles the sequence of groups CH_2–CH_2–CH_2 are allowed to have only three fixed values, 0°, 120° and 240°, which corresponds to *cis*- and *trans*-conformations of the groups. The parameters of the model (Table 1) were adjusted with a series of fast simulations (conformational sampling size ~30–100 thousands and 40 layers in the simulation box) while the accurate data were obtained with several millions of conformations and hundred layers in the box.

Two other, more coarse-grained and less detailed, models are depicted in Fig. 1c and 1d. One of them represents two tails phospholipid with 10 beads and another is simply 3-beads freely joined together. In contrast to the 44-beads model, the conformational space of these models is much more restricted and we need less sampling to produce accurate results. Thus, the simplest 3-beads model is the fastest, and least demanding on computer resources, phospholipid model which can simulate the

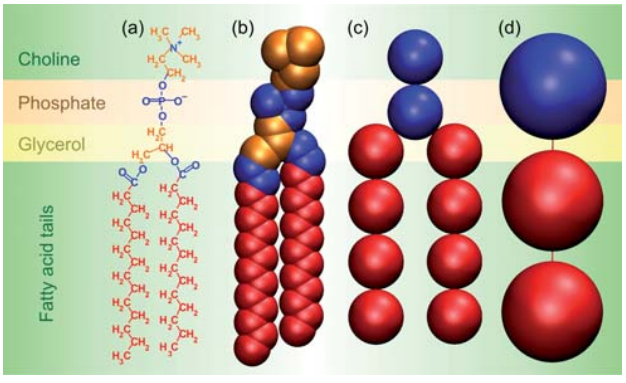

Fig. 1 (a) Chemical structure of the DMPC phospholipid molecule. 44-beads (b), 10-beads (c) and 3-beads (d) models of phospholipid molecules used in the present calculations. Blue beads correspond to hydrophilic monomers, red beads correspond to hydrocarbon monomers in the tails and orange beads correspond to hydrophobic monomers in the heads. The interaction parameters of red and orange beads are the same.

Table 1 Parameters used for the simulation of phospholipid bilayer for three models of DMPC phospholipid molecule

	44B	10B	3B
Units radius/Å	1.90	2.50	4.05
Interaction range/Å	5.70	7.50	12.15
T-T contact energy (kT)	−0.40	−1.50	−2.10
T-S contact energy (kT)	0.00	0.00	0.00
H–S contact energy (kT)	−0.10	−0.20	−0.15
Bond length/Å	1.5	5.0	10.0
Occupied volume fraction ϕ_0	0.700	0.675	0.675
Sampling (number of configurations)	3×10^6	10^6	10^6
Simulation box size/Å	$120.0 \times 120.0 \times 62.7$		

self-assembly of phospholipids into the bilayers with realistic properties of DMPC phospholipid membranes.

It is important to note, that we simulate a finite size box with the fixed volume V and the fixed number of phospholipid molecules N_l with the free energy F given by the expression (10). However, we can extrapolate our data to much larger system with larger number of phospholipids N_l^* and larger number of solvent molecules. The description of a larger system is possible, if we do not take into account any energy contributions related to the perpendicular undulations and bending of the membrane. In this case the simulation box represent a self-similar part of a larger system. The free energy of the larger system F^* is in a simple relation with the free energy per lipid f

$$F^* \approx const + N_l^* f \tag{17}$$

which, in turn, is related to the free energy of the simulation box minus the entropy of the solvent

$$fN_l = F - V\frac{\phi_0}{v_s}\ln\frac{\phi_0}{v_s} \tag{18}$$

where ϕ_0/v_s is the concentration of the pure solvent.

Thus, the calculation of free energy of the box F with different number of molecules in the simulation box gives the free energy of the membrane per lipid f. The minimum of the free energy per lipid f corresponds to the equilibrium density of the membrane, thus the second derivative of this energy with respect to the area per lipid in the minimum gives the compressibility modulus of the layer

$$K = 2A_{eq}f''(A_{eq}) \tag{19}$$

representing a measure of the rigidity of the membrane.

4 Results and discussion

The numerical implementation of the method in the form of two structurally independent modules: the generation of a single molecule conformations and the solution of equations (see Appendix A), permits us to consider several models of the molecule at the same time. Thus, we can compare our three models of phospholipids and test their performance in reproducing the thermodynamic properties of phospholipid membranes.

The most detailed 44-beads model (Fig. 1b) results in equilibrium structures of membranes where the phospholipids are assembled into flat bilayers in fluid phase. Since the output of the method is the probabilities of each molecular conformation in the self-consistent fields, the most probable conformations may be used for the visualization of the resulting structures which correspond to the solutions of the equations. Typical mean field "snapshots" of the equilibrium bilayer structures obtained with the 44-beads model are present at Fig. 2. Although the picture visually resembles instant snapshots of MC simulations, this is not a representation of interacting molecules at a given moment of time, but these are the most probable conformations of a single chain in the fields corresponding to the equilibrium

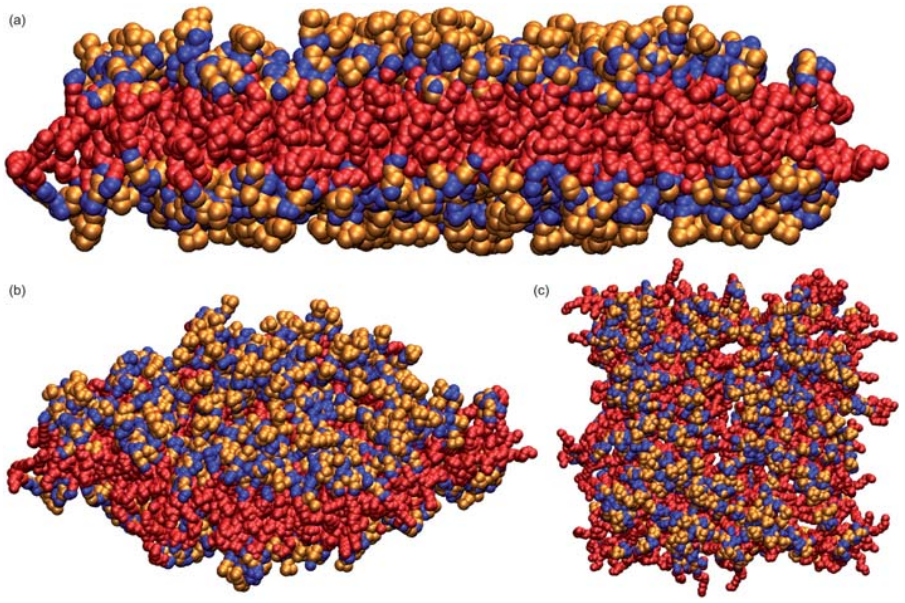

Fig. 2 Typical mean field "snapshots" (set of most-probable conformations of the lipids) of the phospholipid membrane within the 44-beads model.

solution. Such "snapshots" are helpful for visualization purposes in order to distinguish between different molecular structures.

The equations of the SCMF theory may result in several sets of solutions corresponding to various equilibrium and even metastable structures. To this end, the numerical method is implemented in such a way that simultaneously several solutions corresponding to local and global minima of the free energy can be found. The obtained solutions can then be ranged by their free energy or by the concentration profile. Even in the restricted 1D geometry of flat phospholipid bilayers with periodic boundary condition the method finds several self-assembled structures: homogeneous solution of lipids, one single layer, formed either at the center or at the edge of the box and two or even three layers in the box. Each structure has its own free energy which allows to determine the equilibrium properties.

The detailed microscopic information concerning the mechanic and thermodynamic properties of the simulated flat bilayers can be compared directly against the experimental data for phospholipid bilayers.[38–40] Thermodynamic properties of the membranes obtained from the measurements are the thickness of the membrane (determined as a distance between the midpoints of the outer slopes of the H beads concentration profiles), the full thickness of the bilayer region (determined as a thickness of the region where the total concentration of the lipid molecules is larger than zero), the thickness of the hydrophobic core (measured as a distance between the midpoints of the slopes of the T beads concentration profiles), the distances between different groups of the phospholipid molecule, membrane rigidity measured by the compressibility modulus and the interfacial area per lipid molecule. Thus, the coarse-grained parameters of each model of phospholipid molecule are chosen in such a way that all these microscopic properties correspond to the experimental values of the DMPC phospholipid bilayers. The parameters of these three models are summarized in Table 1.

The most detailed 44-beads model provides all information about the composition of the membrane as well as the position of different groups of the molecule in the bilayer. The concentration profile of the bilayer at equilibrium is shown in Fig. 3. The profiles are normalized to unity by division by the occupied volume fraction ϕ_0. One can see, that the terminal groups of the lipid tails are situated in the center of the layer, which is surrounded by the area filled with other carbon groups of the tails. The groups of hydrophilic units representing the "heads" are in the surface layer. Such position of the groups is in agreement with the experimental data for such system.[39] It is noteworthy, that the concentration profile of choline group has two peaks reflecting the position of phospholipid heads in the layer: approximately half of the heads are oriented perpendicular to the layer plane, while the other half is parallel to the layer plane. This is the outcome of the model of the phospholipid molecule and the parametrization of the interactions. This can certainly be improved once the reliable experimental data or results of MD simulations concerning the equilibrium position of the heads in the layer is available.

One of the advantages of the SCMF method is the accurate measurements of the free energies of equilibrium structures. In our model this corresponds to the free energy of formation of flat phospholipid layer. It does not include the entropy of thermal undulations in the perpendicular direction. In particular, undulations may result in the broadening of the phospholipid membrane. However, they become important on the scales much larger than the size of the simulation box and, in principle, can be included as an additional contribution to the free energy of the layer.

The rigidity of the membrane can be obtained from the free energy of the bilayer. Changing the number of lipids in the box, we get the free energy per lipid molecule f as a function of the interfacial area per lipid A (Fig. 4). Although the error bars are quite large because of the large conformational space with respect to the sampling used for the calculations, the energy points can be quite good approximated with the polynomial of the second order. This curve allows us to calculate the compressibility of the layer with respect to compression and stretching in the lateral direction. The second derivative is related to the compressibility modulus defined in eqn (19). The resulting compressibility modulus, the thickness of the membrane, positions of various groups and the area per lipid are shown in

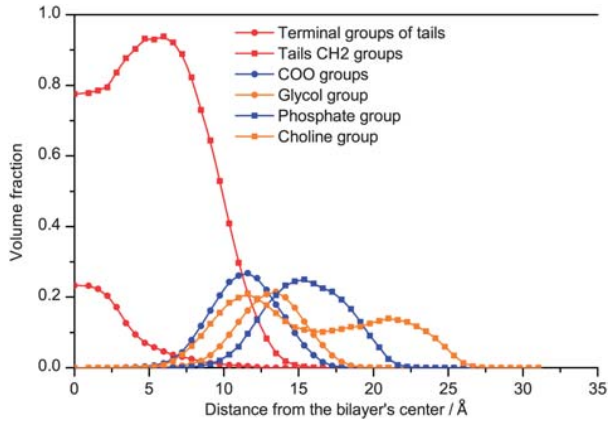

Fig. 3 Detailed equilibrium concentration profile of the phospholipid bilayer obtained with the 44-beads model.

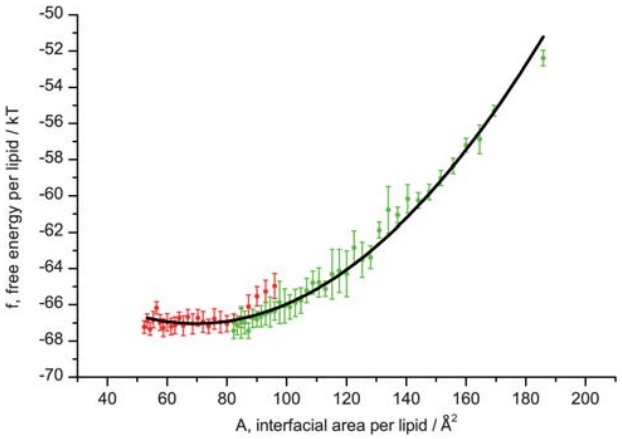

Fig. 4 Free energy per lipid f *vs.* interfacial area per lipid A for the 44-beads lipid model, calculated from solutions with one (red points) and two (green points) bilayers in the simulation box. Parameters of the fitting curve $y = a_0 + a_1x + a_2x^2$ are $a_0 = -61.3 \pm 0.5$, $a_1 = -0.164 \pm 0.010$, $a_2 = (1.17 \pm 0.04) \times 10^{-3}$.

Table 2 Comparison of the equilibrium properties of phospholipid bilayer obtained with three lipid models with experimental data and full atomistic MD simulations of the DMPC lipid bilayer

	44B	10B	3B	DMPC
Membrane thickness/Å	35	36	45	44.2[a]
Full thickness of the bilayer region/Å	51	44	56	53[b]
Thickness of hydrophobic core/Å	24	24	28	26.2[a]
Distance between heads/Å	30	28	36	36[a]
Distance between phosphate groups/Å	30	—	—	32[b]
Distance between choline groups (1st peak) (Å)	22	—	—	37[b,d]
Distance between choline groups (2nd peak) (Å)	42	—	—	37[b,d]
Distance between glycol groups/Å	26	—	—	27[b]
Distance between COO groups/Å	24	—	—	25[b]
Thickness of terminal groups region/Å	6	—	—	10[b]
Interfacial area per lipid/Å^2	70 ± 5	65 ± 11	60 ± 2	59.6[a]
Compress. constant (dyn/cm)	135 ± 11	560 ± 120	269 ± 11	257[c]

[a] Experimental data by Nagle and Tristram-Nagle[39] [b] Calculated from MD simulations data by Damodaran and Merz[6] [c] Experimental data by Mathai *et al.*[40] [d] Average distance between choline groups.

Table 2. The obtained values agree quite well with the experimental data. However, if better agreement is needed, the parameters of the models can be tuned by the additional series of run of calculations with a large number of conformations in the sampling.

The free energy per lipid f (Fig. 4) has a minimum at $A \approx 60$ Å^2, which corresponds to the experimental value of the interfacial area per lipid in the bilayer in the fluid phase. However, the values of A below 50 Å^2 cannot be obtained with the same set of parameters, because this range corresponds to dense packing in the core of the layer. Further decrease of interfacial area per lipid is accompanied with structural rearrangements of the phospholipid environment and strong correlations between the neighboring molecules. These correlations induce phase transitions in lipid membranes,[41] the main transition to the gel phase occurs at $A \approx 40$ Å^2. However, such correlations are well beyond the limit of validity of the mean field theory, where the movements of individual molecules are supposed to be uncorrelated (2).

Similar calculations carried out for the 10-beads model show better reproducibility due to considerably reduced conformational space. In fact, 1 million of conformations is enough for calculations with different sampling to almost coincide in one curve with very small error bars (Fig. 5). The absolute values of the free energy f are shifted with respect to that of the 44-units model, which is the consequence of different sizes of the units and the interactions parameters. However, the energy differences, the density profiles and the compressibility modulus are very close to that obtained with the previous model (Table 2). It is interesting to compare the energies of one and two layers in the box, red and green curves in Fig. 5, correspondingly. The energies are quite similar at low densities of the layer and diverge significantly at high densities. This is consequence of the compression of the two layers due to lack of space in the box for two layers of equilibrium size. The energy per lipid corresponding to the maximal compression of two layers in the box coincides with the energy of a compressed layer. This fact reflects the consistency of our

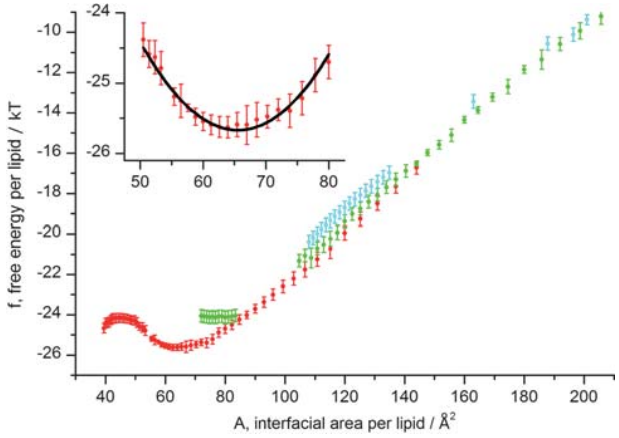

Fig. 5 Free energy per lipid f *vs.* interfacial area per lipid A for the 10-beads lipid model, calculated from solutions with one (red points), two (green points) and three (blue points) bilayers in the simulation box. The inset represents the enlarged region of the minimum. Parameters of the fitting curve $y = a_0 + a_1x + a_2x^2$ are $a_0 = -3.0 \pm 3.0$, $a_1 = -0.68 \pm 0.08$, $a_2 = (5.2 \pm 0.6) \times 10^{-3}$.

picture. On the other hand, high compression of a single layer, A below 50 Å^2, results in gradual splitting of the layer in two with smooth rearrangement of the lipid molecules. Some phospholipids flip and orient their "heads" in the center of the membrane. Thus, a single bilayer smoothly become broader and change its appearance to remind something between a single bilayer with a layer of heads in the center and two tightly compressed bilayers. This process is reflected in the flat part of the energy per lipid curve for A below 50 Å^2, where the distinction between one layer and two layers in the box can hardly be done.

The energy curve for the 3-beads model is presented in Fig. 6. This is the simplest phospholipid model with only 3 beads, thus the conformational space is very limited and the results obtained with the sampling of 1 million of conformations represented here

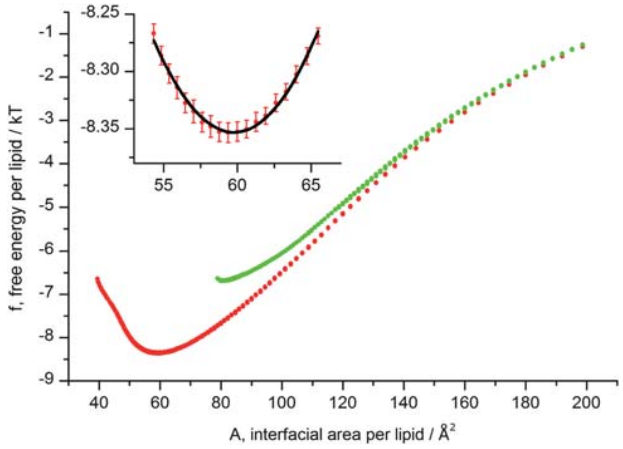

Fig. 6 Free energy per lipid *f vs.* interfacial area per lipid *A* for the 3-beads lipid model, calculated from solutions with one (red points) and two (green points) bilayers in the simulation box. The inset represents the enlarged region of the minimum. Parameters of the fitting curve $y = a_0 + a_1x + a_2x^2$ are $a_0 = -1.4 \pm 0.2$, $a_1 = -0.325 \pm 0.008$, $a_2 = (2.72 \pm 0.06) \times 10^{-3}$.

are close to these obtained with small sampling about 100–300 thousands. The difference between the energies of one and two layers in the box, noted for the 10-beads model, is even more pronounced.

The mean field "snapshots" of the most probable conformations of the layer in equilibrium and the corresponding density profiles for three models are presented in Fig. 7. It shows how the coarse-graining and the decreasing of the model details influence the layer appearance. However, despite obvious differences in details caused by the differences in the molecule structures, the profiles looks quite similar, especially for the most coarse-grained 10- and 3-beads models. In case of the 44-units model, there is a small fraction of the hydrophobic T units at the surface, reflecting the structure of the phospholipid with some hydrophobic T groups in the head. Furthermore, different aspect ratio between T and H units in the models (4 : 1 in 10-beads and 2 : 1 in the 3-beads model) lead to the corresponding difference in the relative density of T and H units. This correspondence is not valid for the 44-beads model, where the beads do overlap and some parts of the molecule are hidden from the solvent. The ratio between the areas under the T and H curves is 4.7 : 1 which is different from the ratio between numbers of T and H beads in the molecule (3.4 : 1).

Finally a few words should be said about the speed performance of the three models. We ran six series of calculations with different conformational sampling of 1–3 millions of conformations. The box is divided in ~100 parallel layers and the number of lipids in the box is varying from 300 to 700 with the step 10. The program runs in parallel on 32-cores AMD machine with 128Gb of RAM. The most time consuming process is the solution of equations while the generation of the sampling at the beginning of calculation is relatively fast and almost does not affect the speed of calculation. In turn, the solution of the equations depends on the number of conformations in the sampling, the number of cells and the number of attempts to solve equations with different initial conditions. Since three models differ in the number of beads, implying different conformational space, the same accuracy of calculations in different models is achieved with different number of conformations in the sampling. The 44-beads model require several

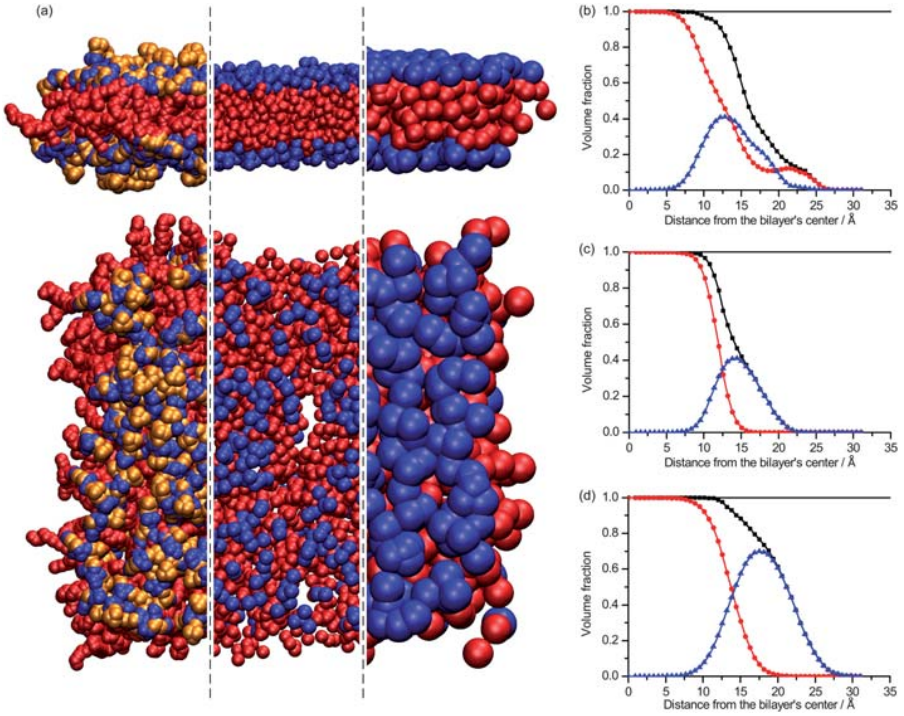

Fig. 7 Mean field equilibrium "snapshots" (set of most-probable conformations of the lipids) and the concentration profiles of tails (T, red lines), heads (H, blue lines) and the phospholipids (T + H, black lines) obtained with 44-, 10- and 3-beads models.

millions of conformations and 48 h of calculations, the 10-beads model require one million of conformations and 17 h, while the 3-beads model can get reliable results with a hundred thousands of conformations in a few hours. Thus, the simplest 3-beads model is the fastest model which can reproduce the essential equilibrium properties of the phospholipid bilayer.

5 Conclusions

In this work we report a computational tool providing relatively fast and stable solution of the equations of the SCMF theory in different geometries and different molecule structures. The SCMF theory is applied for the first time to model the DMPC phospholipid membranes with realistic thermodynamic properties. We show that all three coarse-grained models of phospholipids with the present parameters can adequately describe the equilibrium properties and the molecular structure of DMPC phospholipid bilayers in fluid phase. Among the essential properties of the phospholipid bilayers that correspond to the experimental data are the thickness of the membrane, the positions of different groups of the lipid in the bilayer, the compressibility of the membrane and the equilibrium interfacial area per lipid. The most detailed 44-beads model can reproduce the structure of the phospholipid layer with maximum details. The resulting density profiles of the groups of the phospholipid molecule can be used for the structural modeling in experimental techniques that require the molecular structure of the layer.

However, if one is interested in the average properties of the lipid bilayer, the simplest 3-beads model can be used to model the thermodynamics and the essential properties of self-assembled phospholipid bilayers. This model is faster and computationally more attractive than 44- and 10-beads models. Furthermore, we suggest that the 3-beads model with the parameters found in this work is used for simulation of more complex bilayer structures.

Appendix A Computational details

Here we discuss the implementation details of the algorithm underlying the computational realization of the SCMF theory. The off-lattice realization of the program allows for conformations of the molecules in a real space. The algorithm consist of three independent parts: the generation of the sampling of conformations of molecules of any structure, the discretization of space according to the geometry of the problem and the solution of the SCMF eqn (12). The independence of the parts insures the universality of the method which can be applied for molecules of any structure and their self-assembly in objects of any geometry.

A.1 Conformational sampling generation

First step is the generation of a representative set of conformations of a single molecule. This can be done with different techniques, including bead-to-bead chain growth or MC simulations. The conformations of a single molecule are generated once before solving the equations. They are stored in the RAM memory and not changed during the solution of equations, while the probabilities of each conformation are recalculated with the fields. This static memory allows for highly efficient parallelization of the program within the shared memory OpenMP platform, since the processors communicate very little between each other. The generation of conformations in the sampling is realized as follows:

1. Generation of a new conformation Γ_α of the molecule of type α with random position of the first bead inside the box. We set initial values of the conformation statistical weight $w_\alpha(\Gamma_\alpha) = 1$ and the intramolecular energy $H_\alpha{}^{intra}(\Gamma_\alpha) = 0$.

2. Iterative addition of new beads to the growing molecule and joining them one by one subject to self-avoidance condition. Depending on the final objective, one can use:

(a) Self-avoiding growth with the MC equilibration. The chain is generated as a self-avoiding off-lattice walk and the energy of interaction of the newly joined beads with the rest of the chain is accumulated in $H_\alpha{}^{intra}(\Gamma_\alpha)$. The resulting chain is then equilibrated with MC crankshaft moves and reptations until the full equilibration of the configuration. In this case all conformations have the same statistical weight and $w_\alpha(\Gamma_\alpha) = 1$.

(b) Rosenbluth chain growth.[36] A new bead is placed at a fixed distance from the previous bead either at random angle (freely joined chain) or with additional restrictions on the angles between the beads (chain with angle restrictions). Rosenbluth algorithm generates conformations with biased probability distribution. This bias is then calculated in the conformation weight and removed when the probabilities of each conformation are calculated. In order to calculate the Rosenbluth weight, one should try N_{trial} times to place the new bead at a fixed distance from the previous bead and calculate the number $N_{allowed}$ of successful positions, allowed by self-avoidance condition. If $N_{allowed} > 0$, a new position is accepted with the weight $1/N_{allowed}$, the energy of interaction is accumulated in $H_\alpha{}^{intra}(\Gamma_\alpha)$ and the weight of the conformation $w_\alpha(\Gamma_\alpha)$ is multiplied by the factor $1/N_{allowed}$. If there is no possibility to place the bead, $N_{allowed} = 0$, the generation restarts from the beginning. The Rosenbluth algorithm is simple and efficient enough for generation of phospholipid molecules.

A.2 Discretization of space

Since the solution of equations of the SCMF theory in the integral form (12), (14) is not practical, the equations are simplified by the replacement of the integrals with the sums. The space is discretized according to the geometry of the system and the symmetry considerations. The integrals over the spatial coordinates, $d\boldsymbol{r}$, are replaced by the sums over auxiliary cells i with the same values of the mean fields: $\langle c^a_\beta(\boldsymbol{r})\rangle = c^a_{\beta i}$ and $\lambda(\boldsymbol{r}) = \lambda_i$. The discretization leads to the following approximate relations

$$\begin{aligned} \int \iota^a_\alpha(\Gamma_\alpha, \boldsymbol{r})\langle c^a_\beta(\boldsymbol{r})\rangle d\boldsymbol{r} &\approx \sum_i c^a_{\beta i} \int_i \iota^a_\alpha(\Gamma_\alpha, \boldsymbol{r}) d\boldsymbol{r} \\ \int \lambda(\boldsymbol{r})\phi_\alpha(\Gamma_\alpha, \boldsymbol{r}) d\boldsymbol{r} &\approx \sum_i \lambda_i \int_i \phi_\alpha(\Gamma_\alpha, \boldsymbol{r}) d\boldsymbol{r} \end{aligned} \tag{20}$$

where $\sum_i$ denotes the sum over all auxiliary cells, while $\int_i$ is the integral over the i-th cell. Because of the structure of the equations, the integral over the single i-th cell can be evaluated once in the beginning of calculations, while the sums (20) are calculated during the solution of the equations. Although the number and the geometry of the cells can be arbitrary, their choice will restrict the geometry and the resolution of the resulting solutions. Thus, it is important to choose them accurately for a particular

problem. In case of flat bilayers we choose a planar geometry with the cells parallel to the layer, thus we can only obtain the solutions that can lie in the layer.

The integrals over the conformational space of single molecules are replaced by the sums over the finite samplings generated in the first step

$$\begin{aligned}\phi_{\alpha i} &= \sum_{\Gamma_\alpha} \phi_{\alpha i}(\Gamma_\alpha)\rho_\alpha(\Gamma_\alpha),\\ c^a_{\alpha i} &= \sum_{\Gamma_\alpha} c^a_{\alpha i}(\Gamma_\alpha)\rho_\alpha(\Gamma_\alpha)\end{aligned} \tag{21}$$

where the mean field volume fraction $\phi_{\alpha i}$ and the mean field concentration $c_{\alpha i}{}^a$ of a-beads of the molecule of type α in the cell i are related to the corresponding volume fraction $\phi_{\alpha i}(\Gamma_\alpha)$ and the concentration $c_{\alpha i}{}^a(\Gamma_\alpha)$ of the conformation Γ_α.

The integral expression (11) for the $\rho_\alpha(\Gamma_\alpha)$ yields in form

$$\rho_\alpha(\Gamma_\alpha) = \frac{1}{Z_\alpha w_\alpha(\Gamma_\alpha)} \exp\Bigg(- H^{intra}_\alpha(\Gamma_\alpha) - \sum_{\beta=1}^{M} \left(N_\beta - \delta_{\alpha\beta}\right) \times \sum_{ai} \varepsilon^a_{\alpha i}(\Gamma_\alpha) c^a_{\beta i} + \sum_i \lambda_i v_{\alpha i}(\Gamma_\alpha)\Bigg) \tag{22}$$

where $w_\alpha(\Gamma_\alpha)$ is the Rosenbluth weight calculated during the generation of the chains, and the constant Z_α insures the normalization of the probability $\sum_{\Gamma\alpha}\rho_\alpha(\Gamma_\alpha) = 1$.

The expression for probabilities (22) is accompanied with the following relations

$$v_s\lambda_i \approx \ln\phi_{si} + \sum_{\beta=1}^{M}\left(N_\beta - \delta_{s\beta}\right)\sum_a \varepsilon^a_{si} c^a_{\beta i},$$

$$\phi_{si} = \phi_0 - \sum_{\alpha=1,\alpha\neq s}^{M} N_\alpha \phi_{\alpha i}$$

$$\varepsilon^a_{\alpha i}(\Gamma_\alpha) = \int_i u^a_\alpha(\Gamma_\alpha, \boldsymbol{r}) d\boldsymbol{r},$$

$$v_{\alpha i}(\Gamma_\alpha) = V_i \phi_{\alpha i}(\Gamma_\alpha) = \int_i \phi_\alpha(\Gamma_\alpha, \boldsymbol{r}) d\boldsymbol{r} \tag{23}$$

The quantities $v_{\alpha i}(\Gamma_\alpha)$, $\varepsilon_{\alpha i}{}^a(\Gamma_\alpha)$ and $c_{\alpha i}{}^a(\Gamma_\alpha)$ are calculated using the MC integration technique. The volumes $v_{\alpha i}(\Gamma_\alpha)$ are calculated as follows: one throws randomly N_{trials} points inside the volume occupied by the bead and determine the cell where each of these points hits. Each point contributes to the volume in the cell with the value $v_a/(N_{trials}N_{int})$, where N_{int} is the number of the beads hit by the point and v_a is the volume of the bead. The volume fractions $\phi_{\alpha i}(\Gamma_\alpha)$ are related to the volumes $v_{\alpha i}(\Gamma_\alpha)$ as $\phi_{\alpha i}(\Gamma_\alpha) = v_{\alpha i}(\Gamma_\alpha)/V_i$, where V_i is the volume of the i-th auxiliary cell. The concentrations $c_{\alpha i}{}^a(\Gamma_\alpha)$ are calculated similarly, except that each random point contributes to $c_{\alpha i}{}^a(\Gamma_\alpha)$ with the value $1/N_{trials}$. The interaction energies $\varepsilon_{\alpha i}{}^a(\Gamma_\alpha)$ are calculated with the help of the N_{trials} points thrown for every a at a distance r from the center of the bead b such that $r_{min} < r < r_{max}$, where r_{min} is the minimum distance at which the bead of type a can approach to the b bead, and r_{max} is the maximum distance at which the interaction potential acting between a and b beads is non-zero. If the bead of type a in the position of the trial point does not have any intersection with the beads of the chain, its contribution to the $\varepsilon_{\alpha i}{}^a(\Gamma_\alpha)$ is $4/3\,\pi(r^3_{max} - r^3_{min})U^{ab}(r)/N_{trials}$, where i is the number of the auxiliary cell where the trial point hits, and $U^{ab}(r)$ is the pair potential acting between the beads of types a and b. Since the solvent is implicit in our model, the quantities $\varepsilon_{si}{}^a$ describing the interaction between the solvent and the bead of type a have to be treated separately. We evaluate them by a simple approximate expression

$$\varepsilon^a_{si} \approx 4/3\,\pi(r^3_{sa} - (r_s + r_a)^3)\varepsilon_{sa} \tag{24}$$

where we assume the square well potentials between the solvent molecules s and the beads a with energy ε_{sa} at the distance closer than r_{sa}. Here the radius of solvent is r_s and the radius of the a bead is r_a.

It is noteworthy that the incorporation of the Rosenbluth weight $w_\alpha(\Gamma_\alpha)$ into the expression for probabilities (22) may lead to confusion. Although most of the averages can be calculated with the expressions similar to (21), the averages of expressions containing explicitly the probability ρ_α should be treated separately. For example, the entropy term in the free energy (10) leads to the additional term when we replace the integral with the sum

$$N_\alpha\left\langle \ln\frac{\rho_\alpha N_\alpha}{e}\Lambda_\alpha\right\rangle = N_\alpha\sum_{\Gamma_\alpha}\rho_\alpha(\Gamma_\alpha)\ln\frac{\rho_\alpha(\Gamma_\alpha)N_\alpha}{e}\Lambda_\alpha + N_\alpha\sum_{\Gamma_\alpha}\rho_\alpha(\Gamma_\alpha)\ln w_\alpha(\Gamma_\alpha)\varkappa_\alpha \tag{25}$$

where κ_α is the number of conformations in the sampling of the molecule of type α.

The expressions (12), (22) and (23) form a closed set of algebraical equations with respect to variables $\phi_{\alpha i}$ and $c^a_{\alpha i}$ which can be solved numerically. We must admit however, that the solution of these non-linear equations is not a straightforward task.

A.3 Numerical implemetation

In this work we have implemented the SCMF theory in C++. The program is based on Newton–Raphson technique which provides the efficient and stable solution of the SCMF equations. It has a modular structure which makes it very flexible for modification, further development and extension for new applications.

The first module is the sampling generator, which generates the molecules conformations and calculates the volumes and interactions according to the Appendix A.1. The code for generation of molecules with different structures can be added to this module or changed independently from other parts of the program.

The second module specify the geometry of the problem: 1D spherical, 1D planar, 2D planar, 2D cylindrical, or 3D cubic. It contains the description of the geometry and divide the simulation box into set of auxiliary cells. The modification of this part of code provides an easy way to implement different types of the system geometry. It is worth noting here one technical improvement that significantly increase the performance of the calculations. Since the molecules have small size compared to the size of the box, their contribution to most of the auxiliary cells is zero, thus matrices $\varepsilon^a_{\alpha i}(\Gamma_\alpha)$, $c^a_{\alpha i}(\Gamma_\alpha)$ and $v_{\alpha i}(\Gamma_\alpha)$ have many zero values. In this second module of the program the simple compression of these data is realized *via* elimination of zeros

from these matrices. This helps to save computer memory and, on the next step, speed up the calculations by elimination of the sums over the cells containing zeros.

The core of the third module is the modified Newton–Raphson solver for the solution of SCMF equations. It involves the iterative solver which calculates on each step the matrix of analytical derivatives of eqn (21) with respect to unknown variables along with the analytical expressions including the sums over the conformational sampling. The next approximation of the solution is determined by the inversion of this matrix until the required accuracy is reached. To avoid occasional instability of the Newton–Raphson scheme, the algorithm artificially restrains too big steps which may drop the next approximation outside a reasonable range. The algorithm is able to find several solutions simultaneously by repeating the calculations several times with different initial conditions.

Acknowledgements

The authors are grateful to Josep Bonet and Allan Mackie for introduction into the method SCMF theory, Nigel Slater for his hospitality during the visit of the University of Cambridge and stimulating discussions. The authors gratefully acknowledges financial help from Spanish Ministry of education MICINN *via* project CTQ2008-06469/PPQ, project OPEN ToK (MTKD-CT-2005-030040) and the UK Royal Society for the International Joint Project.

References

1 R. Lipowsky and E. Sackmann, *Structure and Dynamics of Membranes*, Elsevier, Amsterdam, 1995.
2 M. Muller, K. Katsov and M. Schick, *Phys. Rep.*, 2006, **434**, 113–176.
3 M. Venturolia, M. M. Sperottob, M. Kranenburgc and B. Smit, *Phys. Rep.*, 2006, **437**, 1–54.
4 D. Tieleman, S. Marrink and H. Berendsen, *Biochimica et Biophysica Acta*, 1997, **1331**, 235–270.
5 K. V. Damodaran, K. M. Merz and B. P. Gaber, *Biochemistry*, 1992, **31**, 7656.
6 K. V. Damodaran and K. M. Merz, *Biophys. J.*, 1994, **66**, 1076–1087.
7 A. M. Smondyrev and M. L. Berkowitz, *J. Comput. Chem.*, 1999, **20**, 531–545.
8 A. J. Robinson, W. G. Richards, P. J. Thomas and M. M. Hann, *Biophys. J.*, 1994, **67**, 2345–2354.
9 H. Heller, M. Schafer and K. Schulten, *J. Phys. Chem.*, 1993, **97**, 8343.
10 M. Tuckerman, B. Berne and G. Martyna, *J. Chem. Phys.*, 1992, **97**, 1990.
11 A. P. Lyubartsev, *Eur. Biophys. J.*, 2005, **35**, 53–61.
12 M. T. Hyvonen, T. T. Rantala and M. Ala-Korpela, *Biophys. J.*, 1997, **73**, 2907–2923.
13 M. Kotelyanskii and D. N. Theodorou, *Simulation Methods for Polymers*, CRC Press, 2004.
14 R. Goetz and R. Lipowsky, *J. Chem. Phys.*, 1998, **108**, 7397–7409.
15 J. C. Shelley, M. Y. Shelley, R. C. Reeder, S. Bandyopadhyay and M. L. Klein, *J. Phys. Chem. B*, 2001, **105**, 4464–4470.
16 J. C. Shelley, M. Y. Shelley, R. C. Reeder, S. Bandyopadhyay, P. B. Moore and M. L. Klein, *J. Phys. Chem. B*, 2001, **105**, 9785–9792.
17 M. Muller, K. Katsov and M. Schick, *J. Polym. Sci., Part B: Polym. Phys.*, 2003, **41**, 1441–1450.
18 S. Marrink, A. de Vries and A. Mark, *J. Phys. Chem. B*, 2004, **108**, 750.
19 I. R. Cooke, K. Kremer and M. Deserno, *Phys. Rev. E: Stat., Nonlinear, Soft Matter Phys.*, 2005, **72**, 011506.
20 A. Ben-Shaul, I. Szleifer and W. M. Gelbart, *J. Chem. Phys.*, 1985, **83**, 3597.
21 A. Ben-Shaul, I. Szleifer and W. M. Gelbart, *J. Chem. Pys.*, 1986, **85**, 5345.
22 A. D. Mackie, A. Z. Panagiotopoulos and I. Szleifer, *Langmuir*, 1997, **13**, 5022.
23 Z. A. Al-Anber, J. Bonet-Avalos and A. D. Mackie, *J. Chem. Phys.*, 2005, **122**, 104910.
24 Z. A. Al-Anber, J. Bonet-Avalos, M. A. Floriano and A. D. Mackie, *J. Chem. Phys.*, 2003, **118**, 3816–3826.
25 R. Shvartzman-Cohen, C. Ren, I. Szleifer and R. Yerushalmi-Rozen, *Soft Matter*, 2009, **5**, 5003–5011.
26 P. Altevogt, O. Evers, J. Fraaije, N. Maurits and B. van Vlimmeren, *THEOCHEM*, 1999, **463**, 139–143.
27 J. G. E. M. Fraaije, B. A. C. van Vlimmeren, N. M. Maurits, M. Postma, O. A. Evers, C. Hoffmann, P. Altevogt and G. Goldbeck-Wood, *J. Chem. Phys.*, 1997, **106**, 4260–4269.
28 M. Doi, *Pure Appl. Chem.*, 2003, **75**, 1395–1402.
29 A. Soldera, Y. Qi and W. T. Capehart, *J. Chem. Phys.*, 2009, **130**, 064902.
30 H. Mae, M. Omiya and K. Kishimoto, *Journal of Solid Mechanics and Materials Engineering*, 2008, **2**, 1018–1036.
31 M. Muller and G. D. Smith, *J. Polym. Sci., Part B: Polym. Phys.*, 2005, **43**, 934–958.
32 K. C. Daoulas, M. Muller, J. J. de Pablo, P. F. Nealey and G. D. Smith, *Soft Matter*, 2006, **2**, 573–583.
33 K. C. Daoulas and M. Muller, *J. Chem. Phys.*, 2006, **125**, 184904.
34 S. Marcelja, *Nature*, 1973, **241**, 451–453.
35 S. Marcelja, *Biochim. Biophys. Acta, Biomembr.*, 1974, **367**, 165–176.
36 M. N. Rosenbluth and A. Rosenbluth, *J. Chem. Phys.*, 1955, **23**, 356.
37 D. Frenkel and B. Smit, *Understanding molecular simulation: from algorithms to applications*, Academic Press, San Diego, 2002.
38 N. Kucerka, Y. Liu, N. Chu, H. I. Petrache, S. Tristram-Nagle and J. F. Nagle, *Biophys. J.*, 2005, **88**, 2626–2637.
39 J. F. Nagle and S. Tristram-Nagle, *Biochimica et Biophysica Acta*, 2000, **1469**, 159–195.
40 J. C. Mathai, S. Tristram-Nagle, J. F. Nagle and M. L. Zeidel, *J. Gen. Physiol.*, 2008, **131**, 77–85.
41 R. Koynova and M. Caffrey, *Biochimica et Biophysica Acta*, 1998, **1376**, 91–145.

Current Nanoscience, 2011, *7*, 721-726

Equilibrium Insertion of Nanoscale Objects into Phospholipid Bilayers

Sergey Pogodin[1] and Vladimir A. Baulin[1,2]*

[1]*Departament d'Enginyeria Quimica, Universitat Rovira i Virgili, Av. dels Paisos Catalans 26, 43007 Tarragona, Spain,* [2]*ICREA, Passeig Lluis Companys 23, 08010 Barcelona, Spain*

Abstract: Certain membrane proteins, peptides, nanoparticles and nanotubes have rigid structure and fixed shape. They are often viewed as spheres and cylinders with certain surface properties. Single Chain Mean Field theory is used to model the equilibrium insertion of nanoscale spheres and rods into the phospholipid bilayer. The equilibrium structures and the resulting free energies of the nano-objects in the bilayer allow to distinguish different orientations in the bilayer and estimate the energy barrier of insertion.

Keywords: Phospholipid bilayers, nanoparticles, carbon nanotubes, mean field, membranes, self-assembly, peptides, lipids, equilibrium, theory.

1. INTRODUCTION

Biological membranes protect cells against the environment and also provide for selective transport of nanoscale objects across the membranes [1]. Peptides, nanotubes, nanoparticles and other nano-objects with fixed shape can interact with phospholipid bilayers [2], accumulate inside the membranes [3] and penetrate into cells [4-6]. Surface activity of these objects raises issues of biocompatibility and cytotoxicity [7,8], which may limit their biomedical applications. Understanding and controlling the interactions of nanoscale objects with membranes is therefore a key to the design of novel medical treatments and cell-active substances which can modulate the thermodynamic properties of cell membranes.

Although membrane active peptides, membrane proteins, nanotubes and nanoparticles may significantly differ in composition and chemical structure, the membrane activity implies the presence of certain common features providing for such activity. Phospholipid bilayers have alternating hydrophilic and hydrophobic regions which are characterized by the corresponding thickness. Thus, the size and the shape of nanoscale objects need to be compatible with the bilayer structure to ensure their insertion into the bilayer (*e.g.* the concept of hydrophobic matching [9]), cell penetration [10,11] or pore formation [12,13]. The thickness of the hydrophobic core defines the length scale for the size while the planar geometry of the bilayer defines the template for the shape of nanoscale objects able to interact or insert into phospholipid bilayers. The effect of the shape of nanoparticles interacting with phospholipid bilayers have been studied in Ref. [14]. The nanoparticles-lipid bilayer interaction is determined by the contact area and the local curvature of the nanoparticle at the contact point with the bilayer. Thus, nanoscale objects of different nature can be viewed in the first approximation as geometrical objects described only by the shape and the surface properties [14-18].

Many theoretical studies of interaction of phospholipid bilayers with nanoparticles and even peptides consider the simplest shapes: a sphere [3, 19-21] and a cylinder [18, 22-26] with uniform or patterned surface properties. This allows to describe a broad range of objects of similar size within a single concept and provide a general picture on the mechanism and the molecular details of interaction with the bilayers. Coarse-grained Molecular Dynamics (MD) provides the most detailed information about the molecular structure and the dynamics of interaction of nanoscale objects with phospholipid bilayers [3,14,18,19,23,27-31]. However, this method becomes computationally expensive and time consuming when the size of the system and the number of interacting molecules increases [32]. Calculation of equilibrium properties and equilibrium free energies requires equilibration process which may exceed microseconds [32]. One of the alternatives is the use of the self-consistent field theories, where the equilibrium structure of the bilayer is found from the solution of the self-consistency equations. Recently, Single Chain Mean Field (SCMF) theory has been applied for modeling of the phospholipid bilayers at different levels of coarse-graining [33]. It was shown, that essential equilibrium properties of the phospholipid bilayer such as the thickness, position of different groups, the compressibility constant and the area per lipid, can be reproduced with high accuracy. High speed of calculations is obtained by the decoupling of the correlations between the molecules and the fluctuations, taking into account the symmetries in the system. In this manner, the multi-molecule problem is reduced to a single molecule in the external self-consistent field problem. The molecule conformations and the fields are found from the self-consistency condition and gives the free energy of the equilibrium structures as a result of calculations. This method has been applied to estimate the free energies of insertion of a carbon nanotube into a phospholipid bilayer [22] and to elucidate the patterning of a carbon nanotube for physical translocation through the bilayer [34].

In this publication, we first present equations of the SCMF theory for the interaction of phospholipid bilayer and nanoscale objects. This theory is then applied for calculation of equilibrium structures and free energies of resulting structures of phospholipids and nanoscale objects, modeled as spheres and cylinders with given surface properties (Fig. **1**).

2. THEORY

The SCMF theory uses a coarse-grained representation of a phospholipid molecule as a set of spherical beads interacting with the fields through simple effective potentials [33]. The simplest 3-beads model (Fig. **2**) is able to reproduce with high accuracy the equilibrium structure and properties of DMPC phospholipid bilayer, such as the average interfacial area per lipid, the thickness of the bilayer and the core, and the stretching modulus [33]. In this model the phospholipid molecule is represented by two hydrophobic beads (T) and one hydrophilic bead (H) of the same radius 4.05 Å, joined consequently by rigid bonds of length 10.0 Å, and able to bend around the central T-bead. Two T-beads, belonging to different molecules, interact with energy gain $\varepsilon_{TT} = -2.10$ kT at distances

*Address correspondence to this author at the Departament d'Enginyeria Quimica, Universitat Rovira i Virgili, Av. dels Paisos Catalans 26, 43007 Tarragona, Spain; Tel: +34 977 55 85 77; Fax: +34 977 55 96 21;
E-mail: vladimir.baulin@urv.cat

1573-4137/11 $58.00+.00

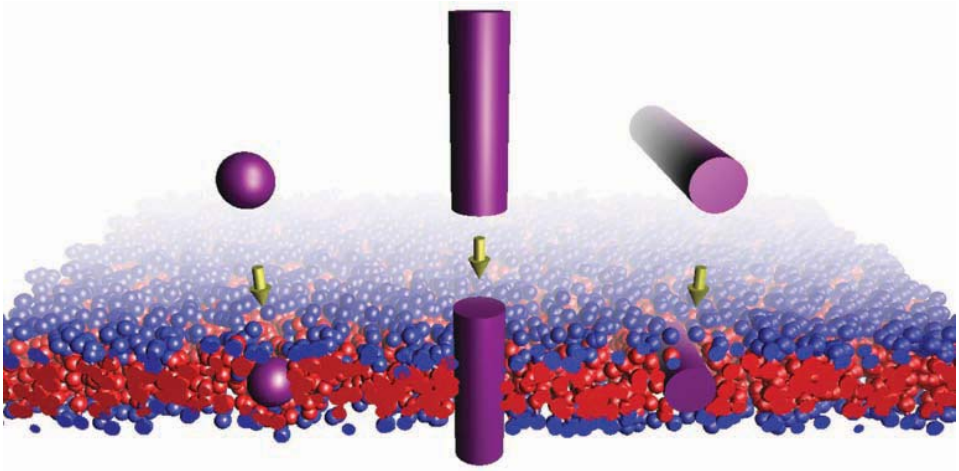

Fig. (1). Three geometries of nanoscale objects considered in the text: insertion of a sphere (left), insertion of a perpendicular cylinder (middle), and insertion of a parallel cylinder (right) into the bilayer.

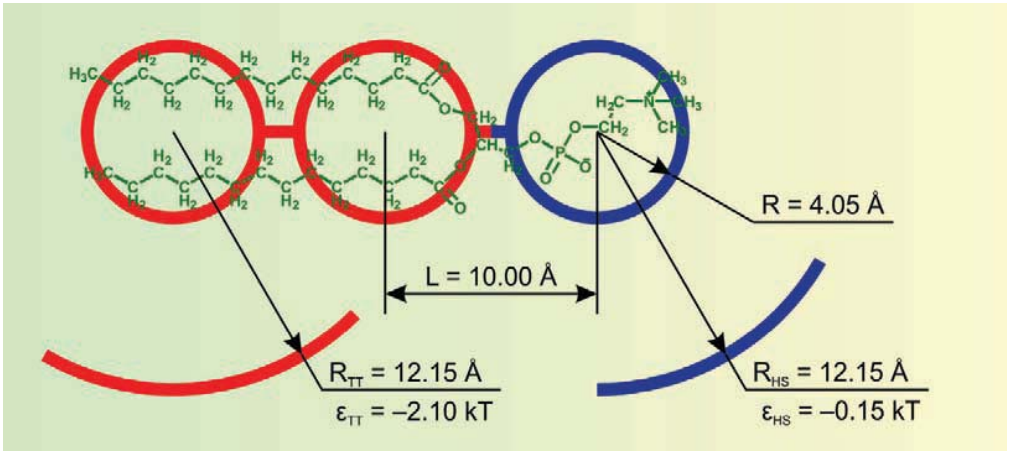

Fig. (2). The 3-beads model of the DMPC phospholipid molecule. R is the radius of the hydrophobic T-beads (red) and hydrophilic H-bead (blue), L is the bonds length, R_{TT} and R_{HS} are the interaction radii of the corresponding stepwise attractive potentials.

between their centers smaller than 12.15 Å. Additionally, the H-beads interact with implicit solvent molecules, assumed as well to be represented by spherical beads of the same radius 4.05 Å, with energy gain $\varepsilon_{HS} = -0.15$ kT at the distances closer than 12.15 Å.

The free energy of a system, containing N lipid molecules and the solvent, depends in general on the total probability distribution function ρ of the system. In the mean field approximation one can split this multi-molecule probability distribution function into a product of the corresponding single-molecule distribution functions. This allows to write the total free energy of the 3-beads model as a sum

$$F = -S_L - S_S + U_0 + U_{TT} + U_{HS} + U_{steric} \quad (1)$$

where S_L and S_S are the entropy contributions of the lipids and the solvent, U_0 describes the intra-molecular and position-dependent energies of the lipids, U_{TT} and U_{HS} represent the inter-molecular interactions between the pairs of T-beads and between H-beads and the solvent, and the last term, U_{steric}, takes into account the hard-core steric repulsions between the molecules.

The entropy part of the free energy is written as

$$-S_L - S_S = N\left\langle \ln\left[\rho(\gamma) N\Lambda\right]\right\rangle + \int c_S(\mathbf{r}) \ln\left[c_S(\mathbf{r})\Lambda_S\right] d\mathbf{r} \quad (2)$$

where $\rho(\gamma)$ is the density of probability of a single lipid molecule to be in the conformation γ (along with relative positions of the beads in the molecule with respect to each other, the conformations also include their spatial position and orientation in the system), $c_S(\mathbf{r})$ is the solvent concentration at the point r, Λ and Λ_S are the de Broglie lengths for the lipids and the solvent respectively, which shift the absolute value of the free-energy but have no effect on the final results. The angular brackets denote the average over $\rho(\gamma)$, and the integral is taken over all the accessible volume of the system.

The intra-molecular interaction energy U_0 is simply the average over $\rho(\gamma)$

$$U_0 = N\left\langle U_0(\gamma)\right\rangle \quad (3)$$

where $U_0(\gamma)$ is the internal energy of the lipid molecule in the conformation γ. It can include interactions between the beads composing the molecules and interaction with the external fields and the walls (or impermeable immobile objects).

The combined inter-molecular energy terms are written as

$$U_{TT} + U_{HS} = \frac{N(N-1)}{2} \int \left\langle u_T(\gamma, \mathrm{r})\right\rangle \left\langle c_T(\gamma, \mathrm{r})\right\rangle d\mathrm{r} + N \int \left\langle u_S(\gamma, \mathrm{r})\right\rangle c_S(\mathrm{r}) d\mathrm{r} \quad (4)$$

where $u_T(\gamma,\mathbf{r})$ and $u_S(\gamma,\mathbf{r})$ are the interaction potentials for T-beads and the solvent at the point $\mathbf{r}$, created by the lipid molecule in the conformation γ, and $c_T(\gamma,\mathbf{r})$ is the concentration of T-beads of the lipid in conformation γ at the point $\mathbf{r}$.

Eq. (4) is valid only if the potentials $u_T(\gamma,\mathbf{r})$ and $u_S(\gamma,\mathbf{r})$ are finite and smooth functions of $\mathbf{r}$ and therefore cannot contain any hard-core steric repulsion interactions, which are included in a separate term, U_{steric}, representing the incompressibility condition at every point $\mathbf{r}$ of the system

$$U_{steric} = \int \lambda(\mathbf{r})\left(\phi_0 - v_S c_S(\mathbf{r}) - N\left\langle\phi(\gamma,\mathbf{r})\right\rangle\right)d\mathbf{r} \quad (5)$$

Here $\lambda(\mathbf{r})$ is the Lagrange multiplier and ϕ_0 is the total volume fraction occupied by the lipids and the solvent ($0 < \phi_0 < 1$), v_S denotes the volume of the solvent molecule, and $\phi(\gamma,\mathbf{r})$ is the volume fraction at the point $\mathbf{r}$ occupied by the lipid in the conformation γ.

To find the equilibrium distribution, one should minimize the total free energy (1) with respect to $\rho(\gamma)$ and the solvent distribution $c_S(\mathbf{r})$ subject to the incompressibility condition (5). The minimization leads to the following set of integral equations

$$\rho(\xi) = \frac{1}{Z}\exp\Big[-U_0(\xi) - (N-1)\int u_T(\xi,\mathbf{r})\left\langle c_T(\gamma,\mathbf{r})\right\rangle d\mathbf{r} - \int u_S(\xi,\mathbf{r})c_S(\mathbf{r})d\mathbf{r} + \int\lambda(\mathbf{r})\phi(\xi,\mathbf{r})d\mathbf{r}\Big] \quad (6)$$

$$v_S\lambda(\mathbf{r}) = \ln\left[v_S c_S(\mathbf{r})\right] + N\left\langle u_S(\gamma,\mathbf{r})\right\rangle \quad (7)$$

$$v_S c_S(\mathbf{r}) = \phi_S(\mathbf{r}) = \phi_0 - N\left\langle\phi(\gamma,\mathbf{r})\right\rangle \quad (8)$$

where the normalization factor Z ensures that $\int\rho(\gamma)d\gamma = 1$. These equations can be solved numerically, if the integrals and the averages are replaced by appropriate sums, which reduce the problem to solution of algebraic equations. To discretize the space, the simulation box is divided into a set of auxiliary cells, where all spatial dependent variables have a constant value. The division into cells should also take into account the symmetry of the solution, which provides the speed up of the calculations. For example, if the lipid system is expected to self-organize into a flat bilayer, the division of the simulation box according to 1D geometry into parallel slits results in considerably smaller number of cells than the 3D division into a cubic grid with the same resolution. The conformational space γ of a single lipid is sampled with the Rosenbluth algorithm [35], the conformations are placed in the box and the spatial distributions $u_T(\gamma,\mathbf{r})$, $u_S(\gamma,\mathbf{r})$, $c_T(\gamma,\mathbf{r})$, $\phi(\gamma,\mathbf{r})$ as well as other necessary conformational-dependent properties are calculated. Finally, the averages of the fields f in the equations (6)-(8) are replaced by the sums

$$\left\langle f(\gamma)\right\rangle = \frac{1}{\kappa}\sum_{\gamma}\frac{\rho_\gamma f_\gamma}{w_\gamma} \quad (9)$$

where f_γ is the value of this field, and ρ_γ is the probability of the conformation γ belonging to the generated sampling (thus ρ_γ is determined only over the sampling, while $\rho(\gamma)$ used above was determined in the full conformational space of the molecule). w_γ is the value of the Rosenbluth weight (*i.e.* biased probability of the conformation γ is introduced into the sampling during the generation). κ is the size of the conformational sampling. Similarly, the integrals over the space are replaced by the sums as

$$\int f(\mathbf{r})d\mathbf{r} = \sum_i f_i V_i \quad (10)$$

where f_i is the value of the field in the i-th auxiliary cell of the simulation box and V_i is the volume of the i-th cell. As a result, the system of integral equations (6)-(8) is reduced to the closed set of algebraic equations of finite but huge number κ of unknown variables ρ_γ. Since the larger κ, the more accurate the solution is, the practical choice of κ which provide a reasonable accuracy is limited by the *representative* sampling. The easiest way to check the accuracy is to perform several simulations with independently generated random samplings and compare their results. Thus we start our simulations with some small value of κ, and then perform series of similar simulations for larger κ till the moment when further increase of κ will not lead to significant change of calculated results. For the simulations reported in this work we used $\kappa = 750000$, which provide accuracy of the calculated energies about ± 10 kT.

The number of auxiliary cells in the box should be high enough to provide acceptable spatial resolution, but if it is relatively small one can decrease the number of independent variables by introducing new independent variables, average concentration of T-beads, $c_{T,i} \equiv \left\langle c_T(\gamma,\mathbf{r}_i)\right\rangle$, potential of the solvent, $u_{S,i} \equiv \left\langle u_S(\gamma,\mathbf{r}_i)\right\rangle$, and the volume fraction occupied by lipids, $\phi_i \equiv \left\langle\phi(\gamma,\mathbf{r}_i)\right\rangle$. Depending on the method of solution of equations[1], such reduction of the number of independent variables can speed up calculations.

The equations of the SCMF theory are written for the canonical (NVT) ensemble. However, the simulation of the phospholipid bilayer with inserted nanoscale object would require the grand-canonical ensemble, since the inserted object may expel the phospholipids out of the simulation box. Fortunately, the SCMF technique is fast enough to perform series of canonical calculations for a part of bilayer with variable number of lipids N in the simulation box. One can consider then the simulation box as an open part of a larger closed system and thus estimate the free energy F^* of the whole system as a function of N. The equilibrium value of N will correspond to the minimum of F^*, thus series of canonical SCMF calculations are equivalent to a grand-canonical calculation. In the simulations performed in the present work (size of the system about $100.0\times100.0\times60.0$ Å, two-dimensional geometry with spatial resolution 2.0 Å, and sampling size $\kappa = 750000$), calculation of one energy point in the grand-canonical ensemble with current version of our SCMF code, demanded, on average, about one day on a 32-cores machine. Full three-dimensional simulations should be significantly slower, but we believe that further improvements of our code will significantly

[1]According to Ref. [33], the independent variables are $c_{T,i}$, $c_{H,i}$ and ϕ_i. One can show that the expression $N\left\langle u_S(\gamma,\mathbf{r})\right\rangle$, which is the average potential experienced by the solvent molecule at the point $\mathbf{r}$, is approximately equal to $N\varepsilon_S\left\langle c_H(\gamma,\mathbf{r})\right\rangle$, where ε_S is the integral of the H-S interaction potential around a solvent molecule. One can easily replace the variables $u_{S,i}$ by $c_{H,i}$. This was indeed necessary in the general case, considered in the previous article, but in this context it can be avoided for the sake of simplicity.

speed-up its' performance, thus making possible three-dimensional simulations in a reasonable time.

3. RESULTS AND DISCUSSION

The equations of the previous section allow to calculate the equilibrium properties and the free energy of the phospholipid bilayer and its interaction with nanoscale objects with a fixed shape. Simulation of a phospholipid bilayer is a one dimensional problem if we neglect the bilayer bending. Since the free energy of a homogenous bilayer is proportional to the area (or the number of lipids in the bilayer) and the interfacial area per lipid and the bilayer thickness are constant along the bilayer, the free energy of a large system F^* can be written as

$$F^* = V^* f_S + N^* f(A), \quad f(A) = \frac{F(V,N,A) - V f_S}{N}, \quad f_S = \frac{\phi_0}{v_S} \ln \frac{\phi_0}{v_S} \quad (11)$$

where V^* is the volume and N^* is the total number of lipids of the large system, f_S is the free energy density of the region occupied by the pure solvent, and $f(A)$ is the free energy per lipid of the bilayer, which depends on the average surface area per lipid A.

The result of the SCMF simulation is the free energy $F(V,N,A)$ of the box of the total volume V with the number of lipids N. These expressions allow to construct the free energy per lipid $f(A)$. The equilibrium area per lipid A_0, which minimizes the total free energy of a large system F^*, can be found by the minimization of $f(A)$, obtained from the series of SCMF simulations, while the simulation corresponding to A_0 gives the equilibrium distribution of T- and H-beads inside the bilayer and the equilibrium thickness (Fig. **3**).

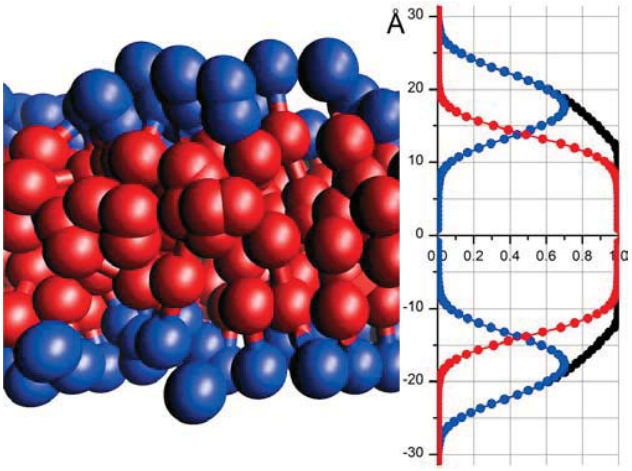

Fig. (3). Mean field snapshot of DMPC bilayer at equilibrium within the 3-beads model (left), and the corresponding concentration profiles (right) of hydrophobic (red), hydrophilic (blue) and total (black) volume fractions of the beads.

Similar approach is applied to study the insertion of a rigid spherical or cylindrical nano-object into the phospholipid bilayer. A part of the object located inside the simulation box is represented by a region prohibited for lipids and the solvent to enter, and the surface of the object can interact preferentially with phospholipid beads. This restricted area is taken into account during the sampling generation by the additional bias and the corresponding contribution to the intra-molecular energy $U_0(\gamma)$. In the case of a spherical object and a cylindrical object oriented perpendicular to the bilayer one can use the two-dimensional cylindrical geometry with the symmetry axis passing through the center of the sphere (cylinder) perpendicular to the bilayer plane. The simulation of a cylindrical object in the parallel orientation has been done within two-dimensional grid geometry *i.e.* assuming infinite cylinder. To limit the bending of the bilayer, which permits the inserted object to escape from the bilayer, the hard walls on the top and bottom of the simulation box have been introduced.

Assuming that a part of the membrane outside the simulation box is not perturbed by the insertion of the object and, thus, is in equilibrium state, we estimate the total free energy change due to the insertion of the object to a given position $\mathbf{p}$ in the box as

$$\Delta F^* = F(V,N,\mathbf{p}) - N f(A_0) - (V - V(\mathbf{p})) f_S \quad (12)$$

where $F(V,N,\mathbf{p})$ is the free energy of the box and $V(\mathbf{p})$ is the volume occupied by the object inside the box.

The results of the free energy calculations for spheres and cylinders of diameter 2.43 nm with homogeneous surface properties are summarized in Fig. (**4**). The surface properties are described by a single interaction parameter between the T-beads and the surface, ε. One can clearly see, that the free energy changes due to the insertion of a sphere, or a cylinder in perpendicular orientation which has a similar contact area with lipids, have relatively close values for all considered levels of hydrophobicity ε. Thus, the shape of the object is not so important as the contact area with lipids. This conclusion is consistent with the previous observations [14]. In contrast, the cylinder in the parallel orientation has a larger contact area with phospholipid tails and disturbs much larger part of the bilayer. Thus, the parallel orientation has sufficiently lower equilibrium free energy than the perpendicular orientation (the points in the plot correspond to a cylinder with the length 10.0 nm, while the numbers in the insets correspond to the energy per nm).

Hydrophilic and hydrophobic objects induce different rearrangement of lipids in the bilayer (see the insets of Fig. **4**). Hydrophilic objects of similar size create pores of similar size with the heads of the lipids oriented inside the pores. Hydrophobic objects attract the tails of phospholipids and they tend to come closer to the surface. For most hydrophobic objects, the meniscus provoked by the wetting of the hydrophobic object can be formed. For intermediate interaction parameters, the pore is not complete and is combined with the partial wetting at the edges, thus provoking the thinning of the bilayer in contact with the nano-object. This diagram also suggest the preferential orientation of cylindrical objects in the bilayer. Hydrophilic cylinder has lower free energy in perpendicular orientation, while the most hydrophobic cylinder has lower free energy in parallel orientation. For an intermediate hydrophobicity, there is a transition in orientation from perpendicular to parallel orientation which depends also on the length of the cylinder. For $\varepsilon = -6.3$ kT the transition from perpendicular to parallel orientation occurs at the length of the cylinder 10 nm, where both orientations have almost the same energies. Longer cylinders would favor parallel orientation.

The uptake of a hydrophobic particle into the core of a bilayer is not the only equilibrium solution of the equations. There exists a solution which corresponds to a hydrophobic particle covered by phospholipids floating around and coexisting with a bilayer (third snapshot from the top in the right column of Fig. **4**). We have compared the free energy of such structure with the energy of the inserted sphere into the bilayer in the most hydrophobic case, $\varepsilon = -10.0$ kT. The bilayer with the incorporated sphere has a lower energy, while the free energy difference with the sphere in the solution is of the order 50.0 kT, indicating that the hydrophobic sphere would unlikely escape. Similar conclusion can be drawn for the case of cylindrical particles lying parallel to the bilayer.

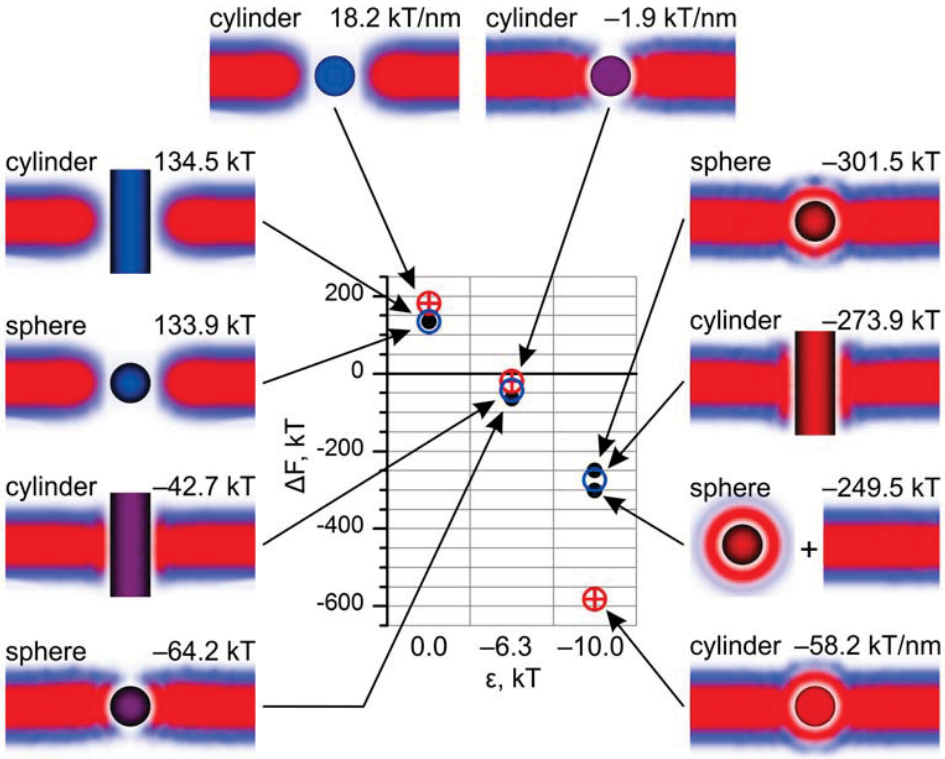

Fig. (4). Snapshots of the equilibrium insertion of a spherical and a cylindrical object into the DMPC bilayer. The color of the objects in the insets illustrates the hydrophobicity level (interaction with T-beads): ε =0.0 (blue), ε =-6.3 kT (purple), ε =-10.0 kT (red). Parallel orientation of a cylinder (denoted by the energy/nm), corresponds to the cylinder of length 10.0 nm.

4. CONCLUSIONS

We have developed the SCMF theory for the interaction of nanoscale objects with phospholipid bilayers. This numerical method provides for detailed microscopic information about the structure of phospholipid bilayers and their essential equilibrium thermodynamic properties. The method gives the total equilibrium free energy of self-assembled structures as the output of calculations, which allows for direct comparison of different equilibrium structures involving nanoscale objects and phospholipid bilayers.

We have applied the SCMF theory to investigate the interaction of phospholipid bilayer with cylindrical and spherical nanoparticles of diameter 2.43 nm and surface properties ranging from hydrophilic to strongly hydrophobic. We have shown that the shape of the nanoparticles is not as important as the contact area with the lipids. Hydrophobic and hydrophilic objects induce different reorganization of lipids around the nanoparticles. More complex nano-objects will be considered in future works.

ACKNOWLEDGEMENTS

The authors acknowledge the UK Royal Society International Joint Project with Cambridge University and Spanish Ministry of education MICINN project CTQ2008-06469/PPQ.

REFERENCES

[1] Alberts, B. *Molecular Biology of the Cell*, 5th ed.; Garland Science: New York, **2008**.

[2] Roiter, Y.; Ornatska, M.; Rammohan, A. R.; Balakrishnan, J.; Heine, D. R.; Minko, S. Interaction of nanoparticles with lipid membrane. *Nanolett.,* **2008**, *8*, 941-944.

[3] Wong-Ekkabut, J.; Baoukina, S.; Triampo, W.; Tang, I.-M.; Tieleman, D. P.; Monticelli, L. Computer simulation study of fullerene translocation through lipid membranes. *Nat. Nanotech.,* **2008**, *3*, 363-368.

[4] Khodakovskaya, M.; Dervishi, E.; Mahmood, M.; Xu, Y.; Li, Z.; Watanabe, F.; Biris, A. S. Carbon nanotubes are able to penetrate plant seed coat and dramatically affect seed germination and plant growth. *ACS Nano,* **2009**, *3*, 3221-3227.

[5] Porter, A. E.; Gass, M.; Muller, K.; Skepper, J. N.; Midgley, P. A.; Welland, M. Direct imaging of single-walled carbon nanotubes in cells. *Nat. Nanotech,.* **2007**, *2*, 713-717.

[6] Verma, A.; Uzun, O.; Hu, Y.; Hu, Y.; Han, H.-S.; Watson, N.; Chen, S.; Irvine, D. J.; Stellacci, F. Surface-structure-regulated cell-membrane penetration by monolayer-protected nanoparticles. *Nat. Mater.,* **2008**, *7*, 588-595.

[7] Liu, J.; Hopfinger, A. J. Identification of possible sources of nanotoxicity from carbon nanotubes inserted into membrane bilayers using membrane interaction quantitative structure-activity relationship analysis. *Chem. Res. Toxicol.,* **2008**, *21*, 459-466.

[8] Cheng, C.; Muller, K. H.; Koziol, K. K. K.; Skepper, J. N.; Midgley, P. A.; Welland, M. E.; Porter, A. E. Toxicity and imaging of multi-walled carbon nanotubes in human macrophage cells. *Biomaterials,* **2009**, *30*, 4152-4160.

[9] Venturoli, M.; Sperotto, M. M.; Kranenburg, M.; Smit, B. Mesoscopic models of biological membranes. *Phys. Rep.,* **2006**, *437*, 1-54.

[10] Stewart, K. M.; Horton, K. L.; Kelley, S. O. Cell-penetrating peptides as delivery vehicles for biology and medicine. *Org. Biomol. Chem.,* **2008**, *6*, 2242-2255.

[11] Zorko, M.; Langel, U. Cell-penetrating peptides: mechanism and kinetics of cargo delivery. *Adv. Drug Deliv. Rev.,* **2005**, *57*, 529-545.

[12] Bayley, H. Membrane-Protein Structure. Piercing Insights. *Nature,* **2009**, *459*, 651-652.

[13] Kafsack, B. F. C.; Pena, J. D. O.; Coppens, I.; Ravindran, S.; Boothroyd, J. C.; Carruthers, V. B. Rapid membrane disruption by a perforin-like protein facilitates parasite exit from host cells. *Science,* **2009**, *323*, 530-533.

[14] Yang, K.; Ma, Y.-Q. Computer simulation of the translocation of nanoparticles with different shapes across a lipid bilayer. *Nat. Nanotech.,* **2010**, *5*, 579-583.

[15] Mouritsen, O. G.; Bloom, M. Mattress model of lipid-protein interactions in membranes. *Biophys. J.,* **1984**, *46*, 141-153.

[16] Jenssen, H.; Hamill, P.; Hancock, R. E. W. Peptide antimicrobial agents. *Clin. Microbiol. Rev.,* **2006**, *19*, 491-511.

[17] Monticelli, L.; Salonen, E.; Ked, P. C.; Vattulainen, I. Effects of carbon nanoparticles on lipid membranes: a molecular simulation perspective. *Soft Matter,* **2009**, *5*, 4433-4445.

[18] Lopez, C. F.; Nielsen, S. O.; Moore, P. B.; Klein, M. L. Understanding Nature's Design for a Nanosyringe. *Proc. Natl. Acad. Sci.,* **2004**, *101*, 4431-4434.

[19] Bedrov, D.; Smith, G. D.; Davande, H.; Li, L. Passive Transport of C60 Fullerenes through a Lipid Membrane: A Molecular Dynamics Simulation Study. *J. Phys. Chem. B,* **2008**, *112*, 2078-2084.

[20] Qiao, R.; Roberts, A. P.; Mount, A. S.; Klaine, S. J.; Ke, P. C. Translocation of C60 and Its Derivatives Across a Lipid Bilayer. *Nano Lett.,* **2007**, *7*, 614-619.

[21] Chiu, C.-C.; DeVane, R.; Klein, M. L.; Shinoda, W.; Moore, P. B.; Nielsen, S. O. Coarse-Grained Potential Models for Phenyl-Based Molecules: II. Application to Fullerenes. *J. Phys. Chem. B,* **2010**, *114*, 6394-6400.

[22] Pogodin, S.; Baulin, V. A. Can a carbon nanotube pierce through a phospholipid bilayer? *ACS Nano,* **2010**, *4*, 5293-5300.

[23] Wallace, E. J.; Sansom, M. S. P. Blocking of carbon nanotube based nanoinjectors by lipids: a simulation study. *Nano Lett.,* **2008**, *8*, 2751-2756.

[24] Huang, H. W. Molecular mechanism of peptide-induced pores in membranes. *Phys. Rev. Lett.,* **2004**, *92*, 198304.

[25] Fosnaric, M.; Kralj-Iglic, V.; Bohinc, K.; Iglic, A.; May, S. Stabilization of pores in lipid bilayers by anisotropic inclusions. *J. Phys. Chem. B,* **2003**, *107*, 12519-12526.

[26] Illya, G.; Deserno, M. Coarse-grained simulation studies of peptide-induced pore formation. *Biophys. J.,* **2008**, *95*, 4163-4173.

[27] Li, Y.; Chen, X.; Gu, N. Computational investigation of interaction between nanoparticles and membranes: hydrophobic/hydrophilic effect. *J. Phys. Chem. B,* **2008**, *112*, 16647-16653.

[28] Nielsen, S. O.; Ensing, B.; Ortiz, V.; Moore, P. B.; Klein, M. L. Lipid bilayer perturbations around a transmembrane nanotube: a coarse grain molecular dynamics study. *Biophys. J.* **2005**, *88*, 3822-3828.

[29] Jusufi, A.; DeVane, R. H.; Shinoda, W.; Klein, M. L. Nanoscale carbon particles and the stability of lipid bilayers. *Soft Matter,* **2011**, *7*, 1139-1146.

[30] Gkeka, P.; Sarkisov, L. Interactions of phospholipid bilayers with several classes of amphiphilic alpha-helical peptides: insights from coarse-grained molecular dynamics simulations. *J. Phys. Chem. B,* **2010**, *114*, 826-839.

[31] Gkeka, P.; Sarkisov, L. Spontaneous formation of a barrel-stave pore in a coarse-grained model of the synthetic LS3 peptide and a DPPC lipid bilayer. *J. Phys. Chem. B,* **2009**, *113*, 6-8.

[32] Muller, M.; Katsov, K.; Schick, M. Biological and synthetic membranes: what can be learned from a coarse-grained description? *Phys. Rep.,* **2006**, *434*, 113-176.

[33] Pogodin, S.; Baulin, V. A. Coarse-grained models of phospholipid membranes within the single chain mean field theory. *Soft Matter,* **2010**, *6*, 2216-2226.

[34] Pogodin, S.; Slater, N. K. H.; Baulin, V. A. Surface patterning of carbon nanotubes can enhance their penetration through a phospholipid bilayer. *ACS Nano,* **2011**, *5*, 1141-1146.

[35] Rosenbluth, M. N.; Rosenbluth, A. Monte Carlo calculation of the average extension of molecular chains. *J. Chem. Phys.,* **1955**, *23*, 356-359.

Received: April 15, 2011 Revised: May 23, 2011 Accepted: June 8, 2011

ARTICLE

Can a Carbon Nanotube Pierce through a Phospholipid Bilayer?

Sergey Pogodin[†] and Vladimir A. Baulin[†,‡,*]

[†]Departament d'Enginyeria Quimica, Universitat Rovira i Virgili 26 Avenue dels Paisos Catalans, 43007 Tarragona, Spain, and [‡]ICREA, 23 Passeig Lluis Companys, 08010 Barcelona, Spain

ABSTRACT Great efficiency to penetrate into living cells is attributed to carbon nanotubes due to a number of direct and indirect observations of carbon nanotubes inside the cells. However, a direct evidence of physical translocation of nanotubes through phospholipid bilayers and the exact microscopic mechanism of their penetration into cells are still lacking. In order to test one of the inferred translocation mechanisms, namely the spontaneous piercing through the membrane induced only by thermal motion, we calculate the energy cost associated with the insertion of a carbon nanotube into a model phospholipid bilayer using the single-chain mean field theory, which is particularly suitable for the accurate measurements of equilibrium free energies. We find that the energy cost of the bilayer rupture is quite high compared to that of the energy of thermal motion. This conclusion may indirectly support other energy-dependent translocation mechanisms, such as, for example, endocytosis.

KEYWORDS: phospholipid bilayer · carbon nanotubes · translocation mechanism · cell membrane

Phospholipid bilayers are designed by nature to protect the interior of cells from the outside environment.[1,2] Despite the weakness of hydrophobic interactions[3] that drive the self-assembly of phospholipids into bilayers, cell membranes represent a serious protective barrier[2,4] for external molecules, proteins, and particles as well as artificial polymers and drugs. This barrier is quite efficient in protecting the interior of the cells, and it is a challenging task to design nano-objects that can penetrate through the phospholipid bilayer without damaging its structure.[5−8] If such nano-objects can be tailored, then they can potentially be used for transmembrane delivery of active components into cells.[9] However, the major difficulty lies in getting a direct microscopic information regarding the interaction of nano-objects with phospholipid layers at the molecular level in order to provide for physical mechanisms of nanoparticle translocation across the membranes. In the absence of such microscopic information it is quite difficult to validate or distinguish between inferred translocation mechanisms that were proposed to explain the internalization by cells of several nano-objects, such as, for example, cell penetrating peptides.[10−13]

Similarly, a consensus has not yet been reached regarding the translocation mechanism of carbon nanotubes through cell membranes. Single-walled carbon nanotubes (SWNTs) have been found inside the cells both in direct imaging experiments using electron microscope,[14,15] spectroscopy,[16] and fluorescent microscopy studies.[17−26] Such experiments suggest that carbon nanotubes can efficiently penetrate into the cells but very little can be said about the pathway and the entry mechanism regulating their internalization. Experimental efforts aimed to distinguish active and passive uptake include comparison of nanotubes internalization by living and dead cells,[27] change of the rate of active biological processes by temperature control,[19] addition of selective chemical agents that inhibit active uptake,[20] and observing nanotubes on the cell membranes by atomic force microscopy (AFM).[28]

However, most of these experiments showing the translocation of carbon nanotubes refer to biological membranes which have complex structure, their properties depend on composition and many external parameters. Biological membranes may undergo several energy consuming processes, such as endocytosis[29] or phase transitions.[2] Thus, it is quite difficult to identify from these experiments a unique translocation mechanism and discard all other possibilities by studying a particular biological system. From this respect, the microscopic mechanism of nanotube translocation through the membrane remains an open question.

*Address correspondence to vladimir.baulin@urv.cat.

Received for review July 15, 2010 and accepted August 25, 2010.

Published online September 1, 2010.
10.1021/nn1016549

A study of a model system of a phospholipid bilayers without inclusions and comprising of one type of phospholipids may shed light on the plausibility of the spontaneous translocation of carbon nanotubes *via* rupture and diffusion of the phospholipid bilayer. If we assume that the driving force for the physical translocation of freely moving SWNTs through the homogeneous phospholipid bilayer is indeed thermal motion, then the energy barrier represented by the phospholipid bilayer should be comparable with the energy of thermal motion. Apparently, the energy barrier depends on the orientation of the SWNT with respect to the bilayer. The minimum energy would correspond to the positions inducing less perturbation to the phospholipid bilayer. Since in the perpendicular orientation to the bilayer plane the SWNT interacts with a minimal number of phospholipids, this orientation would have the minimal energy barrier. Other orientations would induce more perturbations to the bilayer and thus would require higher energies. Hence, an accurate estimation of the energy cost of the SWNTs perpendicular translocation through the phospholipid bilayer would allow to conclude about the possibility of such mechanism.

Calculation of equilibrium energies in computer simulations that provide a microscopic information[30−39] related to the structure and the dynamics of phospholipid bilayers is not straightforward, since the simulations usually deal with a limited number of molecules in the simulation box subject to fluctuations as well as due to the absence of a suitable reference state.[40,41]

Alternative to computer simulations is the use of mean field-type theories that do not include fluctuations and give direct access to the equilibrium free energies as a result of the minimization of the free energy functional. The single-chain mean field (SCMF) theory[42−45] is particulary suitable for such purposes, and in addition to the speed of calculation and high capability of parallelization, it can provide the microscopic details with the accuracy, competing with coarse-grained Monte Carlo (MC) and molecular dynamics (MD) simulations.

The numerical implementation of the SCMF theory was recently improved, and the method was applied to model the equilibrium properties of the dimyristoyl phosphatidylcholine (DMPC) phospholipid bilayers in a fluid phase in ref 46. We use the three-beads model of DMPC phospholipids of this work to model the fluid phase of phospholipid bilayer and estimate the free energy of equilibrium insertion of the SWNT in a perpendicular direction to the bilayer plane using different diameters of carbon nanotubes and different parameters of interaction between nanotubes and the core of the bilayer. This gives the microscopic information about the possibility of spontaneous translocation of SWNTs through the phospholipid bilayer by thermal motion. Our model study has a broader interest than only the study of biologically relevant translocation mechanisms. For example, an AFM tip associated with a carbon nanotube can be used in order to quantify the force of the membrane rupture.[47−50]

FREE ENERGY OF THE NANOTUBE INSERTION

The SCMF theory is a relatively fast and stable tool for obtaining equilibrium properties and free energies of soft matter systems with different geometries and molecular structures.[46] A single molecule is described at a coarse-grained level with an explicit account of intramolecular interactions, while the interactions between different molecules are described through mean molecular fields which are found self-consistently.

In the present work the phospholipid molecule is modeled within the three-beads model with the interaction parameters obtained in ref 46. This model allows for spontaneous self-assembly of phospholipids in bilayers with realistic bulk bilayer properties, such as the average interfacial area per lipid at equilibrium, the thickness of the bilayer and its hydrophobic core, and the compressibility constant. These thermodynamic properties rigidly fix the compression−extension energy curve,[46] the output of the SCMF calculations; the minimum of this curve gives the equilibrium area per lipid, while its second derivative is proportional to the compressibility constant. Thus, this curve gives us confidence in calculated values of the energy upon compression−extension of the bilayer.

The carbon nanotube is modeled as a rigid cylinder of a given diameter which is oriented perpendicularly to the bilayer plane. More precisely, the carbon nanotube represents a cylindrical region in the simulation box which is not accessible for phospholipids. We assume that the cylinder can interact with hydrophobic tails of phospholipids because the driving force for the assembly of the phospholipid bilayer is the hydrophobic interactions, and thus, the interactions between the hydrophobic tails lead to the main contribution in the free energy.

The aim of this work is an accurate measurement of the energy cost of the presence of the SWNT at a fixed position from the bilayer plane. Since the SWNT can perturb the equilibrium structure of the bilayer, the free bilayer may wrap around, bend, or displace in order to minimize the perturbation. In order to avoid such movements, the position of the bilayer in our model is restricted by noninteracting walls at the top and the bottom of the simulation box, and the periodic boundary conditions are applied on the sides. Since the reference state for the free energy calculation is the energy of unperturbed phospholipid bilayer, we assume that the simulation box represents a small part of a much larger system, where the part of the bilayer outside the box

is approximated by the unperturbed bilayer, which serves as a reference state. Thus, calculating the free energy of the small box, containing a part of the lipid bilayer, we can construct the free energy of the larger system. We write the total free energy of the system, F, as a sum of the free energy of the simulation box, F_{box}, and the free energy of the system outside the box, F_{out}, which, in turn, is expressed *via* the free energy density of the unperturbed bilayer given by the reference state, f_l^0, and the entropy of pure solvent, $f_s = (\phi_0/v_s)\ln(\phi_0/v_s)$, where v_s is the volume of the solvent molecule, and ϕ_0 is the bulk solvent volume fraction (see ref 46):

$$F = F_{box} + F_{out} = F_{box} + V_l^{out} f_l^0 + V_s^{out} f_s \quad (1)$$

The volume of the bilayer part lying outside of the simulation box, V_l^{out}, and the volume of pure solvent outside of the box, V_s^{out}, can be expressed *via* the volume of the unperturbed bilayer in the simulation box, V_l^0, and the equilibrium numbers of lipids in the box with the cylinder, N_l, and without cylinder, N_l^0. In addition, we take into account the conservation of the total volume of the system and the total number of lipid and solvent molecules. With this, f_l^0 is related to the free energy F_{box}^0 of the box containing the unperturbed bilayer as

$$f_l^0 = \frac{1}{V_l^0}(F_{box}^0 - (V_{box} - V_l^0) f_s) \quad (2)$$

while the free energy difference with respect to the reference state of unperturbed bilayer yields in the form

$$\Delta F = F_{box} - \frac{N_l}{N_l^0}(F_{box}^0 - V_{box} f_s) - (V_{box} - V_{cyl}^{in}) f_s \quad (3)$$

where V_{box} is the volume of the simulation box, and V_{cyl}^{in} is the part of the cylinder lying inside the box. We used two-dimensional (2D) cylindrical geometry in order to discretize the space such that the symmetry axis coincides with the axis of the cylinder.

RESULTS AND DISCUSSION

We have performed series of SCMF calculations for different positions of perpendicularly oriented SWNT with respect to the DMPC phospholipid bilayer plane for different diameters of the SWNT and interaction parameters between the SWNT and the core of the bilayer. The output of the calculations is the mean field concentration profiles of the heads and tails in the bilayer, demonstrating the structural rearrangements of phospholipids induced by the SWNT at the molecular level and the precise measurements of the equilibrium free energy change for each position of the SWNT. In addition, the SCMF theory gives the probabilities of each phospholipid conformation in the corresponding mean fields. This information allows for visualization of the equilibrium molecular structure of the bilayer disturbed by the presence of the SWNT in the form of mean field "snapshots" representing the most probable conformations of the molecules and their positions in the layer. One of such representative "snapshots" is shown in Figure 1.

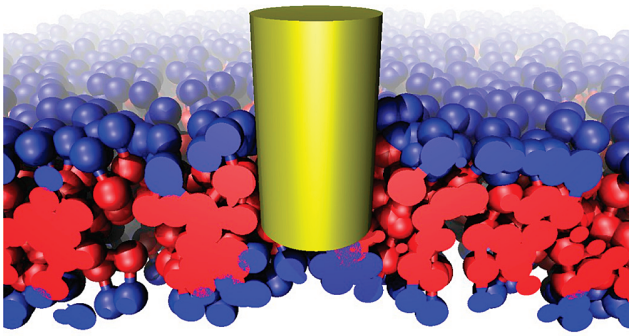

Figure 1. Mean field "snapshot" (set of most-probable conformations of the lipids) of the perpendicular SWNT insertion produced by the SCMF theory. Nanotube diameter is 2.43 nm, nanotube position is −0.63 nm, and interaction parameter between the nanotube and the hydrophobic core is $\varepsilon_T = -6.30$ kT.

Carbon nanotubes, by their chemical structure, can be considered as hydrophobic cylinders.[51] Such objects in aqueous solutions tend to aggregate in bundles, which makes it difficult to observe individual SWNT in solution. In order to prevent such aggregation, the surface of the SWNT is often treated with acids or functionalized[26,51] in such a way that they become slightly hydrophilic. That is why, the energy per contact of the hydrophobic bead with the nanotube, ε_T, in our calculations changes from 0, representing steric repulsion, to −6.3 kT, which corresponds to strong attraction (we assume the interaction distance 8.1 nm).[46] Since carbon nanotubes usually have diameters ranging from 1 to 5 nm, we have chosen three diameters of the cylinder, 1.00, 2.43, and 4.86 nm. The latter diameter is, probably, too big for SWNTs, but it may correspond to multiwalled nanotubes and we include it for completeness.

The free energy cost of the equilibrium insertion of the SWNT as a function of the distance between the SWNT tip and the middle plane of the unperturbed layer for different interaction parameters is shown in Figure 2. Here the SWNT position −3.14 nm corresponds to the SWNT at the bilayer surface, while the position 3.14 nm corresponds to fully inserted SWNT. Insertion of slightly hydrophilic SWNT is not favorable, and the free energy cost increases with the insertion distance until the SWNT pierces completely the bilayer and the curve reaches the plateau, where the nanotube can slide along its length through the bilayer with no energy cost. In turn, the insertion of a hydrophobic SWNT is favorable, and the corresponding insertion curve has a pronounced minimum which corresponds to the partial insertion of the nanotube into the bilayer

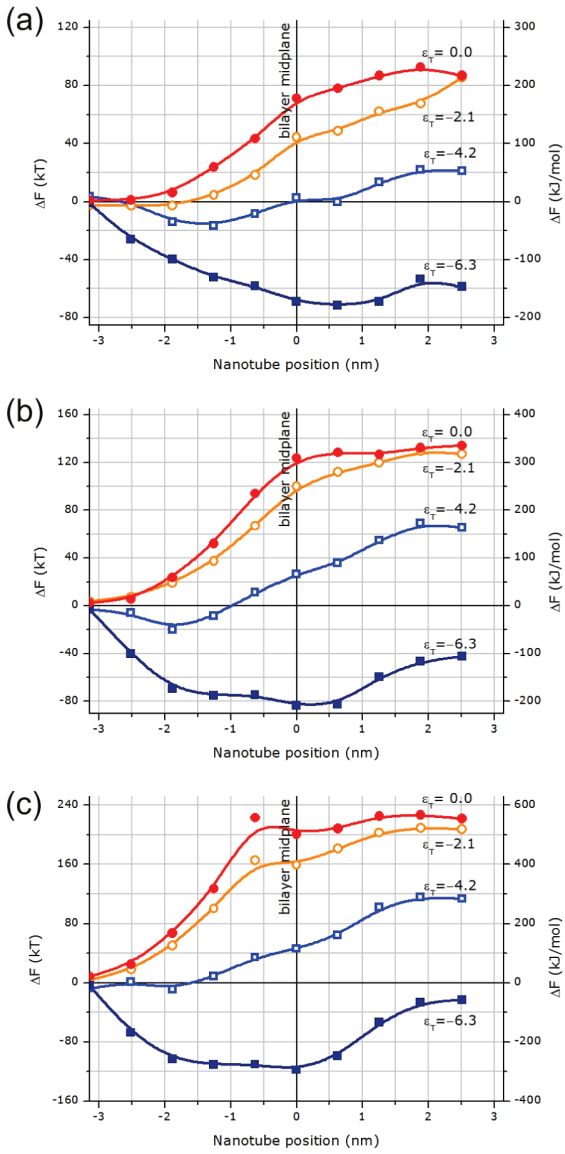

Figure 2. Free energy cost Δ*F versus* nanotube position of SWNTs with diameters 1 (a), 2.43 (b), and 4.86 nm (c) and different interaction parameters with the hydrophobic core of the phospholipid bilayer, ε_T.

when the hydrophobic bottom of the cylinder has maximum contacts with the phospholipid tails. It is noteworthy, that this minimum indicates that the perpendicular position of the hydrophobic nanotube would be less favorable than the parallel insertion into the core of the bilayer when the SWNT can have even a larger number of contacts with the phospholipid tails. The corresponding free energy would be even more negative. The intermediate interaction parameters lead to mixed behavior, the energy gain at a partial insertion, and the energy lost at a full insertion.

Inserted nanotube induces structural changes in the phospholipid bilayer. The SCMF theory allows to visualize the equilibrium structure of the bilayer at each position of the nanotube *via* equilibrium concentration profiles (see Figure 3). One can see how the increasing hydrophobicity of the SWNT changes the character of the interaction with the bilayer and the structural changes around the SWNT. In the case of steric repulsion ($\varepsilon_T = 0.0$ kT), the cylinder compresses the bilayer, and the tails tend to hide from the nanotube and the solvent, however, hydrophobic SWNTs ($\varepsilon_T = -2.1$, -4.2, and -6.3 kT) attract hydrophobic core of the layer which tends to stick to the edges of the nanotube. The surface of the bilayer even lifts up in order to stick to the nanotube and increase the area of contact between the SWNT and the hydrophobic tails of the lipids. This is consistent with the corresponding decrease of the free energy upon insertion of the SWNT observed in Figure 2. Full insertion of the nanotube leads to the pore formation. The energy of the pore formation as well as the structure of the pore strongly depends on the hydrophobicity of the nanotube ε_T. In the most hydrophilic case, the bilayer core is separated from the nanotube by the layer of heads, while in the most hydrophobic case, $\varepsilon_T = -6.3$ kT, the tails touch the surface of the nanotube, and one can observe the wetting of the nanotube with a pronounced rim around the nanotube. Figure 3 also provides information about the breakthrough distances. The hydrophilic nanotube creates a pore in the bilayer when it is inserted in the

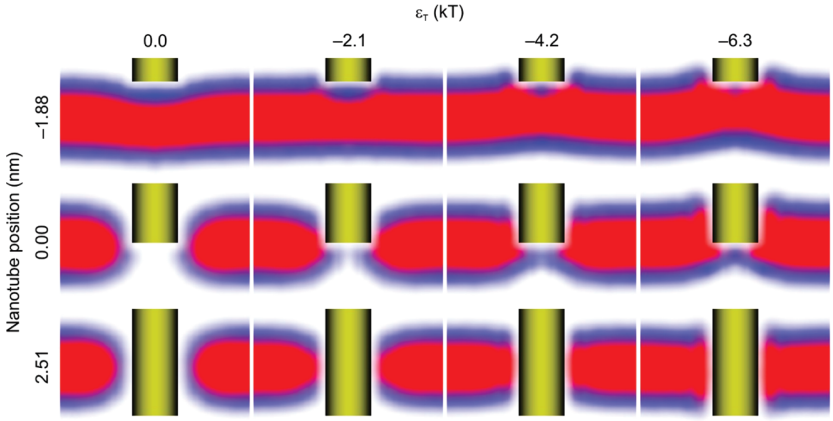

Figure 3. Morphology of the phospholipid bilayer structure induced by the equilibrium insertion of 2.43 nm SWNT for different interaction parameters between the nanotube and the hydrophobic core, ε_T.

TABLE 1. Free Energy Change Due to Full Insertion of the SWNT, ΔF_{full}, the Minimum Free Energy, ΔF_{min}, the Insertion Distance Corresponding to the Minimum of the Free Energy, d_{min} and the Maximal Force to Be Applied to Pierce the Bilayer

diameter	1.00 nm				2.43 nm				4.46 nm			
ε_T (kT)	0.0	−2.1	−4.2	−6.3	0.0	−2.1	−4.2	−6.3	0.0	−2.1	−4.2	−6.3
ΔF_{full} (kT)	87.3	85.9	21.2	− 59.1	134.5	127.4	65.6	− 42.7	222.8	208.1	113.7	− 23.3
ΔF_{min} (kT)	0.8	−3.0	−16.7	−72.1	2.3	3.8	−20.3	−83.8	8.6	3.5	−9.0	−118.6
d_{min} (nm)	−3.14	−2.51	−1.25	0.63	−3.14	−3.14	−1.88	0.00	−3.14	−3.14	−1.88	0.00
max. force (pN)	157	132	74	61	237	206	116	120	517	381	184	241

middle of the bilayer, in turn, hydrophobic nanotubes have to cross almost the full thickness of the bilayer before piercing it. This behavior is consistent with a similar observation in experiments of AFM tip insertion in 1-stearoyl-2-oleoylphosphatidylcholine (SOPC)/cholesterol bilayers.[52]

The numerical values of the free energy cost of translocation through the bilayer are summarized in Table 1. The energy cost to cross the bilayer is quite high for all diameters and interaction parameters (hundreds of kT). Hydrophilic nanotubes have a positive energy barrier, which may be difficult to overcome by thermal motion, while the attraction between hydrophobic nanotubes and phospholipid tails is high enough to entrap the nanotubes in the core of the bilayer. Nanotubes with intermediate hydrophobicity exhibit both effects, steric repulsion due to the pore formation and the enthalpic attraction to the core of the bilayer. Thus, the nanotubes with intermediate parameters will have to cross both barriers, and the resulting energy cost is the sum of the two barriers. Furthermore, the perpendicular orientation of the nanotube has the lowest energy cost for penetration through the layer. This orientation is not necessary the equilibrium one. For example, the hydrophobic nanotube would preferentially orient itself parallel to the layer in the hydrophobic core, where the nanotube would have more contacts with the core. This orientation will have much lower energies, which are proportional to its length. Thus, we would expect that hydrophobic nanotubes with $\varepsilon_T = -4.2$ and -6.3 kT should stick in the hydrophobic core in a parallel orientation. In turn, hydrophilic nanotubes in a parallel orientation will have more steric contacts with both types of phospholipid beads. Thus, the positive barrier would be higher. The translocation through the bilayer also implies the diffusion of the nanotube in a correct orientation close to the bilayer. This would require additional time, thus effectively increasing the energy barrier.

High values of the energy barrier can be understood with the help of a simple estimation. If we consider that the cylinder with the radius $R_{cyl} = 1.2$ nm simply moves apart the lipids and creates a pore with the radius $R_{cyl} + R_{bead}$, where $R_{bead} = 0.4$ nm is the radius of the bead in the phospholipid molecule, then the pore formation energy is due to breaking the contacts between phospholipids lying close to the edge of the pore. Taking into account that the perimeter of the pore is $2\pi(R_{cyl} + R_{bead}) \sim 10$ nm, the area per lipid is 60 Å^2, the energy per lipid due to tail−tail contacts in the three-bead model is ~ -20 kT, and assuming that lipids loose half of the contacts and the membrane is a double layer, we find that the number of lipids at the edge is ~26, *i.e.*, the energy cost for the formation of the pore is ~260 kT, which is comparable by the order of magnitude but higher than the calculated value of 192 kT. The discrepancy is due to contributions of the heads and the rearrangements of the lipids around the pore in order to minimize the energy cost, which does not have a sharp edge. Note, that this energy is comparable with the energy of breaking a chemical bond since typical values of bond energies are also hundreds kT.[53]

The calculated equilibrium force of hundreds of pN corresponds to the energy of hundreds kT, which is an extremely high energy at the molecular level. However, the nanotube can pierce the phospholipid layer if the external force is applied. Carbon nanotubes can be fixed on a AFM tip, and they can be used as "nanoinjectors" or nanoprobes.[47] Such a combination of AFM and carbon nanotube can be used for force measurements. The measurements on living cells[48] have shown that the force of penetration depends on the location over the cell membrane and, possibly, many other factors, especially if the cytoskeleton is involved in the response to the stimulus. The minimal force for piercing of cell membrane measured in these experiments is of order 100 pN, *i.e.*, even higher than suggested by our calculations.

The strength of our method is the direct and accurate calculation of free energies at equilibrium, that allow for judgment about the possibility of spontaneous translocation through the bilayer. The forces obtained in nonequilibrium MD simulations of nanotube penetration with a constant speed[54] are several times higher than in our calculations, and they depend on the speed of pulling, since the layer needs some time to accommodate its structure to the external perturbation. Hence, these calculations at low speed can represent an upper limit for the equilibrium free energy. In contrast, the SCMF method gives directly the equilibrium and the average picture, which does not show the positions of individual phospholipids but the average concentration profiles. That is why our equilibrium

mean field "snapshots" and average concentration profiles look different from the simulation snapshots of nonequilibrium piercing.[54]

The results with different diameters of nanotubes suggest that the thinner a nanotube, the less an energy barrier. Thus, we may conclude that larger objects, such as multiwalled carbon nanotubes composed of several graphitic concentric layers[51] and having diameters more than 4 nm, will have even larger energy barrier, which require the application of an external force to pierce through the bilayer. Finally, an illustration of strong resistance of phospholipid bilayers against piercing is provided in the experiments with microtubules (rigid cylinders of 30 nm in diameter) growing inside the phospholipid vesicles.[55] Growing microtubule exert force on the inner wall of the vesicle at both ends, which leads to large deformation of the surface of the vesicle and the buckling of the microtubule.

CONCLUSIONS

The SCMF theory is used for accurate measurements of the energy cost associated with the perpendicular insertion of carbon nanotubes of different diameters in the phospholipid bilayer. This method gives direct access to the equilibrium free energy and provides microscopic information about the structural rearrangements of the phospholipid bilayer around the inserted nanotubes. This information, though obtained for model dimyristoyl phosphatidylcholine (DMPC) phospholipid bilayers, may contribute to the discussion of the possible mechanisms of translocation of single-walled carbon nanotubes (SWNTs) into cells. In particular, it reflects on the inferred mechanism of spontaneous translocation of SWNTs through phospholipid bilayers by thermal motion.

Our results suggest that hydrophilic or noninteracting SWNTs would require an energy of order of hundreds of kT to cross the phospholipid bilayer in perpendicular orientation. Furthermore, perpendicular orientation is less disruptive for the bilayer, and thus, other orientations would require even higher energies. In turn, more hydrophobic, interacting SWNTs are attracted by the hydrophobic cores, what hinders their translocation through the bilayers and renders difficult the separation of the nanotube from the bilayer simply by thermal motion. Thus, our results for model phospholipid bilayers may suggest that experimentally observed translocation of SWNTs into cells is probably due to other energy-dependent translocation mechanisms, such as, for example, endocytosis.

These results for homogeneous nanotubes may also indicate the ways to reduce the energy cost of translocation through the phospholipid bilayers. For example, inhomogeneous patterning of the nanotube surface can help in design of nano-objects which can freely pass through or preferentially associate with the phospholipid bilayers.

The predicted energy of the bilayer rupture due to the perpendicular insertion of a carbon nanotube can be directly verified by the force measurements of the insertion of the AFM tip functionalized with a carbon nanotube.

METHODS

Single Chain Mean Field Theory. The single-chain mean field (SCMF) theory describes a single molecule surrounded by the mean fields.[42−44,46] It takes explicitly into account the structure of an individual molecule at a coarse-grained level similar to coarse-grained MC or MD simulations. However, as distinct from simulations, the interactions of the molecule with the environment are described through the mean molecular fields. The mean fields determine the most probable conformations of the molecule through the probabilities of individual molecule. In turn, the mean fields are calculated as the average properties of individual conformations. This self-consistence closure defines the set of nonlinear equations that can be solved numerically. The solution of such equations gives the equilibrium structures and the concentration profiles of all components in the system as well as the most probable conformations of individual molecules.

To model the phospholipid bilayer we use the three-bead model of the DMPC phospholipid molecule described in ref 46. The phospholipid molecule is modeled as three spherical beads of diameter $d = 0.81$ nm, joined consequently by stiff bonds of 1.0 nm in length: two hydrophobic, T-beads, representing the tails, and one hydrophilic, H-bead, representing the phospholipid head. The angle between the bonds is free to bend as long as the terminal beads do not intersect each other. The solvent molecule is modeled as a S-bead of the same diameter as the phospholipid beads. The interactions between the beads in this model are given only by two square well potentials with interaction range $r_{int} = 1.215$ nm and depths $\varepsilon_{TT} = -2.10$ kT and $\varepsilon_{HS} = -0.15$ kT for T−T and H−S contacts, respectively. Additional energy is assigned to the T-beads residing at a distance shorter than 8.10 nm from the surface of the cylinder, ε_T (see Table 1). The simulation box 10.00 × 10.00 × 6.27 nm (12.00 × 12.00 × 6.27 nm for the case of the largest nanotube's diameter) is discretized into a grid according to 2D cylindrical geometry with the symmetry axis placed in the center of the box and oriented along the *z*-axis. The grid cells are about 0.5 and 0.3 nm in the radial and vertical directions (comparable with the diameters of the beads in the 3-beads model, 0.81 nm), and the sampling of the molecule conformational space is 400 000 conformations. A series of test calculations have shown that these parameters give enough precision for the energy calculations.

We use the generalized equations of the SCMF method provided in ref 46 which describes the self-assembly of a mixture of an arbitrary number of types of molecules of an arbitrary structure. First step of the SCMF method is the generation of the representative sampling $\{\Gamma\}$ of conformations of a single molecule, where the conformations differ in position and orientation of the molecule in the space and the angle between the bonds of the molecule. If the sampling was generated with a bias, it is corrected with a known weight of each conformation $w(\Gamma)$. The probability of a given conformation Γ of the molecule, placed in the simulation box, containing N lipids is given by[46]

$$\rho(\Gamma) = \frac{1}{Zw(\Gamma)}\exp\left(-H^{intra}(\Gamma) - (N-1)\sum_i \varepsilon_i^T(\Gamma)c_i^T - \sum_i \varepsilon_i^S(\Gamma)\frac{\varphi_i^S}{v_s} + \sum_i V_i\,\lambda_i\,\varphi_i(\Gamma)\right) \quad (4)$$

where Z is the normalization constant, $H^{intra}(\Gamma)$ is the internal energy of the conformation Γ, where we include, as well, its interaction with the nanotube. The simulation box is discretized into a grid cells i of the volume V_i. The interactions of the beads with the fields (c_i^T and c_i^H are the equilibrium concentrations of the beads of each type) are described through interaction fields of a given conformation, $\varepsilon_i^T(\Gamma)$ and $\varepsilon_i^S(\Gamma)$. The Lagrange multiplier λ_i is related to the total volume fraction of the cell i occupied by the solvent, ϕ_i^S *via* $v_s\lambda_i = \ln \phi_i^S + N\varepsilon_i^H c_i^H$, where v_s is the volume of the solvent molecule, and $\varepsilon_i^H = (4/3)\pi(r_{int}^3 - d^3)\,\varepsilon_{HS}$. The condition of local incompressibility relate ϕ_i^S with the volume fraction of the lipids ϕ_i *via* $\phi_i^S + N\phi_i = \phi_0$, where ϕ_0 is the maximal volume fraction occupied by the solvent and all the molecules (equal to 0.675 in this model).[46]

Once the probabilities of the conformations $\rho(\Gamma)$ are known, the molecular mean fields, namely the volume fractions of the molecules and concentrations of the beads of all types, are calculated as averages over all conformations:

$$\phi_i = \sum_{\{\Gamma\}} \phi_i(\Gamma)\rho(\Gamma) \quad (5)$$

$$c_i^{T(H)} = \sum_{\{\Gamma\}} c_i^{T(H)}(\Gamma)\rho(\Gamma) \quad (6)$$

These equations, eqs 4, 5, and 6, define the closed set of nonlinear equations for the probabilities of conformations and the mean fields. Solution of these equations gives the equilibrium properties of the system and the equilibrium free energy of the simulation box, which is written[46] in units kT, as

$$F_{box} = N\langle \ln N\rho(\Gamma)w(\Gamma)\kappa\rangle + \sum_i V_i \frac{\phi_i^S}{v_s} \ln \frac{\phi_i^S}{v_s} + N\langle H^{intra}(\Gamma)\rangle + \frac{1}{2}N(N-1)\sum_i \langle \varepsilon_i^T(\Gamma)\rangle c_i^T + N\sum_i \langle \varepsilon_i^S(\Gamma)\rangle \frac{\phi_i^S}{v_s} \quad (7)$$

where κ is the number of conformations in the sampling $\{\Gamma\}$ and all the averages, denoted by angular brackets are taken as averages over the sampling with probabilities $\rho(\Gamma)$ in analogy to eqs 5 and 6.

The calculation time of one point in the energy curve and full set of microscopic data of the bilayer configuration takes less than 1 day on a single 32-core machine. This time can be drastically decreased by taking advantage of the high capability of parallelization of the SCMF method, which allows the use of more computers and processors.

Acknowledgment. The authors wish to thank Prof. Nigel Slater from Cambridge University for useful discussions, suggestions, comments, and collaboration within the U.K. Royal Society International Joint Project with Cambridge University. We acknowledge the financial help from Spanish Ministry of education MICINN *via* the project CTQ2008-06469/PPQ.

Supporting Information Available: Structural changes in the phospholipid bilayer induced by the equilibrium insertion of a carbon nanotube for different distances of a nanotube from the bilayer midplane. This material is available free of charge *via* the Internet at http://pubs.acs.org/.

REFERENCES AND NOTES

1. Alberts, B. *Molecular Biology of the Cell*, 5th ed.; Garland Science: New York, 2008.
2. Yeagle, P. L. *The Structure of Biological Membranes*, 2nd ed.; CRC Press: Boca Raton, FL, 2005.
3. Tanford, C. The Hydrophobic Effect and the Organization of Living Matter. *Science* **1978**, *200*, 1012–1018.
4. Cooper, G. M.; Hausman, R. E. *The Cell: a Molecular Approach*, 5th ed.; Sinauer Associates Inc.: Sunderland, MA, 2009.
5. Tew, G. N.; Liu, D.; Chen, B.; Doerksen, R. J.; Kaplan, J.; Carroll, P. J.; Klein, M. L.; DeGrado, W. F. De Novo Design of Biomimetic Antimicrobial Polymers. *Proc. Natl. Acad. Sci. U.S.A.* **2002**, *99*, 5110–5114.
6. Stewart, K. M.; Horton, K. L.; Kelley, S. O. Cell-Penetrating Peptides As Delivery Vehicles for Biology and Medicine. *Org. Biomol. Chem.* **2008**, *6*, 2242–2255.
7. Moghimi, S. M.; Hunter, A. C.; Murray, J. C. Nanomedicine: Current Status and Future Prospects. *FASEB J.* **2005**, *19*, 311–330.
8. Kamada, H.; Okamoto, T.; Kawamura, M.; Shibata, H.; Abe, Y.; Ohkawa, A.; Nomura, T.; Sato, M.; Mukai, Y.; Sugita, T.; et al. Creation of Novel Cell-Penetrating Peptides for Intracellular Drug Delivery Using Systematic Phage Display Technology Originated from Tat Transduction Domain. *Biol. Pharm. Bull.* **2007**, *30*, 218–223.
9. Pack, D. W.; Hoffman, A. S.; Pun, S.; Stayton, P. S. Design and Development of Polymers for Gene Delivery. *Nature* **2005**, *4*, 581–593.
10. Jenssen, H.; Hamill, P.; Hancock, R. E. W. Peptide Antimicrobial Agents. *Clin. Microbiol. Rev.* **2006**, *19*, 491–511.
11. Brogden, K. A. Antimicrobial Peptides: Pore Formers or Metabolic Inhibitors in Bacteria. *Nature* **2005**, *3*, 238–250.
12. Hancock, R. E. W.; Sahl, H.-G. Antimicrobial and Host-Defense Peptides as New Anti-Infective Therapeutic Strategies. *Nat. Biotechnol.* **2006**, *24*, 1551–1557.
13. Plank, C.; Zauner, W.; Wagner, E. Application of Membrane-Active Peptides for Drug and Gene Delivery across Cellular Membranes. *Adv. Drug Delivery Rev.* **1998**, *34*, 21–35.
14. Porter, A. E.; Gass, M.; Muller, K.; Skepper, J. N.; Midgley, P. A.; Welland, M. Direct Imaging of Single-Walled Carbon Nanotubes in Cells. *Nature Nanotechnol.* **2007**, *2*, 713–717.
15. Porter, A. E.; Gass, M.; Bendall, J. S.; Muller, K.; Goode, A.; Skepper, J. N.; Midgley, P. A.; Welland, M. Uptake of Noncytotoxic Acid-Treated Single-Walled Carbon Nanotubes into the Cytoplasm of Human Macrophage Cells. *ACS Nano* **2009**, *3*, 1485–1492.
16. Khodakovskaya, M.; Dervishi, E.; Mahmood, M.; Xu, Y.; Li, Z.; Watanabe, F.; Biris, A. S. Carbon Nanotubes are Able to Penetrate Plant Seed Coat and Dramatically Affect Seed Germination and Plant Growth. *ACS Nano* **2009**, *3*, 3221–3227.
17. Cherukuri, P.; Bachilo, S. M.; Litovsky, S. H.; Weisman, R. B. Near-Infrared Fluorescence Microscopy of Single-Walled Carbon Nanotubes in Phagocytic Cells. *J. Am. Chem. Soc.* **2004**, *126*, 15638–15639.
18. Kam, N. W. S.; Jessop, T. C.; Wender, P. A.; Dai, H. Nanotube Molecular Transporters: Internalization of Carbon Nanotube-Protein Conjugates into Mammalian Cells. *J. Am. Chem. Soc.* **2004**, *126*, 6850–6851.
19. Kam, N. W. S.; Dai, H. Carbon Nanotubes As Intracellular Protein Transporters: Generality and Biological Functionality. *J. Am. Chem. Soc.* **2005**, *127*, 6021–6026.
20. Kam, N. W. S.; Liu, Z.; Dai, H. Carbon Nanotubes As Intracellular Transporters for Proteins and DNA: An Investigation of the Uptake Mechanism and Pathway. *Angew. Chem., Int. Ed.* **2006**, *45*, 577–581.
21. Kam, N. W. S.; Dai, H. Single Walled Carbon Nanotubes for Transport and Delivery of Biological Cargos. *Phys. Status Solidi B* **2006**, *243*, 3561–3566.
22. Pantarotto, D.; Briand, J.-P.; Prato, M.; Bianco, A. Translocation of Bioactive Peptides across Cell Membranes by Carbon Nanotubes. *Chem. Commun.* **2004**, *1*, 16–17.
23. Pantarotto, D.; Singh, R.; McCarthy, D.; Erhardt, M.; Briand, J.-P.; Prato, M.; Kostarelos, K.; Bianco, A. Functionalized Carbon Nanotubes for Plasmid DNA Gene Delivery. *Angew. Chem., Int. Ed.* **2004**, *43*, 5242–5246.
24. Liu, Q.; Chen, B.; Wang, Q.; Shi, X.; Xiao, Z.; Lin, J.; Fang, X. Carbon Nanotubes as Molecular Transporters for Walled Plant Cells. *Nano Lett.* **2009**, *9*, 1007–1010.
25. Lu, Q.; Moore, J. M.; Huang, G.; Mount, A. S.; Rao, A. M.; Larcom, L. L.; Ke, P. C. RNA Polymer Translocation with Single-Walled Carbon Nanotubes. *Nano Lett.* **2004**, *4*, 2473–2477.

26. Raffa, V.; Ciofani, G.; Nitodas, S.; Karachalios, T.; DŠAlessandro, D.; Masinie, M.; Cuschieri, A. Can the Properties of Carbon Nanotubes Influence Their Internalization by Living Cells. *Carbon* **2008**, *46*, 1600–1610.
27. Kam, N. W. S.; O'Connell, M.; Wisdom, J. A.; Dai, H. Carbon Nanotubes As Multifunctional Biological Transporters and Near-Infrared Agents for Selective Cancer Cell Destruction. *Proc. Natl. Acad. Sci. U.S.A.* **2005**, *102*, 11600–11605.
28. Lamprecht, C.; Liashkovich, I.; Neves, V.; Danzberger, J.; Heister, E.; Rangl, M.; Coley, H. M.; McFadden, J.; Flahaut, E.; Gruber, H. J.; et al. AFM Imaging of Functionalized Carbon Nanotubes on Biological Membranes. *Nanotechnology* **2009**, *20*, 434001.
29. Miaczynska, M.; Stenmark, H. Mechanisms and Functions of Endocytosis. *J. Cell Biol.* **2008**, *180*, 7–11.
30. Goetz, R.; Lipowsky, R. Computer Simulations of Bilayer Membranes: Self-Assembly and Interfacial Tension. *J. Chem. Phys.* **1998**, *108*, 7397–7409.
31. Tieleman, D.; Marrink, S.; Berendsen, H. A computer Perspective of Membranes: Molecular Dynamics Studies of Lipid Bilayer Systems. *Biochim. Biophys. Acta* **1997**, *1331*, 235–270.
32. Damodaran, K.; Kenneth, M.; Merz, J.; Gaber, B. Structure and Dynamics of the Dilauroylphosphatidylethanolamine Lipid Bilayer. *Biochemistry* **1992**, *31*, 7656.
33. Damodaran, K. V.; Merz, K. M. A Comparison of DMPC and DLPE Based Lipid Bilayers. *Biophys. J.* **1994**, *66*, 1076–1087.
34. Smondyrev, A. M.; Berkowitz, M. L. United Atom Force Field for Phospholipid Membranes: Constant Pressure Molecular Dynamics Simulation of Dipalmitoylphosphatidicholine/Water System. *J. Comput. Chem.* **1999**, *20*, 531–545.
35. Robinson, A. J.; Richards, W. G.; Thomas, P. J.; Hann, M. M. Head Group and Chain Behavior in Biological Membranes: A Molecular Dynamics Computer Simulation. *Biophys. J.* **1994**, *87*, 2345–2354.
36. Heller, H.; Schafer, M.; Schulten, K. Molecular Dynamics Simulation of a Bilayer of 200 Lipids in the Gel and in the Liquid-Crystal Phases. *J. Phys. Chem.* **1993**, *97*, 8343.
37. Tuckerman, M.; Berne, B.; Martyna, G. Reversible Multiple Time Scale Molecular Dynamics. *J. Chem. Phys.* **1992**, *97*, 1990.
38. Lyubartsev, A. P. Multiscale Modeling of Lipids and Lipid Bilayers. *Eur. Biophys. J.* **2005**, *35*, 53–61.
39. Hyvonen, M. T.; Rantala, T. T.; Ala-Korpela, M. Structure and Dynamic Properties of Diunsaturated 1 -Palmitoyl-2-Linoleoyl-sn-Glycero-3-Phosphatidylcholine Lipid Bilayer from Molecular Dynamics Simulation. *Biophys. J.* **1997**, *73*, 2907–2923.
40. Muller, M.; Daoulas, K. C. Chapter Accurate Measurement of Free Energies of Self-Assembling Systems by Computer Simulation. *NIC Symposium*; John von Neumann Institute for Computing: Ulich, Germany, 2008; Vol. 39, pp 255−262.
41. Muller, M.; Daoulas, K. C.; Norizoe, Y. Computing Free Energies of Interfaces in Self-Assembling Systems. *Phys. Chem. Chem. Phys.* **2009**, *11*, 2087–2097.
42. Ben-Shaul, A.; Szleifer, I.; Gelbart, W. M. Chain Organization and Thermodynamics in Micelles and Bilayers. I. Theory. *J. Chem. Phys.* **1985**, *83*, 3597–3611.
43. Ben-Shaul, A.; Szleifer, I.; Gelbart, W. M. Chain Statistics in Micelles and Bilayers: Effects of Surface Roughness and Internal Energy. *J. Chem. Phys.* **1986**, *85*, 5345–5359.
44. Al-Anber, Z. A.; Bonet-Avalos, J.; Mackie, A. D. Prediction of the Critical Micelle Concentration in a Lattice Model for Amphiphiles Using a Single-Chain Mean-Field Theory. *J. Chem. Phys.* **2005**, *122*, 104910.
45. Al-Anber, Z. A.; Bonet-Avalos, J.; Floriano, M. A.; Mackie, A. D. Sphere-to-Rod Transitions of Micelles in Model Nonionic Surfactant Solutions. *J. Chem. Phys.* **2003**, *118*, 3816–3826.
46. Pogodin, S.; Baulin, V. A. Coarse-Grained Models of Phospholipid Membranes within the Single Chain Mean Field Theory. *Soft Matter* **2010**, *6*, 2216–2226.
47. Wilson, N. R.; Macpherson, J. V. Carbon Nanotube Tips for Atomic Force Microscopy. *Nature Nanotechnol.* **2009**, *4*, 483–491.
48. Vakarelski, I. U.; Brown, S. C.; Higashitani, K.; Moudgil, B. M. Penetration of Living Cell Membranes with Fortified Carbon Nanotube Tips. *Langmuir* **2007**, *23*, 10893–10896.
49. Franz, V.; Loi, S.; Muller, H.; Bamberg, E.; Butt, H.-J. Tip Penetration through Lipid Bilayers in Atomic Force Microscopy. *Colloids Surf., B* **2002**, *23*, 191–200.
50. Schrlau, M. G.; Bau, H. H. Carbon-Based Nanoprobes for Cell Biology. *Microfluid. Nanofluid.* **2009**, *7*, 439–450.
51. Klumpp, C.; Kostarelos, K.; Prato, M.; Bianco, A. Functionalized Carbon Nanotubes as Emerging Nanovectors for the Delivery of Therapeutics. *Biochim. Biophys. Acta* **2006**, *1758*, 404–412.
52. Almquist, B. D.; Melosh, N. A. Fusion of Biomimetic Stealth Probes into Lipid Bilayer Cores. *Proc. Natl. Acad. Sci. U.S.A.* **2010**, *107*, 5815–5820.
53. Weast, R. C.; Astle, M. J.; Beyer, W. H. *CRC Handbook of Chemistry and Physics*, 65th ed.; CRC Press: Boca Raton, FL, 1984.
54. Wallace, E. J.; Sansom, M. S. P. Blocking of Carbon Nanotube Based Nanoinjectors by Lipids: a Simulation Study. *Nano Lett.* **2008**, *8*, 2751–2756.
55. Elbaum, M.; Fygenson, D. K.; Libchaber, A. Buckling Microtubules in Vesicles. *Phys. Rev. Lett.* **1996**, *76*, 4078–4081.

Surface Patterning of Carbon Nanotubes Can Enhance Their Penetration through a Phospholipid Bilayer

Sergey Pogodin,[†] Nigel K. H. Slater,[‡] and Vladimir A. Baulin[§,†,*]

[†]Departament d'Enginyeria Quimica, Universitat Rovira i Virgili, 26 Av. dels Paisos Catalans, 43007 Tarragona, Spain, [‡]Department of Chemical Engineering and Biotechnology, University of Cambridge, Pembroke Street, Cambridge CB2 3RA, United Kingdom, and [§]ICREA, 23 Passeig Lluis Companys, 08010 Barcelona, Spain

ABSTRACT Nanotube patterning may occur naturally upon the spontaneous self-assembly of biomolecules onto the surface of single-walled carbon nanotubes (SWNTs). It results in periodically alternating bands of surface properties, ranging from relatively hydrophilic to hydrophobic, along the axis of the nanotube. Single-chain mean field (SCMF) theory has been used to estimate the free energy of systems in which a surface patterned nanotube penetrates a phospholipid bilayer. In contrast to unpatterned nanotubes with uniform surface properties, certain patterned nanotubes have been identified that display a relatively low and approximately constant system free energy (<±10 kT) as the nanotube traverses through the bilayer. These observations support the hypothesis that the spontaneous self-assembly of biomolecules on the surface of SWNTs may facilitate nanotube transduction through cell membranes.

KEYWORDS: phospholipid bilayer · carbon nanotubes · translocation mechanism cell membrane

Understanding the mechanism of transduction of carbon nanotubes through cell membranes is a challenging undertaking from many perspectives. Apart from fundamental interest, details of the mechanism may answer questions about the cytotoxicity of nanotubes[1−4] and their potential use as delivery vehicles[5−10] or to probe bilayer properties.[11,12] However, despite considerable effort devoted to this question, a consensus on the mechanism has not yet been reached, and direct evidence of spontaneous translocation of nanotubes through the membranes of cells is still lacking.

In a recent paper, Pogodin and Baulin[13] considered the thermodynamics of a system in which an uncharged nanotube with uniform surface properties penetrates a phospholipid bilayer. A coarse-grained model of the phospholipid molecule was adopted, which had been previously shown to adequately characterize the key thermodynamic properties of a phospholipid bilayer in a fluid phase.[14] Estimates were made of the free energies of the equilibrium states for the system as the nanotube was progressively moved perpendicularly into the bilayer using a numerical implementation of the single-chain mean field (SCMF) theory.[14] The SCMF methodology and three models of the phospholipid bilayer have been discussed in detail in ref 14. The simplest three-bead model of phospholipids has been proved to be successful in describing the thermodynamic properties of the bilayer. In essence it involves a coarse-grained description of the lipid molecule where the monomers are grouped into two types of beads, one hydrophilic representing the polar heads and two hydrophobic representing the tails of the lipid. The size and the interaction parameters of the beads were adjusted to reproduce the essential thermodynamic properties of a fluid phase of the phospholipid bilayer, such as the thicknesses of the layer and the hydrophobic core, the equilibrium area per lipid, and the compressibility constant.[14]

The objective of these calculations was to determine whether nanotubes of various diameters and surface properties might penetrate a bilayer as a consequence of their thermal motion. Thus, nanotubes of 1.00, 2.43, and 4.86 nm diameter were considered, characterized by an energy per contact with the coarse-grained phospholipid tail, ε_T, ranging from 0 (representing steric repulsion) to −6.3 kT, which corresponds to strong hydrophobic attraction. The perpendicular orientation was chosen since this represents the minimum contact area between nanotube and phospholipids per unit depth of penetration and hence the minimum free energy of interaction. An output of the SCMF calculations was the equilibrium free

*Address correspondence to vladimir.baulin@urv.cat.

Received for review October 14, 2010 and accepted December 23, 2010

Published online January 05, 2011
10.1021/nn102763b

energies and the spatial mean field concentration distribution of the phospholipid heads and tails in the bilayer, which varied as a consequence of nanotube penetration. The model thus demonstrated the structural rearrangement of phospholipids at the molecular level that was induced by insertion of the nanotube and the equilibrium free energy change of the system for each position of the nanotube.

In summary, the calculations showed that the free energy change of the system for $\varepsilon_T = -2.1$ kT rose monotonically with increasing nanotube penetration and was substantial at full penetration (*e.g.*, for the 2.43 nm diameter nanotube the free energy of the system at full penetration was about 100 kT). For $\varepsilon_T = -4.2$ kT, and particularly for $\varepsilon_T = -6.3$ kT, the initial penetration of the nanotube resulted in a significant fall in the system free energy (*e.g.*, to *ca.* −80 kT for penetration of a 2.43 nm diameter nanotube with $\varepsilon_T = -6.3$ kT to the center of the bilayer). Further penetration of these nanotubes then led to a steep rise in the system free energy. Overall, the calculations showed that hydrophilic and weakly hydrophobic nanotubes face a substantial energy barrier to penetration, while intermediate and strongly hydrophobic nanotubes penetrate little or become entrapped in a free energy well within the bilayer.

Inferences can be drawn from these calculations for the transduction of cylindrical nano-objects, such as single-walled carbon nanotubes (SWNTs), through the outer membrane of cells. Untreated SWNTs are significantly hydrophobic, and their thermal motion might lead to their accumulation within the core of the cell membrane, but they are unlikely to translocate across the membrane in view of the steep energy barrier that they face to pass out of the membrane core. Hydrophilically functionalized SWNTs, for example, pegylated SWNTs,[15] face a substantial energy barrier in even penetrating the membrane to its core. These thermodynamic calculations create a conundrum since numerous experimental reports exist that show the accumulation of SWNTs within the cytoplasm of cells.[16,17] How may this be?

Unlike the model system that is envisaged in ref 13, the environment around a cell is complex and comprises of diverse biomolecular species that might interact with SWNTs. Indeed, a number of publications have reported the ordered self-assembly of polar lipids,[18,19] single-stranded DNA,[20−22] polysaccharides,[23,24] amphiphilic proteins,[25−27] and even vitamins[28] onto nanotubes. The electrostatics also give rise to the most general patterns on the nanotubes.[29] This self-assembled patterning occurs spontaneously upon mixing the nanotubes with the patterning agent in aqueous solution. The resulting molecular structures commonly take the form of discrete hydrophilic rings along the axis of the nanotube in the case of polar lipids, to helices for polysaccharides and DNA. Thus, in practice, in cell culture systems nanotubes may not have homogeneous surface properties but may display a distinct regular patterning. Furthermore, it is not evident that a nanotube that has been naturally patterned in this way interacts with phospholipid bilayers in a similar manner to a naked nanotube or to a nanotube with a homogeneous adsorption layer. Our point of view is supported by experimental evidence that ordered arrangements of hydrophilic and hydrophobic surface functional groups can alter the penetration of spherical nanoparticles through the cell membranes.[30]

Consider then a patterned hydrophobic nanotube. Along the nanotube the self-assembly of polar lipids (or other biomolecular species) leads to equispaced rings of different relative hydrophobicity to the naked nanotube. Moving along the axis of the nanotube, the surface characteristics alternate periodically, as indicated in Figure 1A. The spatially segregated surface characteristics of such a nanotube are thus substantially different from the uniform surface character assumed in the previous SCMF calculations,[13] and this may influence the free energy change of the system when the nanotube penetrates a phospholipid bilayer. Note that the surface patterning has bigger effect on the translocation through a bilayer than the shape or geometry of nanoparticles,[31] especially for small particles.

Comparison of the energy curves of uniform nanotubes at different positions[13] suggests that alternation of stripes with certain interaction can, in principle, reduce considerably the energy barrier of translocation. For example, two stripes with opposite energies placed together may cancel the contribution of each other. Since the thickness of the hydrophobic core is about 2 nm, the width of alternating stripes in this case should be of the order of 1 nm so that the core is in contact simultaneously with two opposite stripes. Two distinct patterns were considered for a 1 nm diameter nanotube (Figure 1A, S1 and S2) that differ only in the relative widths of the two sets of rings (*i.e.*, whereas B = 1.00 nm for S1, D = 0.90 nm and E = 1.10 nm for S2). Both S1 and S2 are characterized by alternating rings of interaction energy $\varepsilon_T = -2.1$ and -6.3 kT, respectively. A larger nanotube of diameter 2.43 nm was also considered. In this case, five different patterns were considered (Figure 1A, L1−L5). The effect of the bottom of the nanotube was also investigated, and L4 and L5 only differ in the interaction of the bottom part, while P1 has an edge with the same interaction parameter as L4. The corresponding concentration profiles of nanotubes with similar patterns, S2, P1, L4, and L5, are shown in Figure 1B. We emphasize that these patterns are purely representative, and their dimensions and energies are not those for any specific biomolecular system.

The concentration profiles for the patterns L1−L3 look identical, while the energy of penetration of these patterns is quite different. This is because the same

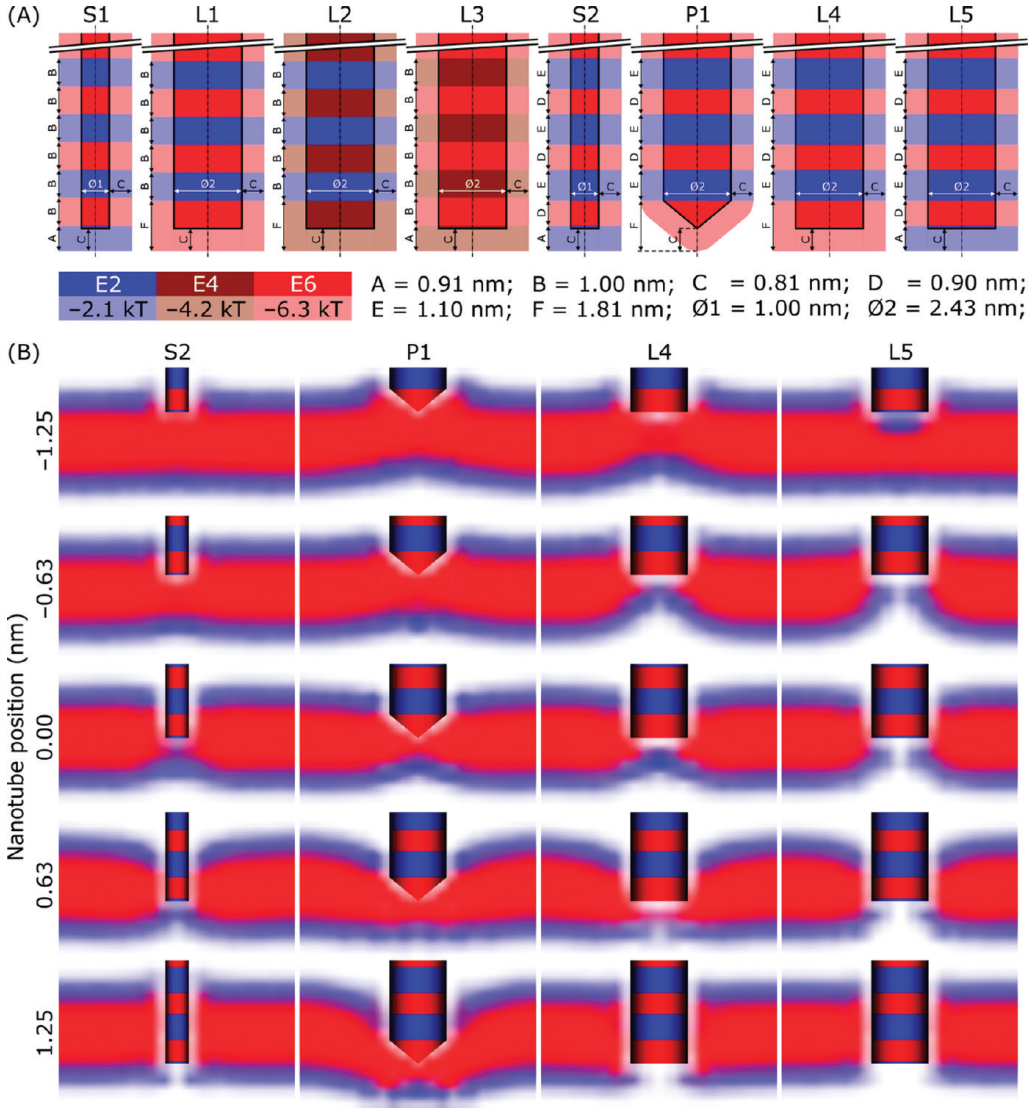

Figure 1. (A) Possible patterns of carbon nanotubes. Dense colors indicate the magnitude of the interaction parameter with the phospholipid tails, ε_T, for the corresponding section of nanotube. Translucent coloring is provided to indicate the interaction range where the phospholipids feel the attraction. (B) Concentration profiles of the phospholipid bilayer interacting with differently patterned nanotubes. Complete set of concentration profiles is available in Supporting Information Section.

positions of the lipids around the nanotube may lead to different enthalpic contributions. Thus, the snapshots usually provided by MD simulations may not be sufficient to distinguish between different scenarios, while the equilibrium energy of insertion may be crucial for understanding the mechanisms of insertion into phospholipid bilayers.

The free energy of penetration of these variously patterned nanotubes into a coarse-grained representation of a phospholipid bilayer was estimated using a numerical implementation of SCMF, in the manner described by Pogodin and Baulin.[13] The resulting free energies for the small nanotubes are shown in Figure 2. For the nanotube pattern S1 with equisized rings (Figure 1A, S1), the system free energy always lies within the range 0 to −20 kT. Neglecting the end of the nanotube, the mean interaction energy along the length of S1 is −4.2 kT. Comparing S1 with the free energy for penetration of a nanotube with a uniform surface of interaction energy E4 of −4.2 kT (Figure 2, E4), it is evident that no steep energy barrier is encountered by the patterned nanotube. Variation of the relative sizes of the rings (to give Figure 1A, S2) results in the free energy of the system being always within the range less than ±10 kT, allowing relatively unimpeded passage of the nanotube through the bilayer. Note that the oscillations of the energy curve are due to abrupt passage from one stripe to another. However, one can expect that a helical pattern would allow for smooth transition from one minimum to another, similar to

screwdriving. Since the error bar of these curves is about a few kT, this pattern implies a zero energy cost of translocation.

A similar behavior was observed for the larger diameter nanotube (Figure 3A, L1−L3). Judicious choice of patterning (L3) resulted in free energies for penetration within the range −20 to +10 kT with no steep energy barrier. Injudicious patterning (L1 and L2) resulted in free energy profiles that varied significantly with depth of penetration, and both presented very significant energy barriers to penetration. The result for pattern L1 suggests a critical dependence upon the interaction energy of the end face of the nanotube, since the pattern L1 differs from that of a smaller nanotube S1 only insofar as the end face has been changed to the highest hydrophobicity (*cf.* −6.3 and −2.1 kT in L1 and S1, respectively). The free energy profile for L1 is thus similar in characteristic to the uniformly hydrophobic nanotube, though presents a significantly steeper energy barrier to full penetration. For L2 the effect is opposite, the lower hydrophobicity of the end face and rings causes the free energy profile to resemble that of a nanotube of uniformly low hydrophobicity and again presents a steep energy barrier at a relatively low extent of penetration. Finally, the error bars on the point at 0 nm for curve L3 in Figure 3A are included to show the standard error of six separate SCMF calculations for this arrangement and the extent of penetration (approximately 10 kT). The characteristic values of the energies, forces, and pressures for different patterns are summarized in Table 1.

The effect of the end face was investigated in Figure 3B. The pattern of L4, L5, and P1 is similar to a successful patterning of the small nanotube S2, only the end face is different. The larger nanotube L5 has the same end face as S2 and shows no steep energy barrier for penetration, although the energy is slightly shifted to positive values. The same pattern but different end face, L4, results in serious changes in the penetration energy in the beginning of insertion. In fact, the energy curve for L4 follows the curve for homogeneous nanotube E6, which has the same interaction parameter as the end face. In turn, when the nanotubes are fully inserted, the end face does not influence, and the curves L4 and L5 coincide. Modification of the shape of the end of the nanotube does not lead to serious changes. Since our calculations consider equilibrium insertion, only the area of contact of different stripes matters, and the nanotube with sharp tip P1 behaves similar to L4. However, one can expect that the shape of the tip may be important for dynamics of the insertion.

In the calculations reported here, no attempt has been made to determine the optimum surface patterning along the axes of the nanotubes that results in the most uniform system free energy throughout bilayer penetration; this can be done separately for each particular system. Nor have we sought to determine the optimal sets of ε_T's. Rather, calculations have been conducted for discrete patterns of combinations of

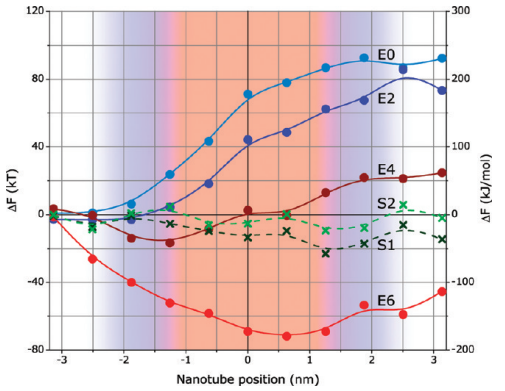

Figure 2. Free energy cost Δ*F versus* nanotube position of patterned SWNTs with diameter 1.00 nm S1 and S2 in comparison with uniform nanotubes with different interaction parameters with the hydrophobic core of the phospholipid bilayer, ε_T.[13] Unperturbed phospolipid bilayer location is indicated by the translucent coloring.

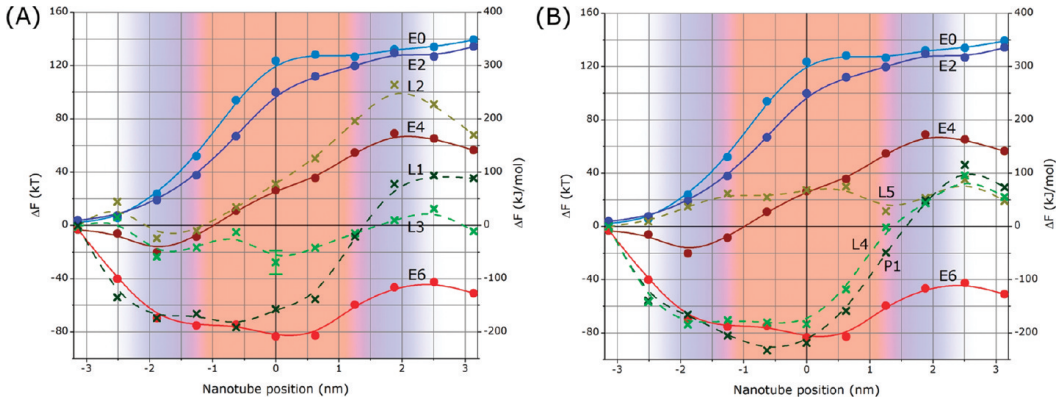

Figure 3. Free energy cost Δ*F versus* nanotube position of SWNTs with diameters 2.43 nm with different patterns, L1−L3 (A), and different end faces, L4, L5, and P1 (B), in comparison to uniform nanotubes with different interaction parameters with the hydrophobic core of the phospholipid bilayer, ε_T.[13] The unperturbed phospolipid bilayer location is indicated by the translucent coloring.

TABLE 1. Energy Cost of Full Insertion, ΔF_{full}, Maximal Amplitude (Positive or Negative) of the Insertion Free Energy, ΔF_{max}, Insertion Distance Corresponding to the Minimum Energy, d_{min}, Maximal Force and Pressure, for Piercing the DMPC Phospholipid Bilayer

	S1	S2	P1	L1	L2	L3	L4	L5
ΔF_{full} (kT)	−15	−2	29	36	68	−4	22	19
ΔF_{max} (kT)	−17	−9	−93	−77	105	−24	−74	37
d_{min} (nm)	1.88	1.25	−0.63	−0.63	−1.88	−1.88	−1.88	−3.14
max. force (pN)	56	51	275	286	184	68	241	78
max. pressure (MPa)	72	64	59	62	40	15	52	17

previously reported ε_T's for homogeneous nanotubes.[13] Nevertheless, for the systems studied, the effect of nanotube patterning had a significant effect upon the system free energy change during bilayer penetration, and some patterns were shown to result in a relatively uniform free energy throughout penetration. In the most preferable case, S2, any free energy barrier to penetration is <10 kT, which is comparable in magnitude to the standard error in the SCMF free energy calculation. Extrapolating these observations to the practical case of cell membrane penetration by SWNTs, it is tempting to speculate that patterning of the tubes by one or by other of the biomolecules that are commonly present in cell culture supernatants may significantly enhance the possibility of their transduction through cell membranes.

Acknowledgment. The authors acknowledge the United Kingdom Royal Society International Joint Project with Cambridge University and the Spanish Ministry of education MICINN project CTQ2008-06469/PPQ.

Supporting Information Available: Concentration profiles of the equilibrium insertion of the patterned carbon nanotubes into phospholipid bilayer are shown for different distances of a nanotube from the bilayer midplane. This material is available free of charge *via* the Internet at http://pubs.acs.org.

REFERENCES AND NOTES

1. Cheng, C.; Muller, K. H.; Koziol, K. K. K.; Skepper, J. N.; Midgley, P. A.; Welland, M. E.; Porter, A. E. Toxicity and Imaging of Multi-Walled Carbon Nanotubes in Human Macrophage Cells. *Biomaterials* **2009,** *30*, 4152–4160.
2. Davoren, M.; Herzog, E.; Casey, A.; Cottineau, B.; Chambers, G.; Byrne, H. J.; Lyng, F. M. Vitro Toxicity Evaluation of Single Walled Carbon Nanotubes on Human A549 Lung Cells. *Toxicol. in Vitro* **2007,** *21*, 438–448.
3. Liu, J.; Hopfinger, A. J. Identification of Possible Sources of Nanotoxicity from Carbon Nanotubes Inserted into Membrane Bilayers Using Membrane Interaction Quantitative Structure-Activity Relationship Analysis. *Chem. Res. Toxicol.* **2008,** *21*, 459–466.
4. Smart, S.; Cassady, A.; Lu, G.; Martin, D. The Biocompatibility of Carbon Nanotubes. *Carbon* **2006,** *44*, 1034–1047.
5. Kam, N. W. S.; Dai, H. Carbon Nanotubes As Intracellular Protein Transporters: Generality and Biological Functionality. *J. Am. Chem. Soc.* **2005,** *127*, 6021–6026.
6. Kam, N. W. S.; Liu, Z.; Dai, H. Carbon Nanotubes As Intracellular Transporters for Proteins and DNA: An Investigation of the Uptake Mechanism and Pathway. *Angew. Chem., Int. Ed.* **2006,** *45*, 577–581.
7. Pantarotto, D.; Briand, J.-P.; Prato, M.; Bianco, A. Translocation of Bioactive Peptides across Cell Membranes by Carbon Nanotubes. *Chem. Commun.* **2004,** *1*, 16–17.
8. Pantarotto, D.; Singh, R.; McCarthy, D.; Erhardt, M.; Briand, J.-P.; Prato, M.; Kostarelos, K.; Bianco, A. Functionalized Carbon Nanotubes for Plasmid DNA Gene Delivery. *Angew. Chem., Int. Ed.* **2004,** *43*, 5242–5246.
9. Klumpp, C.; Kostarelos, K.; Prato, M.; Bianco, A. Functionalized Carbon Nanotubes as Emerging Nanovectors for the Delivery of Therapeutics. *Biochim. Biophys. Acta* **2006,** *1758*, 404–412.
10. Liu, Q.; Chen, B.; Wang, Q.; Shi, X.; Xiao, Z.; Lin, J.; Fang, X. Carbon Nanotubes as Molecular Transporters for Walled Plant Cells. *Nano Lett.* **2009,** *9*, 1007–1010.
11. Balasubramanian, K.; Burghard, M. Biosensors Based on Carbon Nanotubes. *Anal. Bioanal. Chem.* **2006,** *385*, 452–468.
12. Kouklin, N. A.; Kim, W. E.; Lazareck, A. D.; Xu, J. M. Carbon Nanotube Probes for Single-Cell Experimentation and Assays. *Appl. Phys. Lett.* **2005,** *87*, 173901.
13. Pogodin, S.; Baulin, V. A. Can a Carbon Nanotube Pierce through a Phospholipid Bilayer?. *ACS Nano* **2010,** *4*, 5293–5300.
14. Pogodin, S.; Baulin, V. A. Coarse-Grained Models of Phospholipid Membranes within the Single Chain Mean Field Theory. *Soft Matter* **2010,** *6*, 2216–2226.
15. Chattopadhyay, J.; de Jesus Cortez, F.; Chakraborty, S.; Slater, N.; Billups, W. Synthesis of Water-Soluble PEGylated Single-Walled Carbon Nanotubes. *Chem. Mater.* **2006,** *18*, 5864–5868.
16. Porter, A. E.; Gass, M.; Muller, K.; Skepper, J. N.; Midgley, P. A.; Welland, M. Direct Imaging of Single-Walled Carbon Nanotubes in Cells. *Nat. Nanotechnol.* **2007,** *2*, 713–717.
17. Porter, A. E.; Gass, M.; Bendall, J. S.; Muller, K.; Goode, A.; Skepper, J. N.; Midgley, P. A.; Welland, M. Uptake of Noncytotoxic Acid-Treated Single-Walled Carbon Nanotubes into the Cytoplasm of Human Macrophage Cells. *ACS Nano* **2009,** *3*, 1485–1492.
18. Richard, C.; Balavoine, F.; Schultz, P.; Ebbesen, T. W.; Mioskowski, C. Supramolecular Self-Assembly of Lipid Derivatives on Carbon Nanotubes. *Science* **2003,** *300*, 775–778.
19. Thauvin, C.; Rickling, S.; Schultz, P.; Celia, H.; Meunier, S.; Mioskowski, C. Carbon Nanotubes as Templates for Polymerized Lipid Assemblies. *Nat. Nanotechnol.* **2008,** *3*, 743–748.
20. Gigliotti, B.; Sakizzie, B.; Bethune, D. S.; Shelby, R. M.; Cha, J. N. Sequence-Independent Helical Wrapping of Single-Walled Carbon Nanotubes by Long Genomic DNA. *Nano Lett.* **2006,** *6*, 159–164.
21. Tu, X.; Manohar, S.; Jagota, A.; Zheng, M. DNA Sequence Motifs for Structure-Specific Recognition and Separation of Carbon Nanotubes. *Nature* **2009,** *460*, 250–253.
22. Campbell, J. F.; Tessmer, I.; Thorp, H. H.; Erie, D. A. Atomic Force Microscopy Studies of DNA-Wrapped Carbon Nanotube Structure and Binding to Quantum Dots. *J. Am. Chem. Soc.* **2008,** *130*, 10648–10655.
23. Zhang, X.; Meng, L.; Lu, Q. Cell Behaviors on Polysaccharide-Wrapped Single-Wall Carbon Nanotubes: A Quantitative Study of the Surface Properties of Biomimetic Nanofibrous Scaffolds. *ACS Nano* **2009,** *3*, 3200–3206.
24. Numata, M.; Asai, M.; Kaneko, K.; Bae, A.-H.; Hasegawa, T.; Sakurai, K.; Shinkai, S. Inclusion of Cut and As-Grown Single-Walled Carbon Nanotubes in the Helical Superstructure of Schizophyllan and Curdlan (betta-1,3-Glucans). *J. Am. Chem. Soc.* **2005,** *127*, 5875–5884.

25. Dieckmann, G. R.; Dalton, A. B.; Johnson, P. A.; Razal, J.; Chen, J.; Giordano, G. M.; Munoz, E.; Musselman, I. H.; Baughman, R. H.; Draper, R. K. Controlled Assembly of Carbon Nanotubes by Designed Amphiphilic Peptide Helices. *J. Am. Chem. Soc.* **2003,** *125*, 1770–1777.
26. Dalton, A. B.; Ortiz-Acevedo, A.; Zorbas, V.; Brunner, E.; Sampson, W. M.; Collins, S.; Razal, J. M.; Yoshida, M. M.; Baughman, R. H.; Drapper, R. K.; et al. Hierarchical Self-Assembly of Peptide-Coated Carbon Nanotubes. *Adv. Funct. Mater.* **2004,** *14*, 1147–1151.
27. Zorbas, V.; Ortiz-Acevedo, A.; Dalton, A. B.; Yoshida, M. M.; Dieckmann, G. R.; Draper, R. K.; Baughman, R. H.; Jose-Yacaman, M.; Musselman, I. H. Preparation and Characterization of Individual Peptide-Wrapped Single-Walled Carbon Nanotubes. *J. Am. Chem. Soc.* **2004,** *126*, 7222–7227.
28. Ju, S.-Y.; Doll, J.; Sharma, I.; Papadimitrakopoulos, F. Selection of Carbon Nanotubes with Specific Chiralities Using Helical Assemblies of Flavin Mononucleotide. *Nat. Nanotechnol.* **2008,** *3*, 356–362.
29. Vernizzi, G.; Kohlstedt, K. L.; Olvera de la Cruz, M. The Electrostatic Origin of Chiral Patterns on Nanofibers. *Soft Matter* **2009,** *5*, 736–739.
30. Verma, A.; Uzun, O.; Hu, Y.; Hu, Y.; Han, H.-S.; Watson, N.; Chen, S.; Irvine, D. J.; Stellacci, F. Surface-Structure-Regulated Cell-Membrane Penetration by Monolayer-Protected Nanoparticles. *Nat. Mater.* **2008,** *7*, 588–595.
31. Yang, K.; Ma, Y.-Q. Computer Simulation of the Translocation of Nanoparticles with Different Shapes across a Lipid Bilayer. *Nat. Nanotechnol.* **2010,** *5*, 579–583.

Biomolecule Surface Patterning May Enhance Membrane Association

Sergey Pogodin,[†] Nigel K. H. Slater,[‡] and Vladimir A. Baulin[†,§,*]

[†]Departament d'Enginyeria Quimica, Universitat Rovira i Virgili, 26 Av. dels Paisos Catalans, 43007 Tarragona, Spain, [‡]Department of Chemical Engineering and Biotechnology, University of Cambridge, Pembroke Street, Cambridge CB2 3RA, United Kingdom, and [§]ICREA, 23 Passeig Lluis Companys, 08010 Barcelona, Spain.

ABSTRACT Under dehydration conditions, amphipathic late embryogenesis abundant proteins fold spontaneously from a random conformation into α-helical structures, and this transition is promoted by the presence of membranes. To gain insight into the thermodynamics of membrane association, we model the resulting α-helical structures as infinite rigid cylinders patterned with hydrophobic and hydrophilic stripes oriented parallel to their axis. Statistical thermodynamic calculations using single chain mean field theory show that the relative thickness of the stripes controls the free energy of interaction of the α-helices with a phospholipid bilayer, as does the bilayer structure and the depth of the equilibrium penetration of the cylinders into the bilayer. The results may suggest the optimal thickness of the stripes to mimic the association of such protein with membranes.

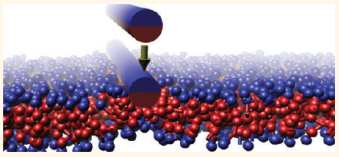

KEYWORDS: phospholipid bilayer · cell membrane · LEA proteins · desiccation stress proteins · membrane activity

Certain biological molecules interact with cell membranes to affect some functional properties. Late embryogenesis abundant (LEA) proteins are an example of such molecules. These proteins are expressed in plant and some animal cells in response to desiccation conditions, and they increase the ability of such cells to withstand desiccation stress.[1] They are widespread among higher plants but have also been found in some microorganisms and nematodes exposed to water deficit.[2] LEA proteins may exist in the form of random coils[3,4] and can spontaneously self-assemble into α-helices upon desiccation stress.[5] Such an α-helix structure in turn provides an ordered pattern of alternating hydrophilic and hydrophobic stripes that run along the axis of the helix,[3] which may facilitate the interaction and insertion of the protein into the phospholipid membrane. Recently, Popova *et al.*[6] have shown that the fraction of LEA7 protein that takes up the α-helix conformation is increased when it is dried in the presence of liposomes, indicating that phospholipid membranes associate closely with LEA proteins and play a critical role in stabilizing their α-helix conformation. LEA proteins are amphiphilic and when in the α-helix conformation can be approximately described as solid rods with a distinct axial arrangement of hydrophilic and hydrophobic stripes. An entirely distinct class of membrane-active peptides, pore-forming peptides,[7] also have surface patterning with a hydrophilic stripe along the backbone of an α-helix. However, the mechanism of association of these proteins with the phospholipid membrane is very different. Membrane pores are formed due to the concerted self-assembly of several peptides on the membrane with a preferential orientation of peptides perpendicular to the bilayer plane; the so-called "Barrel and Stave" mechanism.[8] To allow for such an orientation, the length of the pore-forming peptides does not usually exceed the thickness of the bilayer.[9,10] In contrast, LEA proteins adopt a more random structure and are much longer.[11] As a consequence, they lie as single molecules parallel to the surface of the membrane bilayer. The hydrophobic groups on the side of the backbone control the depth of insertion of the LEA proteins into the bilayer.

To gain insight into the factors that influence the interaction of such a rod with a phospholipid bilayer, we have calculated the free energy of association as a function of stripe geometry and position of the rod relative to the center of the bilayer.

In a previous paper,[12] we showed that single chain mean field (SCMF) theory could be used to calculate the equilibrium structures for insertion of a hydrophobically patterned rod into a phospholipid bilayer with the rod axis oriented perpendicular to the layer. These calculations aimed to determine the effect of patterning upon the puncture of the bilayer by the rod. Here, equilibrium structures of association of a hydrophobically patterned rod with a bilayer

* Address correspondence to vladimir.baulin@urv.cat.

Received for review October 24, 2011 and accepted January 12, 2012.

Published online
10.1021/nn204736b

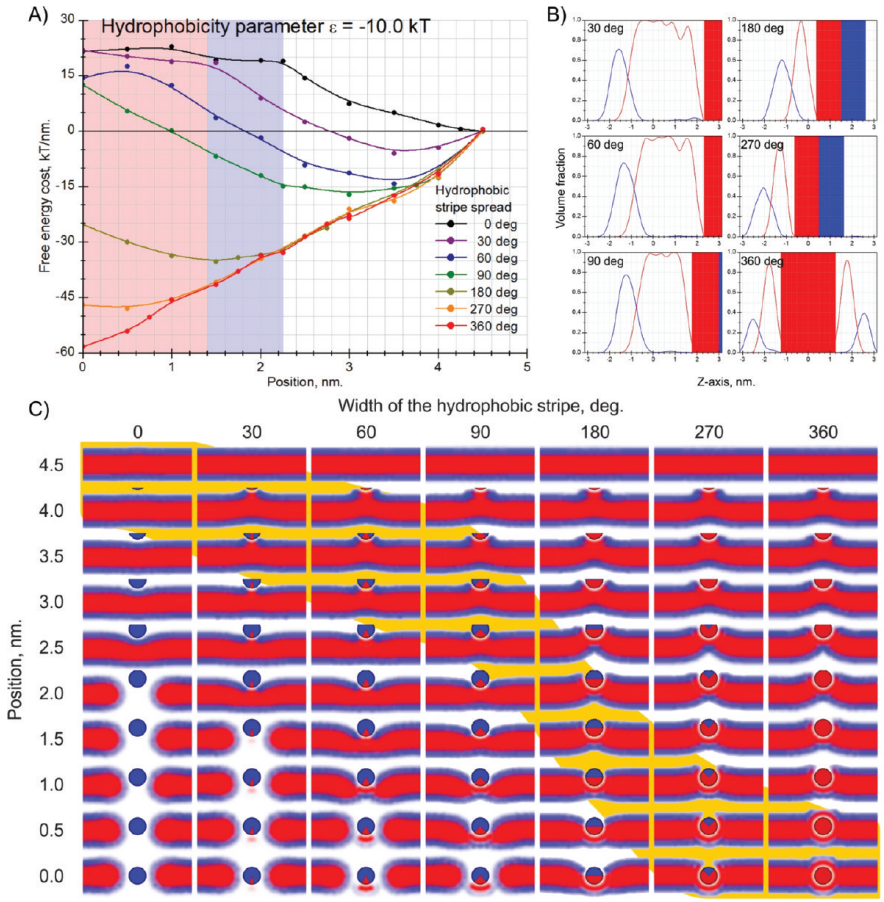

Figure 1. Insertion of a hydrophilic cylinder, $\varepsilon = 0$, with a hydrophobic stripe, $\varepsilon = -10$ kT, into phospholipid bilayer. (A) Free-energy cost of insertion of cylinders with different width of the hydrophobic stripe (in degrees) as a function of the center position. (B) Concentration profiles of tails (red lines) and heads (blue lines) in the central cross section. Red and blue stripes represent the cylinder with corresponding stripes. (C) Perturbation of the bilayer (blue, heads H; red, tails T) upon insertion of the cylinder. The pink and blue areas at the background show the regions of hydrophobic core and hydrophilic surface of the unperturbed bilayer. Yellow band represents the minimum of the free energy (A), which corresponds to the equilibrium position of the cylinder.

are simulated with the rod axis oriented parallel to the layer. These calculations aim to mimic the behavior of moieties such as LEA proteins that may associate with, but not puncture, bilayers.

RESULTS AND DISCUSSION

Equilibrium structures of a rigid rod inside a phospholipid bilayer are simulated within the SCMF theory.[13] A phospholipid molecule is represented at a coarse-grained level within the three-bead model,[13] which is found to describe adequately the mechanical properties of the phospholipid bilayer at equilibrium. The infinite rod lying parallel to the bilayer represents the excluded area for the lipids and water molecules, while the interactions between phospholipids in the bilayer are described through the mean fields. The results of SCMF calculations are presented in Figure 1 and Figure 2. The free-energy differences are calculated per unit cylinder length and neglect end effects. This approximation of infinitely long cylinder is reasonable for cylinders in which the lateral surface area is much larger than the end-cap area. The interaction of lipids with the cylinder are described by a single parameter ε that is the energy of interaction of phospholipid tails T with the surface of the cylinder: $\varepsilon = 0$ implies only steric repulsion, while negative values reflect the attraction of T beads to the surface of the cylinder.

Insertion of a completely hydrophilic cylinder, $\varepsilon = 0$, into a bilayer is energetically unfavorable (black lines in Figure 1A and Figure 2A). The energy penalty increases with the length of the cylinder. The hydrophilic cylinder compresses the bilayer at small penetrations and breaks it at distances about 2.0−2.5 nm from the center. The insertion free energy increases monotonously with depth of penetration and reaches a plateau of height 21.0 ± 2.0 kT/nm. The rupture of the bilayer is similar to a first-order transition in the bulk. Two solutions, one corresponding to the compressed bilayer and another to the broken bilayer, can coexist at some distance, while for other distances, one solution

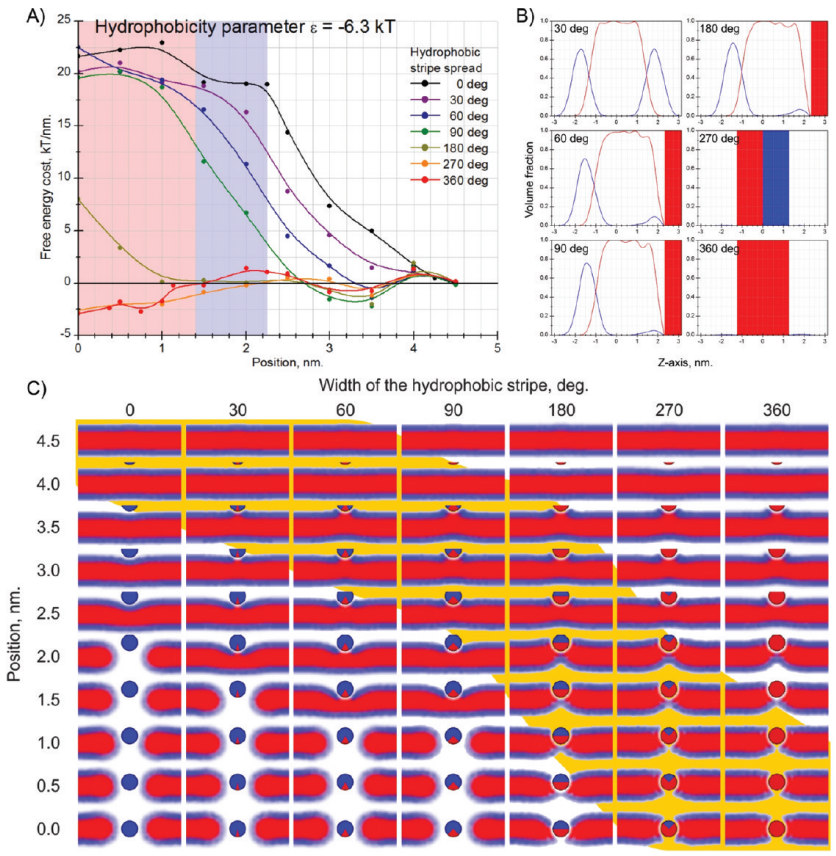

Figure 2. Same as Figure 1, but the stripe is less hydrophobic, $\varepsilon = -6.3$ kT.

is stable and another is metastable. Thus, the cylinder can follow the metastable branch with higher free energy of compressed and intact bilayer before abrupt rupture, accompanied with sudden drop of the free energy. Another reason for the dispersion of the points at the plateau are the error of calculations. Thus, it can be used to estimate the accuracy of the calculations (±2 kT/nm).

The presence of a parallel hydrophobic stripe on a hydrophilic cylinder makes the penetration of the cylinder inside the bilayer more favorable. This stripe is described by its width or projected angle (in degrees) in Figure 1 and Figure 2. We explore only the orientation with the stripe faced down to the bilayer since this is the lowest energy orientation, but these calculations can also be used to estimate the energy of rotation of the cylinder in the bilayer.

For relatively narrow stripes (with the projected angle in the range of 30−90°), phospholipid heads move apart from the cylinder to accommodate the insertion at low penetrations, which allows for the energetically favorable contact between the stripe and the hydrophobic core of the membrane and leads to the wetting of the stripe. The contact line moves up the hydrophilic cylinder surface, forming a rim, and increases the contact with the bilayer core. At higher penetrations, the cylinder compresses the bilayer and eventually breaks the membrane. The breakage distance between the cylinder and the membrane centers decreases with an increasing width of the stripe from 1.5−2.0 nm (the stripe of 30° projected angle) to 0.0−0.5 nm (90° stripe), and the free energy of penetration becomes lower. The equilibrium position of the cylinder within the bilayer (yellow band in Figure 1C corresponding to the minimum of the energy in Figure 1A) also shifts to the center of the bilayer with increasing width of the stripe. Thus, the width of the stripe controls not only the hydrophobicity of the cylinder and the insertion energy into the bilayer but also the equilibrium position with respect to the bilayer core (Figure 1B).

The mean field concentration profiles in Figure 1B,C demonstrate that hydrophobic interactions of $\varepsilon = -10.0$ kT are high enough for the cylinder to partially adsorb phospholipids from the bilayer. The hydrophobic stripe is covered with the phospholipids even after the rupture of the bilayer. For larger widths of the hydrophobic stripe (180−360°), the rupture of both leaflets of the bilayer does not occur and the cylinder is covered by phospholipids in the entire range of penetrations from 0.0 to 4.5 nm from the bilayer center. The bilayer only bends around the cylinder at small

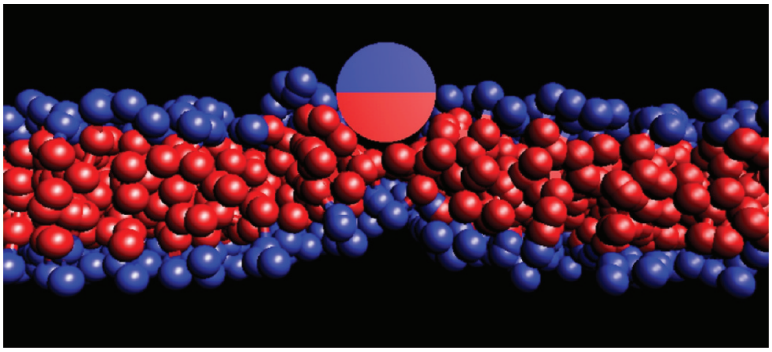

Figure 3. Amphiphilic cylinder (stripe width 180°, $\varepsilon = -10.0$ kT) and the most probable conformations of lipids.

penetrations, 1.5−4.0 nm, and covers the whole hydrophobic part of its surface at larger penetrations, 0.0−1.5 nm.

The SCMF method provides the probability of conformations of molecules in a given field. Thus, it allows for visualization of the solutions of the mean field equations in the form of the most probable conformations of molecules in the mean fields that correspond to the solution of the equations.[13] The example of most probable conformations of phospholipids, which correspond to the equilibrium position of the amphiphilic cylinder in the bilayer, is shown in Figure 3.

At lower hydrophobicity ($\varepsilon = -6.3$ kT, Figure 2), the behavior of the system is different in many aspects. The compression of the bilayer for relatively small (30−90°) widths of the hydrophobic stripe leads to the rupture of the membrane farther from the bilayer center than for the same stripes with higher hydrophobicity. Similarly, the equilibrium position of the cylinder with the same stripes but lower hydrophobicity is shifted closer to the surface of the bilayer. The overall surface of narrow stripes is too small to allow for the contact with two edges of the broken layer.

Hydrophobic stripes of larger width and $\varepsilon = -6.3$ kT induce small perturbations to the structure of the bilayer due to rearrangements of lipids around the stripe at relatively small penetrations. Phospholipid heads pushed apart by the inserted cylinder enable contact of the stripe with the hydrophobic core of the bilayer. Penetration of the cylinder to 2.0−2.5 nm from the bilayer center induces the rupture of the bilayer into two parts. Each part of the broken layer contacts with the stripe at their edges. The equilibrium position of the cylinders with large hydrophobic stripes (180−360°) is in the center of the bilayer. However, the interaction energy $\varepsilon = -6.3$ kT is insufficient for phospholipids to cover the cylinder from all sides, and the cylinder forms a pore in the bilayer (the central cross section concentration profiles in Figure 2B are different from the corresponding profiles in Figure 1B for 180−360° stripes).

The main difference between $\varepsilon = -10.0$ and -6.3 kT cases is the difference in the free energy of insertion of

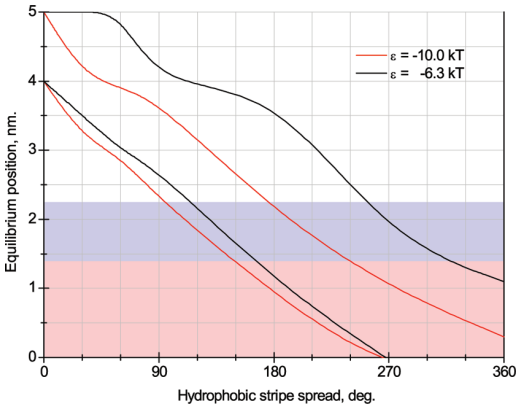

Figure 4. Range of the cylinder equilibrium position *versus* width of the hydrophobic stripe on its surface. The equilibrium position is in the region between the two red lines in the case of the stripe with higher hydrophobicity and between the two black lines in the case of the stripe with lower hydrophobicity. Rose and blue stripes designate the core and the heads regions of the bilayer.

the cylinder with large widths of the hydrophobic stripe (180−360°) (Figure 1A and Figure 2A). The more hydrophobic cylinder ($\varepsilon = -10.0$ kT) is fully covered with lipid tails, and thus its free energy of insertion is much lower than that of the partially covered cylinder with $\varepsilon = -6.3$ kT. Furthermore, the free-energy plots for more hydrophobic cylinder $\varepsilon = -10.0$ kT have pronounced minima, while the plots corresponding to $\varepsilon = -6.3$ kT have wide regions of relatively constant energies around their minima which correspond to the equilibrium position. Taking into account that the free-energy calculations presented here have an accuracy of about ±2.0 kT/nm and the minima are shallow, one can plot the areas where the free-energy cost of the cylinder insertion inside the membrane differs from its minimum value by less than 2.0 kT/nm (Figure 4). The region of equilibrium positions is wider and is on average shifted from the center of the bilayer for lower hydrophobicity. Thus, our results suggest that the cylinders with wide and low hydrophobicity stripes are able to change their position within a large range around the core of the bilayer with little or no energy cost.

The shallow minima of less hydrophobic ($\varepsilon = -6.3$ kT) and wide (180−360°) stripes can also be due to a particularity of the methodology used for the calculations. The vertical size of the simulation box is fixed for both cases, and the walls restrict the movement of the bilayer, and so the absence of complete covering of the hydrophobic part of the cylinder with the phospholipids in case of $\varepsilon = -6.3$ kT leaves more free space inside the simulation box to bend the bilayer. As a result, small shifts of the cylinder inside the box for less than 1.5 nm from the equilibrium lead to bending of the bilayer together with the cylinder without reorganization of the bilayer structure. In contrast, there is almost no free space in the case of the cylinder with $\varepsilon = -10.0$ kT, and small deviations of the position lead to significant reorganization of lipids covering the hydrophobic stripe, which has a higher free-energy cost. However, this difference is only significant for two points of the free energy corresponding to wide stripes.

Although the minimum free-energy orientation is with the stripe faced down to the bilayer, an estimate can be made of the free energy of the cylinder rotating around its axis. In the cases of completely hydrophilic, and completely hydrophobic cylinders, there are no changes to the free energy. Rotation of the cylinder with the stripe leads to contact of the bilayer edges and the hydrophobic core of the cylinder as well as contact between the heads of the bilayer phospholipids with a hydrophilic part of the cylinder. Thus, there is an energy barrier for rotation that can be estimated as follows. The maximum height of the barrier for rotation of the cylinder at position 0.0 nm from the bilayer center for 90° will be equal, approximately, to the average of the free-energy costs of insertion into this position of completely hydrophobic and completely hydrophilic cylinders (from which we can estimate the energy of rotation for each position). In all others cases, the equilibrium positions found for the orientation "stripe-down" will be the true equilibrium position for any rotation of the cylinder because in all of these positions the hydrophobic core of the bilayer has the maximum possible contact with the hydrophobic stripe of the cylinder. Hence, any rotation of the cylinder will not increase the contact area but will significantly deform the bilayer, causing the free-energy loss.

CONCLUSION

Our results demonstrate physical principles of the association of rod-shaped objects with a specific surface pattern and self-assembled phospholipid bilayers. In particular, a hydrophobic stripe along the axis of the cylinder can mimic self-assembled peptides with a secondary periodic structure such as α-helices. The position of the cylinder in the bilayer as well as the free energy of association depends on the geometry of the stripe, that is, the width and the hydrophobicity. This microscopic information, in turn, can be used for the design of artificial polymers with enhanced association with phospholipid bilayers.

MATERIALS AND METHODS

Within the SCMF theory,[13] the phospholipid molecule is modeled at a coarse-grained level, while the interactions between the molecules in the bilayer are represented by the mean fields. The three-bead model[12−15] describes a phospholipid molecule as a sequence of three spherical beads of a radius 4.05 Å, one hydrophilic (H) and two hydrophobic (T), joined consequently with the bond length of 10.0 Å. Two T beads of neighboring molecules interact with the energy $\varepsilon_{TT} = -2.10$ kT if the distance between the centers of the molecules is smaller than 12.15 Å. The H beads interact with implicit solvent molecules with the energy $\varepsilon_{HS} = -0.15$ kT if the distance between the centers of the molecules is smaller than 12.15 Å. The solvent molecules are considered as spherical beads of the same radius, 4.05 Å. The phospholipid molecule is free to bend around the central bead.

A cylinder with a diameter of 24.3 Å and longitudinal hydrophobic stripe on the surface is inserted into the phospholipid bilayer at different positions in the simulation box. The position of the cylinder is fixed parallel to the bilayer with the orientation "stripe-down". The hydrophobic part of the surface of the cylinder interacts with the T beads with the energy, ε, if the centers of the molecules are at the distance closer than 8.1 Å, while the hydrophilic stripe has only steric repulsion interactions with phospholipids and water molecules. This allows one to describe the hydrophobicity of the cylinder with a stripe by its width and a single interaction parameter, ε. We consider an infinite cylinder, where the cylinder length is equal to the size of the simulation box in the corresponding direction, and use the periodic boundary conditions.

In cases where the cylinder penetration is unfavorable, the phospholipid bilayer tends to bend and escape the inserted cylinder to minimize the equilibrium free energy. To restrict the bending of the phospholipid bilayer, we introduce hard walls at the top and bottom of the simulation box. This allows the estimation of free energy of insertion at a given position according to the procedure described in ref 13.

Conflict of Interest: The authors declare no competing financial interest.

Acknowledgment. P.S. and V.A.B. acknowledge the Spanish Ministry of education MICINN project CTQ2008-06469/PPQ. P.S., V.A.B., and N.K.H.S. thank the Royal Society for the provision of an International Joint Project grant that facilitated aspects of the work.

REFERENCES AND NOTES

1. Garay-Arroyo, A.; Colmenero-Flores, J. M.; Garciarrubio, A.; Covarrubias, A. A. Highly Hydrophilic Proteins in Prokaryotes and Eukaryotes Are Common during Conditions of Water Deficit. *J. Biol. Chem.* **2000**, *275*, 5668–5674.
2. Browne, J.; Tunnacliffe, A.; Burnell, A. Anhydrobiosis: Plant Desiccation Gene Found in a Nematode. *Nature* **2002**, *416*, 38.
3. Tolleter, D.; Jaquinod, M.; Mangavel, C.; Passirani, C.; Saulnier, P.; Manon, S.; Teyssier, E.; Payet, N.; Avelange-Macherel, M.-H.; Macherel, D. Structure and Function of a Mitochondrial Late Embryogenesis Abundant Protein Are Revealed by Desiccation. *Plant Cell* **2007**, *19*, 1580–1589.

4. Wise, M. J.; Tunnacliffe, A. POPP the Question: What Do LEA Proteins Do? *Trends Plant Sci.* **2004**, *9*, 13–17.
5. Goyal, K.; Tisi, L.; Basran, A.; Browne, J.; Burnell, A.; Zurdo, J.; Tunnacliffe, A. Transition from Natively Unfolded to Folded State Induced by Desiccation in an Anhydrobiotic Nematode Protein. *J. Biol. Chem.* **2003**, *278*, 12977–12984.
6. Popova, A. V.; Hundertmark, M.; Seckler, R.; Hincha, D. K. Structural Transitions in the Intrinsically Disordered Plant Dehydration Stress Protein LEA7 upon Drying Are Modulated by the Presence of Membranes. *Biochim. Biophys. Acta* **2011**, *1808*, 1879–1887.
7. Panchal, R. G.; Smart, M. L.; Bowser, D. N.; Williams, D. A.; Petrou, S. Pore-Forming Proteins and Their Application in Biotechnology. *Curr. Pharm. Biotechnol.* **2002**, *3*, 99–115.
8. Yang, L.; Harroun, T. A.; Weiss, T. M.; Ding, L.; Huang, H. W. Barrel-Stave Model or Toroidal Model? A Case Study on Melittin Pores. *Biophys. J.* **2001**, *81*, 1475–1485.
9. Illya, G.; Deserno, M. Coarse-Grained Simulation Studies of Peptide-Induced Pore Formation. *Biophys. J.* **2008**, *95*, 4163–4173.
10. Gkeka, P.; Sarkisov, L. Interactions of Phospholipid Bilayers with Several Classes of Amphiphilic α-Helical Peptides: Insights from Coarse-Grained Molecular Dynamics Simulations. *J. Phys. Chem. B* **2010**, *114*, 826–839.
11. Tunnacliffe, A.; Wise, M. J. The Continuing Conundrum of the LEA Proteins. *Naturwissenschaften* **2007**, *94*, 791–812.
12. Pogodin, S.; Slater, N. K. H.; Baulin, V. A. Surface Patterning of Carbon Nanotubes Can Enhance Their Penetration through a Phospholipid Bilayer. *ACS Nano* **2011**, *5*, 1141–1146.
13. Pogodin, S.; Baulin, V. A. Coarse-Grained Models of Phospholipid Membranes within the Single Chain Mean Field Theory. *Soft Matter* **2010**, *6*, 2216–2226.
14. Pogodin, S.; Baulin, V. A. Can a Carbon Nanotube Pierce through a Phospholipid Bilayer? *ACS Nano* **2010**, *4*, 5293–5300.
15. Pogodin, S.; Baulin, V. A. Equilibrium Insertion of Nanoscale Objects into Phospholipid Bilayers. *Curr. Nanosci.* **2011**, *7*, 721–726.

Chapter 7

Conclusions

This chapter summarizes the results obtained in the work.

Working SCMF computer simulation code was developed, tested, and successfully applied for investigation of molecular systems, namely of the DMPC phospholipid membranes and their interactions with nano-objects, such as nanotubes with homogeneous and patterned surfaces and LEA-protein-like patterned cylinders. It was shown that the method is able adequately reproduce experimentally relevant equilibrium properties of such systems. In addition, the developed method can be applied for broad spectrum of problems which are far beyond the scope of the present work. In view of this perspective, there is a lot of room for improvement of the computer implementation of the method. It seems, that if such improvements and future optimizations of the method will be performed, the SCMF can become really powerful and popular tool for investigation of behavior of different molecular systems.

Few models of the DMPC phospholipid molecules with different levels of coarse-graining were proposed. Each of them reproduced such essential properties of the DMPC membrane, as its thickness, density and elasticity. Each of this model was found able to adequately reproduce relevant properties of the bilayer, the most simple and less computationally expensive "three-beads" model was chosen for the use in subsequent research.

Simulation of carbon nanotubes with homogeneous surface properties revealed that such nanotubes are not able to translocate, by means of thermal diffusion, through the phospholipid bilayer due to high free-energy barrier at the pathway of such translocation. We have found that the hydrophobic nanotubes will be entrapped inside the bilayer with orientation parallel to its plane, while the hydrophilically modified nanotubes won't be able to pierce into the bilayer even in the most advantageous perpendicular orientation with respect to the bilayer. Nanotubes with intermediate hydrophobicity properties will show intermediate behavior, with pos-

sibility to be adsorbed at the bilayer's surface.

Further investigations demonstrated, that the ability of a carbon nanotube to penetrate through a lipid membrane can be significantly enhanced by smart patterning of the nanotube by altering periodical regions of higher and lower hydrophobicity. Correct pattern may considerably decrease the translocation energy-barrier, making the nanotube diffusion through the membrane much easier.

In the final part of the work some investigation of adsorption of LEA-protein-like object onto phospholipid membranes was carried out. It was shown, that the ratio between widths of longitudinal hydrophobic and hydrophilic regions, presented at the surface of LEA-proteins in helical state, controls the depth of the protein penetration into the bilayer, and, as well, the corresponding free-energy of association with the membrane.

In summary, the goals of study were achieved, and further directions of the research and development of the SCMF method were indicated.

Chapter 8

Publications, conferences and summer schools

8.1 Publications in refereed journals with ISI citation index

1. **Authors**: Elena P. Ivanova, Jafar Hasan, Hayden K. Webb, Vi Khanh Truong, Gregory S. Watson, Jolanta A. Watson, Vladimir A. Baulin, Sergey Pogodin, James Y. Wang, Mark J. Tobin, Christian Löbbe, and Russell J. Crawford
   Title: Natural antibacterial surfaces: cicada *Psaltoda claripennis* wings kill *Pseudomonas aeruginosa* cells
   Journal: just submitted

2. **Authors**: Sergey Pogodin, Nigel K. H. Slater, and Vladimir A. Baulin
   Title: Biomolecule surface patterning may enhance membrane association
   Journal: ACS Nano
   Volume: 6 **Pages**: 1308 - 1313 **Year**: 2012
   ISI category: Nanoscience & Nanotechnology
   Impact factor: 9.865 **AIF**: 4.154
   Position in the category: 5

3. **Authors**: Andriy Yaroshchuk, Emiliy Zholkovskiy, Sergey Pogodin, and Vladimir A. Baulin
   Title: Coupled concentration polarization and electroosmotic circulation near micro/nanointerfaces: Taylor-Aris model of hydrodynamic dispersion and limits of its applicability
   Journal: Langmuir
   Volume: 27 **Pages**: 11710 - 11721 **Year**: 2011
   ISI category: Chemistry, Multidisciplinary

Impact factor: 4.269 **AIF**: 4.299
Position in the category: 24
Cited: 2 times

4. **Authors**: Sergey Pogodin, and Vladimir A. Baulin
Title: Equilibrium insertion of nanoscale objects into phospholipid bilayers
Journal: Current Nanoscience
Volume: 7 **Pages**: 721 - 726 **Year**: 2011
ISI category: Nanoscience & Nanotechnology
Impact factor: 1.879 **AIF**: 4.154
Position in the category: 36

5. **Authors**: Sergey Pogodin, Nigel K. H. Slater, and Vladimir A. Baulin
Title: Surface patterning of carbon nanotubes can enhance their penetration through a phospholipid bilayer
Journal: ACS Nano
Volume: 5 **Pages**: 1141 - 1146 **Year**: 2011
ISI category: Nanoscience & Nanotechnology
Impact factor: 9.865 **AIF**: 4.154
Position in the category: 5
Cited: 4 times

6. **Authors**: Sergey Pogodin, and Vladimir A. Baulin
Title: Can a carbon nanotube pierce through a phospholipid bilayer?
Journal: ACS Nano
Volume: 4 **Pages**: 5293 - 5300 **Year**: 2010
ISI category: Nanoscience & Nanotechnology
Impact factor: 9.865 **AIF**: 4.154
Position in the category: 5
Cited: 7 times

7. **Authors**: Sergey Pogodin, and Vladimir A. Baulin
Title: Coarse-grained models of phospholipid membranes within the single chain mean field theory
Journal: Soft Matter
Volume: 6 **Pages**: 2216 - 2226 **Year**: 2010
ISI category: Polymer science
Impact factor: 4.457 **AIF**: 2.458

Position in the category: 6
Cited: 7 times

8. **Authors**: S. I. Kuchanov, and S. G. Pogodin
Title: Theoretical consideration of bulk free-radical copolymerization with allowance for the preferential sorption of monomers into globular nanoreactors
Journal: Journal of chemical physics
Volume: 128 **Pages**: 244902 **Year**: 2008
ISI category: Physics, Atomic, Molecular & Chemical
Impact factor: 2.921 **AIF**: 2.483
Position in the category: 7

9. **Authors**: S. Kuchanov, S. Pogodin, G. ten Brinke, and A. Khokhlov
Title: Polymer globule as a nanoreactor
Journal: Macromolecules
Volume: 41 **Pages**: 2689 - 2693 **Year**: 2008
ISI category: Polymer science
Impact factor: 4.838 **AIF**: 2.458
Position in the category: 5
Cited: 2

8.2 Participation in conferences and summer schools

1. **Event**: Workshop on biomaterials and their interactions with biological and model membranes
Location: Salou, Spain **Month and year**: September 2011
Type of participation: oral presentation
Authors: Sergey Pogodin, Nigel K. H. Slater, and Vladimir A. Baulin
Title: Simulation of nanoparticles penetration through a phospholipid bilayer

2. **Event**: European polymer congress EPF-2011
Location: Granada, Spain **Month and year**: June 2011
Type of participation: oral presentation
Authors: Sergey Pogodin, Nigel K. H. Slater, and Vladimir A. Baulin
Title: Simulation of nanoparticles penetration through a phospholipid bilayer

3. **Event**: Gordon research conference “Environmental Nanotechnology”
Location: Waterville Valley NH, USA **Month and year**: May 2011
Type of participation: poster presentation

Authors: Sergey Pogodin, and Vladimir A. Baulin
Title: Simulation of nanoparticles penetration through a phospholipid bilayer

4. **Event**: International symposium on functional polymers for nanomedicine
   Location: Hangzhou, China **Month and year**: May 2011
   Type of participation: poster presentation
   Authors: Sergey Pogodin, and Vladimir A. Baulin
   Title: Simulation of nanoparticles penetration through a phospholipid bilayer

5. **Event**: MACRO 2010
   Location: Glasgow, UK **Month and year**: July 2010
   Type of participation: poster presentation
   Authors: Sergey Pogodin, and Vladimir A. Baulin
   Title: Single chain mean field technique for simulation of complex molecular systems

6. **Event**: Soft matter conference 2010
   Location: Granada, Spain **Month and year**: July 2010
   Type of participation: poster presentation
   Authors: Sergey Pogodin, and Vladimir A. Baulin
   Title: Single chain mean field technique for simulation of complex molecular systems

7. **Event**: Multiscale molecular modelling
   Location: Edinburgh, UK **Month and year**: July 2010
   Type of participation: poster presentation
   Authors: Sergey Pogodin, and Vladimir A. Baulin
   Title: Single chain mean field technique for simulation of complex molecular systems

8. **Event**: CSC summer school in scientific and high-performance computing
   Location: Finland **Month and year**: June 2010

9. **Event**: 8-th poster exhibition of doctoral students of the Chemical Engineering Department of the Rovira i Virgili University
   Location: Tarragona, Spain **Month and year**: April 2010
   Type of participation: poster presentation
   Authors: Sergey Pogodin, and Vladimir A. Baulin
   Title: Single chain mean field technique for simulation of complex molecular systems

10. **Event**: Summer school "Methods in molecular simulation"
    Location: Sheffield, UK **Month and year**: July 2009

11. **Event**: 7-th poster exhibition of doctoral students of the Chemical Engineering Department of the Rovira i Virgili University
    Location: Tarragona, Spain **Month and year**: April 2009
    Type of participation: poster presentation
    Authors: Sergey Pogodin, and Vladimir A. Baulin
    Title: Single chain mean field technique for simulation of complex molecular systems

12. **Event**: Summer school "Multiscale simulation methods in molecular sciences"
    Location: Jülich, Germany **Month and year**: March 2009

13. **Event**: Summer school "Long range interacting systems"
    Location: Les Houches, France **Month and year**: August 2008

UNIVERSITAT ROVIRA I VIRGILI
COMPUTER SIMULATION OF NANOPARTICLES TRANSLOCATION THROUGH PHOSPHOLIPID MEMBRANES WITHIN SINGLE CHAIN MEAN FIELD APPROACH
Sergey Pogodin
DL: T. 290-2012

UNIVERSITAT ROVIRA I VIRGILI
COMPUTER SIMULATION OF NANOPARTICLES TRANSLOCATION THROUGH PHOSPHOLIPID MEMBRANES WITHIN SINGLE CHAIN MEAN FIELD APPROACH
Sergey Pogodin
DL: T. 290-2012

UNIVERSITAT ROVIRA I VIRGILI
COMPUTER SIMULATION OF NANOPARTICLES TRANSLOCATION THROUGH PHOSPHOLIPID MEMBRANES WITHIN SINGLE CHAIN MEAN FIELD APPROACH
Sergey Pogodin
DL: T. 290-2012